FOOD EARLY SOLUTIONS FOR AFRICA (FESA)

FESA MICRO-INSURANCE

Methodology, validation, contract design

August 2010

EARS Earth Environment Monitoring – Delft

FESA Micro-Insurance

Methodology, validation, contract design

August 2010

Authors

Andries Rosema**,** Marjolein de Weirdt**,** Steven Foppes, Charlotte Wilczok
EARS Earth Environment Monitoring BV, Delft, Netherlands

Foreword: Prof. Dr. Kees Stigter, founding president of the International Society for Agricultural Meteorology

Project

Food Early Solutions for Africa (FESA) – Micro Insurance
Milennium Project 00038
Directorate General for International Cooperation
Ministry of Foreign Affairs, the Netherlands

Cover photograph

Africa as observed through Meteosat. Copyright EUMETSAT, Darmstadt.

CONTENTS

FOREWORD

by Prof. Dr. Kees Stigter, founding president of the International Society for Agricultural Meteorology (www.agrometeorology.org)

When working in poor countries and the large poorer (very often rural) parts of somewhat better off countries, meeting consequences of weather and climate related disasters is always part of one's experience. But it is these days increasingly so in the context of climate change. In only the past four months (Nov. 2009 – Febr. 2010) (i) I witnessed in areas of Cambodia the effect of recent large scale floods, travelling by road from Phnom Penh to much more northern Siem Reap after one week of Workshops on coping with weather related pests and diseases; (ii) I felt in the coastal north of West Java (particularly Indramayu region) and valleys near Yogyakarta (Wareng/Gunungkidul) in Central Java the increasing desperation of rice farmers trying to cope with persistent drought during an El-Nino year, while trying for one week to assist local scientists in finding lasting solutions with these farmers, and (iii) I read in the newspapers in Lesotho (southern Africa) about the troubles of lowland subsistence farmers not being able to pay back their loans to the government because of droughts and floods over the past four years, while giving a Roving Seminar of one week on agrometeorological services in its capital Maseru. In all these cases also politicians were to blame for not coming to the rescue of these areas, in long overdue preparedness or in immediate relief measures. In more than one case these politicians even being part of the problem instead of the solution.

In such and many comparable situations immediate solutions are needed that save poor farmers from complete ruination and that do not wreck their future chances of restoring their farming systems for production in better seasons and years. Community based individual insurance on a large scale can be a very good contribution to such solutions, but special care has to be taken that the schemes are also available to the more vulnerable low-income individuals. The Wikipedia learns that micro-insurance in principle links multiple small units into larger structures, creating networks that enhance both insurance functions (through broader risk pools) and support structures for improved governance (i.e. training, data banks, research facilities, access to reinsurance etc). This mechanism's main objective is to pool both risks and resources of whole groups for the purpose of providing financial protection to all members against the financial consequences of mutually determined risks. This means that:
- transactions are low-cost (and reflect members' willingness to pay);
- clients are essentially low-net-worth (but not necessarily uniformly poor);
- communities are involved in the important phases of the process (such as package design and rationing of benefits).

Micro-insurance is a low cost, high volume business. Unless costs are contained, agricultural micro-insurance cannot be sustainable. Making products compulsory is one of the few ways micro-insurance schemes can reach the high volumes they need to become sustainable. Advantages and disadvantages of this have to be outweighed carefully. When carefully prepared, drought micro-insurance can play a great role in climate adaptation strategies, combating impoverishment and obtaining a more sustainable development.

I have always believed that science can support many poverty alleviation attempts, when we take care that also the applied scientists understand contexts as given above. The story below confirms that also in developing countries relevant applied research can easily be done. When I worked as a resident professor at the University of Dar es

Salaam in the late seventies and early eighties, trustable potential evaporation (at that time just renamed as reference crop evaporation) calculations were internationally an important issue for support of determining crop water requirements. In the strongest physics based equation in use, the radiation term is in the tropics often the most important one. Therefore simple trustable solar radiation quantification with a high spatial representativity was crucial. In this context we were interested in differences between point cloudiness and aerial cloudiness, which were due to the problem that cloudiness was commonly observed twice a day visually by observers from a meteorological station. This gave point cloudiness while satellites had just started to quantify areal cloudiness.

Now we found at the time that the complement of “sunshine duration”, measured with a Campbell Stokes instrument, could be called “shade duration”. This “shade duration” came much closer to the areal cloudiness observed by satellites and thus also “sunshine duration” was indeed rather representative for radiation received at the earth surface. We even found that twice a day data at observational hours in Tanzania, corrected for the problem of being point cloudiness, represented well the average areal cloudiness for the day. This made satellite data users very happy because satellites did measure areal cloudiness in one place twice a day. But this way there was also a simple spatially representative proxy for solar radiation received at the earth surface, with a high spatial density.

The above story came back to me when reading the report before you. What is needed in drought micro-insurance is a best possible proxy (index) of agricultural drought. Rainfall is an extremely useful parameter to be measured by farmers on their plots, to relate it to their growth of crops, but it is substantially less suitable for purposes of representing agricultural drought for reasons well dealt with in this report. The index used here is that of satellite derived Relative Evapotranspiration (RE) that represents actual water use by the crops. And in addition a satellite derived Relative crop Yield (RY) index is used to represent the effect of lack of water, so drought, on yields, that is crop losses. The risk of the latter, due to drought, is then related to the probability that RY or RE falls below a trigger value related to insurance pay out. This is all detailed in this report but the lesson is that the satellite data, once well calibrated with historical data, do not necessitate further ground backing for insurance pay out. Such historical data do hardly exist for any meteorological parameters related to drought that are measured in the classical way. It was already difficult enough to find historical yield data that could be trusted.

One should finally not be amazed that a large part of this report subsequently deals with validation exercises. Contrary to the relatively simple cloudiness/radiation example from Tanzania, the approach used here is much more complicated, the parameters/indexes much more complex and assessments often indirect. But the validation exercises are much more promising than they can be for the other approaches. Together with the fact that these indexes can be produced at low costs, that is what gives me the necessary trust in the approach. The final task will be to bring that sense of trust also to the stakeholders involved, through serious attempts to inform them about the seasonal developments derived from this new approach.

1 INTRODUCTION

Insurance is a long existing risk sharing mechanism, which is recognized as being an essential requirement for socio-economic development. Insurance against drought and other adverse climatic events has raised considerable interest during the past decade and is advocated as a tool to:

- Protect the population against adverse climatic events, so as to decrease poverty and foster economic development.
- Prepare for disasters and provide funding for immediate disaster mitigation, as an alternative to providing emergency aid after a disaster has occurred and has been assessed.
- Provide a mechanism to adapt to and cope with climatic change.

However, traditional insurance is still too expensive to be affordable to the poor. Micro-insurance seeks innovative ways to reduce these costs and to provide an affordable but reliable mechanism of risk sharing.

Risk sharing has an important social-economic spin-off. It prevents farmers from falling into the “poverty trap”, which occurs if after crop failure they have to sell their productive assets and thus loose their capability of gaining an income through farming. Reversely, having insurance may allow them to obtain credit from a bank and to invest in the intensification of agricultural production by buying fertilizers, pesticides and higher quality seeds. In this way poor farmers can considerably increase their crop production and income. And for this very reason micro-insurance is an essential tool in reaching Millennium Development Goal Nr. 1: the reduction of extreme poverty and hunger.

This document is prepared in the framework of Millennium project no 38: *FESA Micro-Insurance*, a project commissioned by the Netherlands Minister of Development Cooperation, as a contribution to reaching the UN Millennium Development Goals. The project aims to develop an abundant satellite based climatic data source and a related drought insurance system that can reach every farmer in Africa. In this report we study the suitability of Meteosat derived climatic data for this purpose. Focus will be on Meteosat derived evapotranspiration, derived through the earth surface energy balance. Since 1993, EARS is receiving hourly Meteosat data for this purpose and is operating a corresponding satellite data processing line. It operates independently, not needing other input data. Actual evapotranspiration data are closely related to crop growth. This is what drought insurance is particularly targeting at and for this reason we also discuss the use of these data for crop yield estimation.

Besides evapotranspiration data, EARS is also operating a rainfall processing line to generate daily rainfall data fields for Africa. The methodology is based on counting cloud level frequencies. It uses calibration with ground measured rain gauge data and consequently is not independent of the availability and quality of such ground measurements. The use of rainfall data is not advocated because of its dependence on ground data and because of the unknown faith of the precipitation, in view of surface run-off and deep percolation. Nevertheless a long term rainfall data base will also be developed as an alternative to the evapotranspiration data.

1.1 Traditional crop insurance

In developing countries the traditional type of crop insurance has widely failed (Pierro 2008). In a business sense traditional agricultural insurance is considered inherently non-sustainable and has always been subsidized (Roth et al. 2009). The causes for lack of success are:

- High correlated risk, causing high costs for re-insurance.
- Adverse selection: farmers with high-risk represent the majority of buyers.
- Moral hazard: farmers loose incentives to make a best effort.
- Fraud: evidence is manipulated to support a claim.
- Lack of transparency, particularly in relation to claim assessment.
- Late pay-out due to extensive claim verification.
- High costs, due to extensive monitoring, administration, claim verification.

1.2 Index-based insurance

In response to the aforementioned problems, index based crop insurance has been explored in recent years. In such insurance the farmer is not insured against crop loss, but against the adverse climatic conditions that cause crop loss. In relation to drought the index could for example be the rainfall during the growing season. The positive elements of such index-based insurance could be:

- Low costs of monitoring and administration
- Low moral hazard, as the index does not depend on the farmer
- Less adverse selection
- Transparent: trigger and pay-out can easily be verified
- Fast pay out, since no damage assessment is needed
- Potential to be economically self-sustainable

However, index insurance also introduces some problems or demands, in particular:

- High basis risk: the index may be insufficiently representative for the loss to be covered, leading to inappropriate payouts.
- Need for long time series of the index so as to be able to assess the risk and develop and price the insurance.
- High data requirements may require high investments in measuring stations and may increase the costs.

In relation to drought, rainfall seems a logical index, particularly because it is close to people's perception of drought. Rainfall is indeed the source of water for plant growth, but not all rainfall is used by the plants, Part of the rainfall runs off, and part percolates to greater depth outside the reach of the plant roots. Moreover rain does not necessarily fall at the time plants use the water. This introduces considerable uncertainties and may pose considerable problems in the formulation of the insurance.

The problem could be addressed by involving a soil water balance model, which is fed by the precipitation and simulates how much water remains available in the root zone to the plants. For such a model to work properly, knowledge of the soil infiltration coefficient, water holding capacity and water conductivity is required. Such information is usually not available or can only be estimated roughly on the basis of soil type and soil depth. An example is the Water Requirements Satisfaction Index (WRSI) developed at FAO by *Gommes (1983)* which provides an estimate of the water availability to the crop relative to its water needs. The WRSI has been used in a disaster insurance contract by AXA with the Ethiopian government and also in

insurance contracts, which were a part of the Millennium Villages Project *(Hellmuth et al. 2009)*.

More elaborate approaches go beyond the water availability and use coupled crop growth models to estimate the effects of water availability on crop yield. The Agriculture Insurance Company of India has used the INFOCROP model. By replacing the rainfall indicator with the WRSI or even an estimate of crop yield as index, the intrinsic basis risk may certainly be reduced, but an important shortcoming that remains is the spatial basis risk related to the sparse availability of reliable rainfall input data.

Rainfall in Africa is very variable. To adequately represent the spatial variation of convective rainfall systems, the distance between rainfall stations should not be more than a few kilometres. Current drought insurance practice requires the insured to live within a distance of 25 km from a suitable rainfall station. This, however, is very questionable and will already imply a high spatial basis risk, leading to cases of inappropriate payout. In fact the number of suitable rainfall stations in Africa is very low. This tends to cause a high spatial basis risk and limits scaling up of the insurance. Scaling up is badly needed to make drought insurance self-sustainable. A possible solution could be to establish many new rainfall stations. Rainfall stations, however, are costly, not only from the investment point of view, but particularly in terms of operational costs. Moreover building more rainfall stations does not solve the need of long time series to assess and price the risk.

1.3 Satellite indices

Because of the problems related to ground measured indices, as discussed in the previous section, there is a growing interest in satellite data. Such data are continuous in space, could reduce spatial basis risk and thus offer potential for insurance scaling up. On the other hand, some of these approaches may introduce a higher intrinsic basis risk in the sense that the quantity measured from space shows insufficient bearing on the type of risk to be insured, i.e. the risk of drought and crop failure.

Satellites may cover entire regions with sufficient spatial and temporal resolution to adequately represent the variability of weather and crop conditions. In relation to micro-insurance important questions are:

- Do satellite derived indices really represent drought and crop yield, in other words: do they not introduce high intrinsic basis risk, and
- Do these indices provide high performance at low-costs, are they cost-effective?

With respect to cost-effectiveness, geostationary meteorological satellites show high potential. They are characterized by:

- sufficient spatial resolution (3-5 km grid size)
- adequate temporal resolution (1 hourly repetition)
- reliable operational systems, backed by a large user community
- regional to continental data coverage
- low data costs

On the basis of geostationary satellites several type of data products are currently known, which are discussed in the following sub-sections.

1.3.1 Reflection indices

Well known is the Normalized Difference Vegetation Index (NDVI), which is based on the earth surface reflection in the red (R) and near infrared (NIR) spectral band: NDVI=(NIR-R)/(NIR+R). The reflection spectrum of bare soil or rock is quite flat. Plant leaves, however have a low reflection in the red (due to absorption by chlorophyll) and a very high reflection in the near infrared (due to low absorption and strong scattering). Therefore the NDVI is low for soil and rock, and high for a plant canopy. The NDVI is essentially an indicator of canopy closure. The index is sometimes used as an indicator of the quality of the growing season and of crop yields to be expected. This is however questionable because the NDVI is only a measure of greenness and vegetation cover and gives no direct information on water limitation to crop yield.

There are also other indices that have been proposed as indicators of crop growth. An example is APAR and fAPAR. They are used in the supposition that "absorbed photosynthetic active radiation" is an indicator of crop growth. Although this indicator may represent light interception, it does give information on the partitioning of absorbed solar energy between photosynthetic electron transport and heat. In this sense these indices do not offer significantly more information than the NDVI.

1.3.2 Precipitation

The use of satellite data for rainfall monitoring has already a long history, which is well documented in *Barrett and Martin (1981)* and *Kidder and Vonder Haar (1995)*. Operational monitoring of rainfall over the African continent has been pioneered since the 1980's by the TAMSAT group at the University of Reading, UK and by EARS in Delft, the Netherlands. EARS was the first to map rainfall across the African continent and has also implemented its technology for east and southeast Asia.

For rainfall monitoring two types of satellites may be used: the more general meteorological satellites providing imaging capability in the visible and thermal infrared, and dedicated satellites providing micro-wave imaging instruments. Examples of the first are the METEOSAT, GOES and FY2 geostationary meteorological satellites. An example of the latter is the Tropical Rainfall Mapping Mission (TRMM). The latter however suffers from a relatively low spatial resolution and low repeat coverage.

The methods used by the TAMSAT group and by EARS are based on the TIR band on board of geostationary meteorological satellites. On the basis of radiation temperature measurements, clouds are classified according to their height. This is typically done every hour and the presence of these cloud height classes is counted during a certain period, usually a day or a 10-daily period (dekad). The resulting figure is usually called "cloud duration". Subsequently a statistical relation between the cloud duration(s) and the rainfall is sought by means of mathematical regression analysis.

In the TAMSAT approach only very high or so-called "cold clouds" are used. The relation between rainfall and "cold cloud duration" (CCD) is calibrated against historical data from available rainfall stations. A disadvantage of this approach is that the calibration coefficients have appeared to be very variable in time and space and historical calibration coefficients may not be valid today. Another disadvantage is that

the use of only the CCD makes the methodology less suitable for advective and orographic rainfall and thus restricts continent wide application.

The method developed by EARS is based on multiple cloud height classes and corresponding cloud durations (CD's), as well as on a rainstorm vigour indicator called "cloud top temperature threshold excess" (CTTE). Calibration is done in near real time by means of multiple regression against WMO-GTS rain gauge data. The limited availability of GTS rainfall stations in Africa, however, may also impose a limitation to this real time approach.

A disadvantage of rainfall as crop growth indicator is, that it is not known how much of the precipitation is available to the crop. A considerable part of the precipitation may run off, depending on soil infiltration characteristics and slope. Of the rain that infiltrates the soil, a considerable part may percolate to deeper layers outside the reach of plant roots. However, as discussed in section 1.4, an additional water balance and crop growth model could help to address this problem and "translate" precipitation in information more closely related to crop production deficit, although such a model would require additional information on soil type and depth.

1.3.3 Evapotranspiration

Besides developing satellite based mapping of rainfall, EARS has been pioneering the derivation of actual evapotranspiration data from Meteosat since the early 1980's. In this way the company has become the only routine provider of both satellite rainfall and evapotranspiration data.

In principle evapotranspiration consists of two components. One is water loss through the plant leaves, also called transpiration, and the other one is water loss from bare soil. However bare soil evaporation is very small. This is caused by the fast development of a dry surface layer, which isolates the soil from further water loss to the atmosphere. Transpiration from plants is by far the dominant component.

It is well documented in the plant physiological literature that evapotranspiration from plants is proportional to CO_2 uptake and consequently to plant growth and crop yield (*Stewart et al. 1973, 1977, Doorenbos and Kassam 1979, Slabbers et al. 1979*). For this reason actual evapotranspiration is fundamentally a better indicator of crop growth than precipitation. An operational advantage of the satellite derived evapotranspiration data is that, contrary to rainfall data production, no additional data from other ground-based sources are required, once the system is tuned.

1.3.4 Crop yield

On the basis of crop growth being proportional to evapotranspiration, several crop growth models have been developed. The traditional models were always fed with rain gauge data. A soil water balance model is then used to estimate how much of the precipitation is available to the crop and can be evaporated. Well known is the WOFOST model of Alterra in Wageningen and the related CGMS, applied by the EU Joint Research Centre to estimate and forecast crop yields in Europe, using a network of meteorological stations. EARS has developed a similar crop growth model (ECGM), which makes directly use of the satellite derived evapotranspiration and radiation data as input. The algorithm is based on solid physical and physiological principles, which follow the work of *Monteith*, *Stewart*, *Doorenbos and Kassam*, and

others. The ECGM is capable of generating crop yield estimates for every location in Africa and Europe and is currently operationally used for crop yield forecasting of maize, wheat, sorghum, millet and potato. However, the model can be applied to many other crops.

1.4 Report objective and scope

Meteorological satellites provide abundant information that is suitable for the development of a drought micro insurance system that overcomes the disadvantages of indices measured on the ground, in particular high basis risk and high data collection costs. In this report we investigate the suitability of Meteosat based evapotranspiration and crop yield products. They have the following distinct advantages over satellite based rainfall products:

- They are closer to the actual risk to be addressed, i.e. crop failure due to drought
- They do not depend on measured ground data
- They show better data distribution characteristics

These are important advantages, which may lead to high cost efficacy and which may allow for relatively easy insurance scaling up.

The use of satellite derived evapotranspiration and related crop yield estimates for crop insurance purposes has not earlier been explored. Moreover there are almost no operational providers of such data. This may have contributed to a lack of knowledge and awareness in this field. It is the objective of the current project to investigate and test this new possibility and to develop a drought micro-insurance approach with continental coverage.

In chapter 2 we will first describe how the temperature, radiation, evapotranspiration and rainfall are derived from the geostationary satellite data by means of the Energy and Water Balance Monitoring System (EWBMS). In chapter 3 the simulation of crop growth and the estimation of crop yields through the EARS Crop Growth Model (ECGM) is presented. Chapter 4 addresses the validation of the data generated in this way. Detailed validation results are added in Annex A to C at the end of this report. Chapter 5 reports the generation of a 28 year data base of relative evapotranspiration (RE) and relative yield (RY) from hourly Meteosat data. This chapter also addresses the properties of evapotranspiration data in comparison with precipitation data.

In chapter 6, elements of contract design are studied, starting from the current state of the art, as represented by the multi-phase contract structure developed by IRI at Columbia University. This contract structure is expected to be highly sensitive to the precise start of the growing season. For this reason a method is developed to determine the sowing window and the actual start of the growing season automatically. A spreadsheet approach is developed to perform a burn analysis on the basis of both evapotranspiration and rainfall data. In addition approaches for scaling up, while limiting data processing and administrative costs, are explored. These concern modelling of the triggers on the basis of climatic mean values and a zoning approach to contract design. They are believed to enable the development of a single contract. At the end of this chapter building trust among farmers and stakeholders is addressed. Finally, chapter 7 summarizes the results and draws conclusions.

2 DERIVING CLIMATIC DATA FROM METEOSAT

Climatic data are derived from Meteosat by means of the Energy and Water Balance Monitoring System (EWBMS), a software system that is used to process hourly geostationary meteorological satellite data to daily climatic data fields. A schematic overview is presented in figure 2.1. There are two parallel processing lines, one to derive the rainfall and one to derive the components of the energy balance: radiation and evapotranspiration. In addition there are sub-systems that use the previous data to generate dedicated products for specific applications, such as river flow forecasts, drought maps, and crop yield forecasts. In the following sections of this chapter the methodology that is used to derive these data is briefly described.

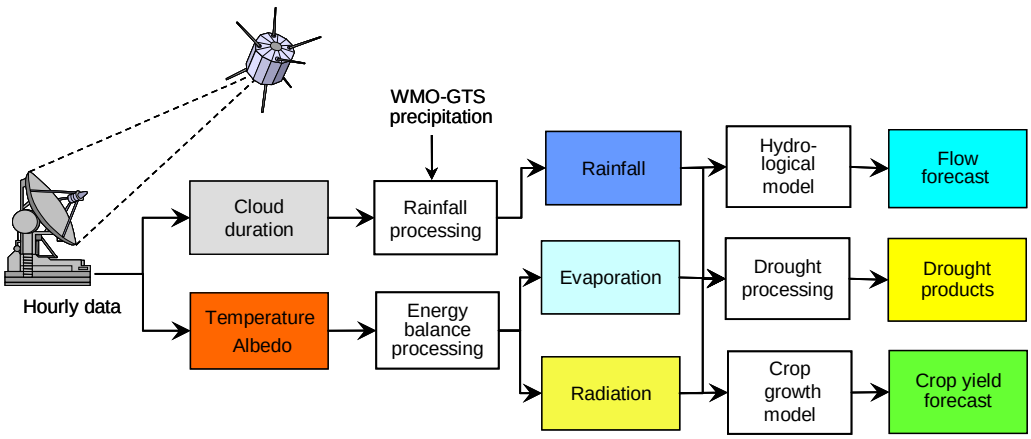

Figure 2.1: Overview of the Energy and Water Balance Monitoring System

2.1 Rainfall Monitoring

A statistical technique has been developed which is based on the duration of cloud presence. Clouds are first identified and classified in certain height classes on the basis of their cloud top temperature, as measured every hour in the satellite thermal infrared images. The presence of clouds at the different cloud levels is then counted during a period of 1 day or 10 days. This leads to cloud duration numbers (CD). Also the temperature threshold excess (TTE) is determined, this is the difference in temperature between thunderstorm cloud tops and the underlying temperature threshold, and is an indicator of rainstorm vigour. To relate these quantitative rainfall indicators to rainfall as measured in the ground, use is made of rain gauge data that are available in near real time from the World Meteorological Organisation (WMO) through their Global Telecommunications System (GTS). Subsequently local regression equations are derived between the satellite data and the WMO-GTS rain gauge data, i.e. one regression equation for each rain gauge station:

$$R_{j,est} = a_{j,0} + \Sigma\, a_{j,n}.CD_n + b_j.TTE \qquad (1)$$

Here $R_{j,est}$ is the rainfall estimate, CD_n is the cloud duration at cloud level n and TTE is the temperature threshold excess at the corresponding location. This regression equation is established for each rainfall station using the rainfall and the satellite derived cloud data at this station and the nearest 11 surrounding stations. The regression equation, however, is an imperfect estimator of rainfall. Therefore at each station the residual D_j between the estimated and the observed rainfall is also determined

$$D_j = R_{j,obs} - R_{j,est} \qquad (2)$$

Subsequently the coefficients $a_{j,n}$, b_j and the residual D_j are interpolated between the GTS rainfall stations using a weighted inverse distance technique so as to obtain the corresponding values for each pixel (i). The rainfall field is finally calculated pixel by pixel and using the interpolated coefficients and residual:

$$R_i = a_{i,0} + \Sigma\, a_{i,n}.CD_n + b_i.TTE + D_i \qquad (3)$$

2.2 Evapotranspiration Monitoring

While rainfall monitoring is a statistical technique, based on cloud top temperatures, evapotranspiration monitoring is largely deterministic and based on the energy balance and the physics of energy and mass exchange at the earth surface. The calculation of actual evapotranspiration data is carried out in several steps: calibration, atmospheric correction, air temperature mapping, and calculation of the net radiation, calculation of the sensible heat flux and determination of the actual evapotranspiration. The various steps are briefly discussed in the following sections.

2.2.1 Calibration

Calibration is the conversion of satellite digital numbers to meaningful physical values. For the thermal infrared band calibration coefficients are send with the data that allow their conversion into “planetary” temperatures. For the visual satellite band the digital number is converted in the ‘planetary’ albedo (reflectivity). Here usually a vicarious calibration is used based on the known albedo’s of certain references, in particular Cumulonimbus clouds, which have a reflectivity of 92%. Hereafter the planetary albedo and planetary temperature have to be converted to the corresponding surface albedo and surface temperature. This is done by means of atmospheric correction algorithms

2.2.2 Atmospheric Correction

The atmospheric correction procedures are also based on reference information inside the image and can therefore be performed automatically. Data are processed in batches of 10 days (dekad).

In the visual band a 'cloud-free' planetary albedo map is extracted by preparing 10-daily minimum value composites. Hereafter the planetary albedo's of each pixel are converted to surface albedo's using a two-flux atmospheric transmission model based on Kondratyev (1969). In this model the planetary albedo is a function of the surface albedo and the atmospheric optical depth. The influence of the optical depth is strong for low surface albedo. The lowest surface albedo is about 0.07 (forest). The procedure searches in the image for the lowest planetary albedo. From this pair of values the atmospheric optical depth may be calculated. Having this value each observed planetary albedo is subsequently converted to the corresponding surface albedo. The atmospheric optical depth is also used in calculating the amount of solar radiation reaching the surface.

In the thermal infrared band a different method of atmospheric correction is used. The relation between the planetary temperature (T_0') and the surface temperature (T_0) is described as:

$$(T_0-T_a) = [k/\cos(i_o)](T_0'-T_a) \quad (4)$$

where k is the correction coefficient and i_o the observation zenith angle. The highest planetary temperature is extracted from the thermal image data. This value is assumed to correspond with the condition of no evapotranspiration. For this special case the actual surface temperature may be calculated from the daily net radiation. With this pair of planetary and actual surface temperature the correction coefficient (k) is determined. Subsequently all planetary temperatures may be converted to actual surface temperatures.

2.2.3 Air temperature mapping

A novel technique has been developed to estimate and map the air temperature at the top of the boundary layer (T_a) from satellite data. The method is based on the relation between noon surface temperatures ($T_{0,n}$) and midnight surface temperatures ($T_{0,m}$), which may be written as.

$$T_{0,n} = a \,.T_{0,m} + b \quad (5)$$

The coefficients a and b of this relation depend on the solar zenith angle. They may be derived on the basis of regression between observed noon and midnight temperatures. A more stable approach is to derive them by means of a physical-mathematic model of the daily temperature cycle under solar radiation. Now, in addition we note that in the (theoretical) case of perfect heat transfer between the surface and the atmosphere we would have

$$T_{0,n} = T_{0,m} = T_a \quad (6)$$

Consequently the air temperature then follows from

$$T_a = b/(1-a) \quad (7)$$

2.2.4 Observation height air temperature

The observation height air temperature (oha-temperature) is the air temperature at standard observation height, usually 2 meter (T_{2m}). This temperature is not needed for generating the actual evapotranspiration, since the latter depends on the difference between surface and boundary layer air temperature (bla-temperature). Nevertheless the oha-temperature may be useful, as from tradition various relations are based on this measured temperature. This temperature also offers an approach to validation, whereas oha-temperatures may be obtained 3 hourly through the WMO-GTS network.

The oha-temperature results from the turbulent mixing of air parcels rising from the surface and descending from the top of the boundary layer. So one can expect the oha-temperature to be a weighed mean of the surface temperature and the bla-temperature:

$$T_{2m}=a.T_a + (1-a).T_0. \quad (8)$$

In practice the relation is determined empirically by regression with observed temperatures and then reads:

$$T_{2m} = a.T_a + b.T_0 + c \quad (9)$$

2.2.5 Net Radiation

Once the temperature data fields have been derived, the algorithm continues with the calculation of the radiation components. There are both short-wave (solar) and long wave (thermal, terrestrial) radiation components involved. The net radiation (I_n) represents the radiation absorbed at the surface and converted into heat. It may be calculated as

$$I_n = (1\text{-}A)\, I_g - L_n \tag{10}$$

I_g is the daily solar or "global" radiation at the earth surface and A is the surface albedo or reflectivity. The calculation of the global radiation is again based on an extended version of Kondratyevs two-flux model (1969). The long wave radiation term, denoted L_n, consists of two components: (1) the upward long-wave radiation from the surface (L_u) and the downward long wave radiation from the atmosphere (L_d). These long wave radiation fluxes, according to the law of Stephan-Bolzman, depend on respectively the surface and the air temperature. However, also the emission coefficients have to be taken into account. The formulation of the net long wave radiation is

$$L_n = L_u - L_d = \varepsilon_0 \sigma T_0^4 - (1\text{-}\varepsilon_0)\, \varepsilon_a \sigma T_a^4 \tag{11}$$

When a pixel is cloud covered, the light transmission (t) through the clouds is first calculated from the cloud albedo and then the net radiation is estimated with:

$$I_{nc} = (1\text{-}A)\, t\, I_g \qquad (L_n \approx 0) \tag{12}$$

Under clouds the long wave radiation fluxes almost cancel and are therefore neglected.

2.2.6 Sensible Heat Flux

The sensible heat flux into the atmosphere is proportional to the average temperature difference across the atmospheric boundary layer (T_0-T_a). This temperature difference is directly derived from the satellite data. The simple formulation is:

$$H = C.v_a.(T_0\text{-}T_a) \tag{13}$$

The daily average surface temperature T_0 is obtained as the average of the noon and midnight values of the surface temperature. C is the turbulent heat transfer coefficient, which depends on the aerodynamic roughness of the area and the height of vegetation. A theoretical model after Businger (1965) has been used to establish its value range.

2.2.7 Actual Evapotranspiration

Having determined the net radiation I_n (section 2.2.5) and the sensible heat flux H (section 2.2.6) the latent heat flux LE, i.e. the actual evapotranspiration in energy units, is obtained from the energy balance

$$LE = I_n - H - P \tag{14}$$

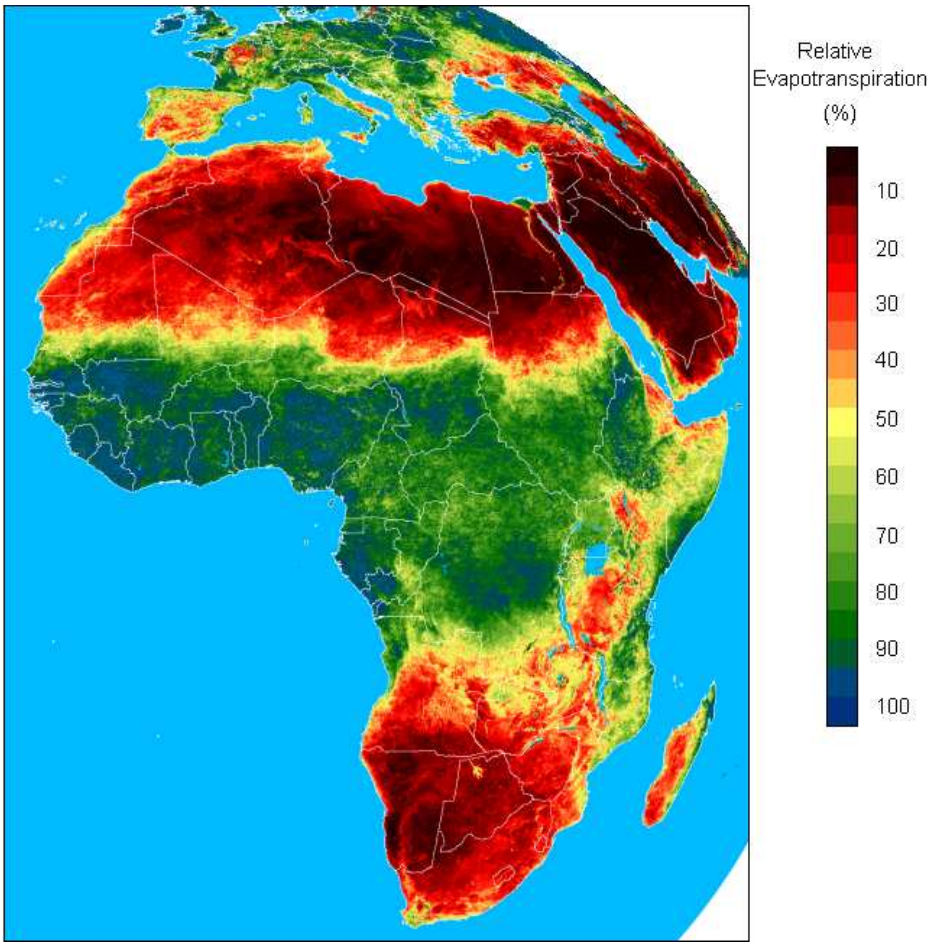

Figure 2.2: The relative evapotranspiration across Europe and Africa as derived from Meteosat for the first 10 days of September 2005

P is the radiation used for photosynthetic electron transport, approximately 10% of the daily solar radiation in case of full vegetation cover. The daily soil heat flux is very small and therefore neglected.

In case of cloud cover the net radiation at the surface is estimated from the cloud albedo. The actual evapotranspiration then follows from the assumption that energy partitioning, i.e. the Bowen ration, is the same as on the previous cloud free day.

2.2.8 Relative evapotranspiration

The actual evapotranspiration, as derived in the previous section, depends on soil water availability to the plants, and on the net radiation. In practice it is useful to have a pure soil water availability measure to characterize agricultural drought. This is achieved as follows. First the potential evapotranspiration is calculated using a Priestly-Taylor approach, derived by simplifying the Penman equation

$$LE_P = c.\ I_n \qquad (15)$$

Where $c \approx 0.8$. Next the relative evapotranspiration (RE) is defined as

$$RE = LE / LE_p \qquad (16)$$

The resulting relative evapotranspiration is fairly independent of the net radiation and, as we will see in the next chapter, a good measure of plant growth reduction due to water limitation or drought.

As shown in figure 2.3, RE is also quite well related to measured plant available water content, which is the traditional indicator of agricultural drought. It is however not the same. From the theoretical point of view RE is a better measure of agricultural drought as it is directly related to crop growth. Uptake of water by plant roots is governed by soil water tension, rather than soil water content. The relation between the last two, depends also on soil type.

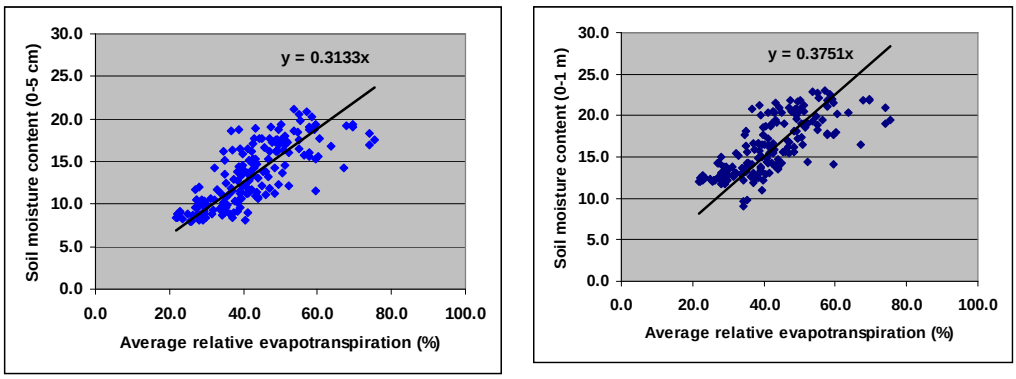

Figure 2.3: Empirical relation between satellite derived 2-monthly RE and plant available soil moisture content in the top 5 cm (left) and top 1 m of soil (right). (Soil moisture data: courtesy University of Salamaca, Spain)

3 CROP YIELD ESTIMATION AND FORECASTING

Crop yields are derived from the EWBMS radiation and evapotranspiration outputs by means of a crop growth model. The EARS Crop Growth model (ECGM) simulates biomass production during the growing season. The ECGM is a relatively simple model. Detailed models, like WOFOST (*Supit, 1994*), estimate the partitioning of dry matter among various plant organs during different crop growth stages. The ECGM considers the whole plant as a single storage organ. The economic yield of the crop is supposed to be proportional to the dry matter produced. For input the model uses the global solar radiation and the relative evapotranspiration generated from Meteosat with the EWBMS. The simulation of the biomass development is performed daily and involves the calculation of: (1) photosynthetic active radiation or PAR, (2) photosynthetic light use efficiency, (3) light interception/surface vegetation cover, (4) gross photosynthesis, (5) maintenance respiration, (6) biomass production. Figure 3.1 presents a schematic representation.

The ECGM calculates the daily increase of biomass with:

$$B_t = B_{t-1} + \Delta B \qquad (17)$$

where B_t : Biomass at simulation day t [kg/m^2]
$B_{(t-1)}$: Biomass at simulation day t-1 [kg/m^2]
ΔB : Daily biomass increase [$kg/m^2.day$]

The daily biomass increase is obtained as the difference between the photosynthesis (P) and the maintenance respiration (R).

$$\Delta B = P - R \qquad (18)$$

where P : Photosynthesis rate [$kg/m^2 day$]
R : Maintenance respiration rate [$kg/m^2.day$]

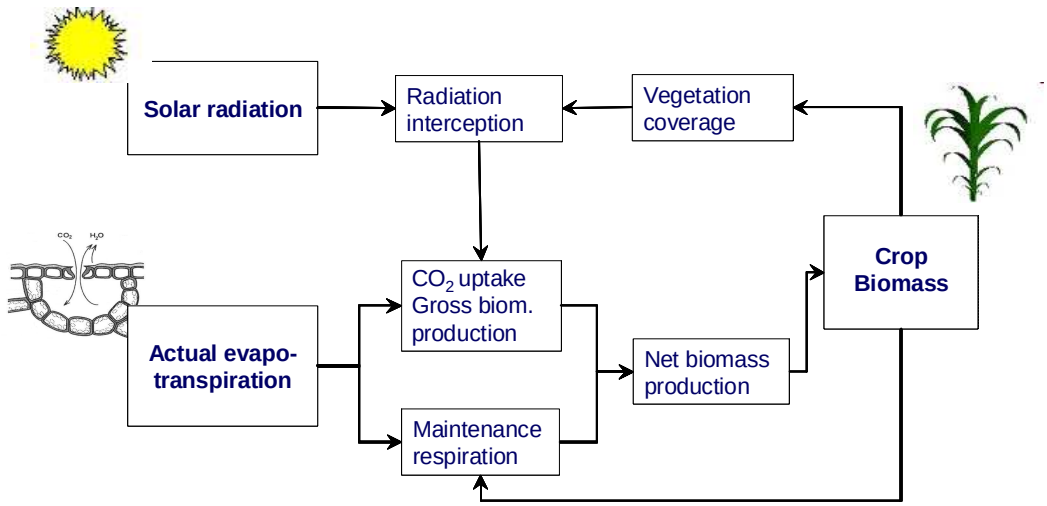

Figure 3.1: Schematic representation of the EARS Crop Growth Model (ECGM)

3.1 Conversion of solar energy into dry matter

The ECGM makes use of a principle put forward by Monteith (1977), who demonstrated that the dry matter production has an almost unique relation with the total radiation intercepted by the foliage, independent of crop type. 1 Joule is roughly equivalent to $14E^{-10}$ kg dry matter. This equivalency implies that the daily dry matter production may be expressed in terms of the daily average global radiation (I_{gd}) with

$$\Delta B = a.C.I_g \qquad (19)$$

where ΔB : biomass production [$kg/m^2.day$]
C : fraction of soil covered by the vegetation biomass
Ig : daily global radiation [J/m2s]
a : conversion constant ($\approx 1.2E^{-4}$)

Monteith's results were obtained for crops in England, so in a relatively small geographical area and most likely in the absence of drought stress. It is known, however, that with the increase of light level, the efficiency of light use for photosynthesis decreases. It is also known that water shortage will lead to stomata closure and by consequence limitation of photosynthesis. Therefore to generalize this approach, we have to include these elements

3.2 Water limitation to growth

CO_2 uptake and consequently dry matter production will be reduced due to stomata closure as a result of limited water availability to the plant. Since water vapour and CO_2 largely share the same diffusion path, there is strong relation between evapotranspiration and CO_2 assimilation (*Slabbers et al. 1979*). A practical approach has been developed by *Stewart (1977)* and was verified on the basis of experimental data from all over the world by *Doorenbos and Kassam (1979)* and is hence referred to as the "*SDK relation*":

$$(1-RY) = k\ (1-RE) \qquad (20)$$

where RY : relative yield ($=Y/Y_p$)
RE : relative evapotranspiration ($=LE/LE_p$)
k : yield response factor [-]

The yield response factor is crop specific and indicates the drought sensitivity of a crop. For example the value for maize is 1.25, for winter wheat 1.0 and for sorghum 0.9. Values higher than 1 indicate a drought sensitive, lower than 1 a drought resistant crop.

3.3 Light use efficiency

Plants only use part of the absorbed radiation for photosynthesis. Only 50% of the absorbed solar radiation is photosynthetic active radiation (PAR). As a result of the absorption of radiation by the plant, electrons are excited. But not all excited electrons drive photosynthesis. A considerable and variable part of the excitation energy is dissipated into heat. At very low light levels only 20% is dissipated, but this amount will increase with increase of light level, and may reach 80 or 90% during the

middle of the day. The light use efficiency as a function of light level has been investigated by *Rosema et al. (1998)*. It was shown that the instantaneous photosynthetic light use efficiency ϕ could be described with:

$$\phi = 1 / (1.25 + 2.r_e.I_g) \quad (21)$$

where ϕ : photosynthetic efficiency of light
r_e : effective electron transport resistance
I_g : global radiation (W/m^2)

The electron transport resistance (r_e) is a plant specific constant, which indirectly represents its ability to assimilate CO_2 with open stomata. Using a model describing the daily course of solar radiation and related photosynthetic light use, we have investigated the application of the previous relation on a daily average basis, with the following result.

$$\phi_d = (d/12)^{0.5} / (1.25 + 4.r_e.I_{gd}) \quad (22)$$

where: ϕ_d : mean daily photosynthetic light use efficiency
r_e : effective electron transport resistance
I_{gd} : Daily average global radiation [W/m^2]
d : daylight duration [hr]

This equation can be applied during the whole year and for regions located between the equator and 60 degrees latitude.

3.4 Dry matter production

Based on the aforementioned elements equation (19) is now generalized by replacing the conversion constant *a* by $b.R_g.\phi_d$:

$$P = b \cdot C \cdot R_g \cdot \phi_d \cdot I_{gd} \quad (23)$$

Since $a = b.R_g.\phi_d \approx 1.2E^{-4}$, and in England we would mostly expect $R_g \approx 1$ and $\phi_d \approx 0.2$ we find for the new conversion factor: $b \approx 6E^{-4}$

3.5 Respiration loss

From the daily dry matter production we have to subtract the amount of carbohydrates used for respiration. There are two different types of respiration: growth respiration and maintenance respiration. Growth respiration is the energy needed to build plant dry matter from the primary assimilation products. This amount is usually 20-30% of the dry matter production P. This term is already included in the conversion constant b. Maintenance respiration is the amount of energy needed for maintenance of the total biomass present. This term is proportional to the total biomass. The maintenance respiration increases with the temperature. It is usually expressed as:

$$R = c \cdot B_t \cdot Q_{10}^{(Ta-Tr)/10} \quad (24)$$

The maintenance coefficient (c) is in principle crop dependent. The magnitude of the relative increase of respiration rate (Q_{10}) is about 2. In the CGM model we have modified this equation, using the relative evapotranspiration instead of the temperature

$$R = c \,.\, B_t \,.\, Q_{10}^{(1\text{-}RE)} \qquad (25)$$

3.6 Net dry matter production

With the appropriate substitutions we obtain the general equation for the daily dry matter production

$$\Delta B = P - R = b \,.\, C \,.\, R_g \,.\, \phi_d \,.\, I_{gd} - c \,.\, B_t \,.\, Q_{10}^{(1\text{-}RE)} \qquad (26)$$

Based on this equation it is now possible to simulate the dry matter production during the growing season. In the Crop Growth model there is the option not to simulate any crop growth if daily average temperatures at observation height (obtained from the Energy Balance Mapping System) are below 5°C. In figure 3.2a-b simulation results are shown for different levels of water availability (relative evapotranspiration) and for different levels of light. Water limitation has a more than proportional effect on the biomass development. Light limitation has a less than proportional effect. Simulations may be done for a number of crops, including maize, wheat, sorghum, cotton, barley, potato and rangeland, for which yield response coefficients have been published (Doorenbos and Kassam 1979).

3.7 Crop calendar

The calculations of crop growth discussed in the previous sections have to be applied from the beginning to the end of the growing season, in accordance with the so-called crop calendar. Crop calendar dates, such as the start of the growing season and the time of harvesting have been published by FAO for all countries. They are used to set the time limits of the growing season. In addition the software uses an RE trigger to start "actual" growth. It is usually assumed that crop growth starts when RE ≥ 0.4.

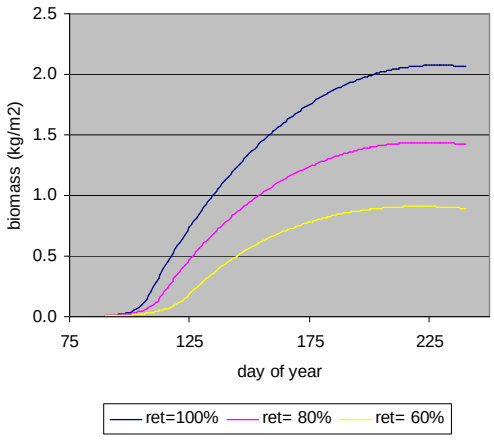

Figure 3.2a: The influence of changes in relative evapotranspiration on the simulated biomass of wheat.

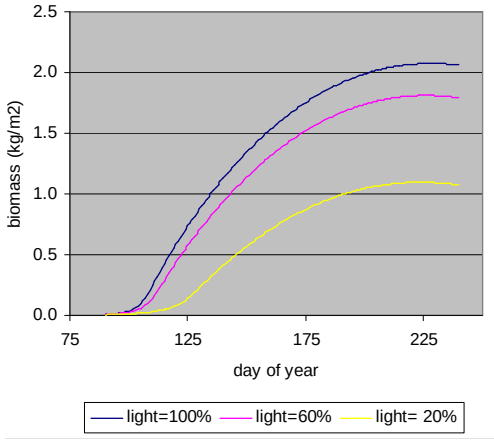

Figure 3.2b: The influence of changes in light level on the simulated biomass of wheat.

3.8 Relative and difference yield

It is very difficult, if not impossible, to make an accurate *absolute* crop yield estimate in kg/ha on the basis of a model alone. The reason is that many other growth factors play a role, for example soil type, seed quality, use of fertilizer and pesticides. All these are not known over large area's. Therefore we follow a relative approach and first generate the relative biomass (RB) from the satellite data as the ratio of the simulated actual biomass (B) and the simulated potential biomass (B_P) in the current year. The latter is obtained with the model by assuming no water limitation (RE=1) during the growing season. The relative economic yield (RY) is then assumed to be equal to the relative biomass (RB):

$$RY=Y/Y_P \approx RB = B/B_P \quad (27)$$

RY and RB are instable during the beginning of the growing season. However, halfway the growing season, after about 70 growing days, RY and RB stabilize and their correlation with end of season yields becomes almost constant, as illustrated in figure 3.3. Therefore the relative yield after 70 growing days can be considered a forecast of the relative yield at harvest. From this relative yield the forecasted absolute yield (Y) could be determined if the potential crop yield (Y_P) is known, which is usually not the case. For this reason the satellite data of the previous five years are also processed to generate the satellite derived relative yields of the previous 5-year and their average $RY_@$ as well. Then the difference yield (DY) is defined as:

$$DY = (RY-RY_@) / RY_@ \quad (28)$$

Since the potential yield is about constant, the previous equation reduces to

$$DY = (Y-Y_@)/Y_@ \quad (29)$$

RY and DY are both data products of the satellite monitoring system. The previous equation is used to forecast the current season crop yield with

$$Y = Y_@ (1+DY) \quad (30)$$

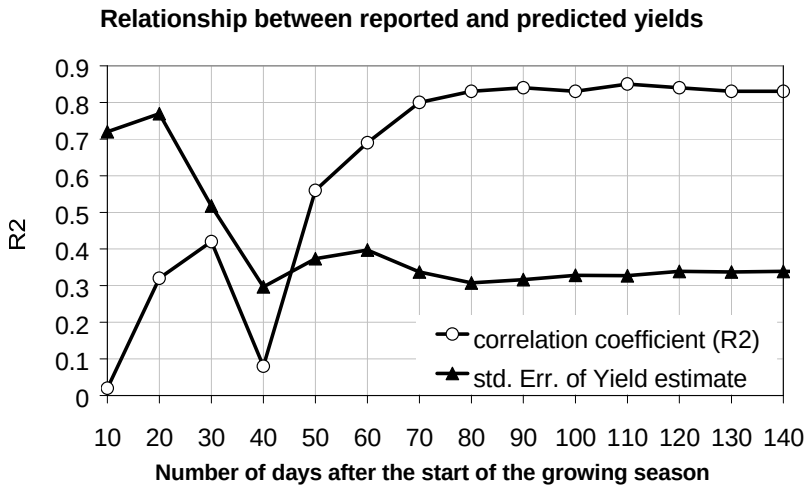

Figure 3.3: Development of correlation between reported and predicted maize crop yield and the standard error of yield estimate. Zimbabwe, 1994/1995 growing season

In this equation Y is the forecasted crop yield, $Y_{@}$ the reported average yield of the same crop in the same area in the previous 5-year, and DY the difference yield derived with the EWBMS-ECGM system from the satellite data.

Figures 3.4 and 3.5 show examples of Sorghum/millet and Maize DY forecasts produced and issued through Reliefweb in 2008. First forecasts where generated at the end of July and then updated every 10 days incorporating the latest satellite data. The examples shown are against the end of the season and include the satellite data from the beginning of the growing season up to and including the first 10 days (dekad) of September.

3.9 Combination with geographic information

Difference yield maps, as presented in figure 3.4 and 3.5, usually give a first general impression of regional drought problems and related crop yield patterns. But for practical use there is often a need for data tables that provide direct quantitative figures for administrative regions such as provinces and districts. The Food and Agricultural Organisation of the United Nations (FAO) has developed a standardized classification of administrative regions in three levels: GAUL 0, 1 and 2 and provides the related digital maps of the boundaries between these regions. We use this classification for generating tables of average RY or DY values for these regions. At GAUL level 2 this amounts to some 1000 regions.

When averaging values within a region, care is taken that the most accurate possible result is obtained. Use is made of a land-use map to exclude all pixels with a non-agricultural land use from the averaging process, and to include only those pixels, which are within the FAO crop growing areas. EARS has developed a dedicated Geographic Information System (GIS) called “ImageShow2” for use with EWBMS and ECGM products, and which is capable of carrying out such tasks in a fast and efficient way. An example of averages by administrative is shown in figure 3.6.

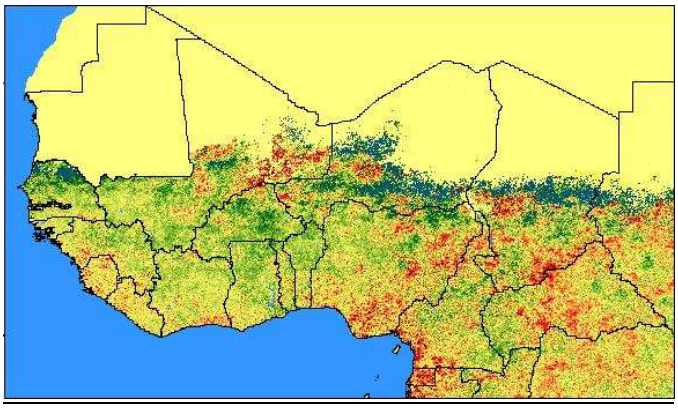

Figure 3.4: Sorghum/millet difference yield (DY) forecast for West Africa, 11 September 2008

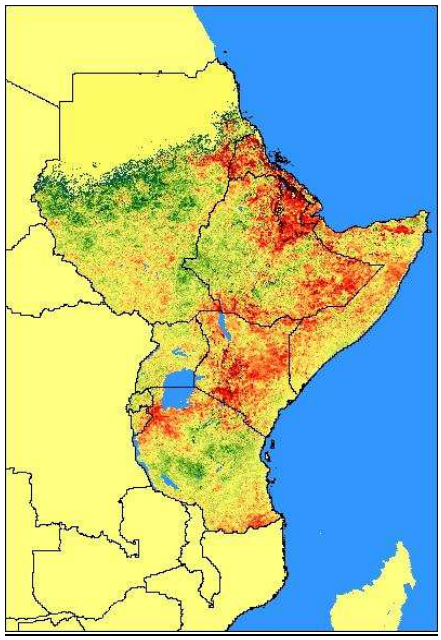

Figure 3.5: Maize difference yield (DY) forecast for East Africa, 11 September 2008

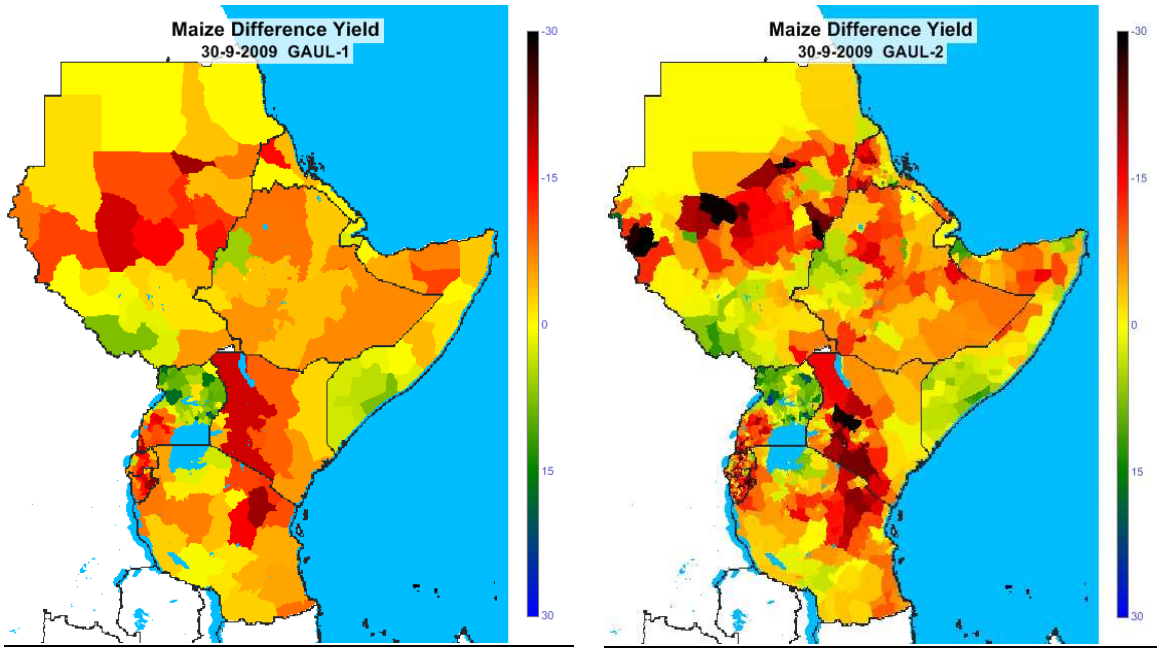

(a) *(b)*

Figure 3.6: Crop yield forecast for East Africa on 30 September 2009, (a) averaged by province and (b) averaged by district according to the GAUL classification

4 VALIDATION OF METEOSAT DERIVED DATA

In the previous chapters we have presented the FESA methodology to derive climatic data and crop yield estimates from the Meteosat geostationary meteorological satellite series. Meteosat derived evapotranspiration data and yield estimates have a high potential to be used for drought micro-insurance. As explained in section 3.2 they are very close to crop growth, more close than precipitation. But Meteosat derived evapotranspiration and yield data are quite new and not widely used yet. This is caused by the fact that actual evapotranspiration data were never routinely available before. EARS is still the sole operational provider of such data. But the key role of evapotranspiration in relation to crop growth is well understood for some 40 years, thanks to the work of *Stewart (1973)*, *Slabbers et al. (1979)*, *Doorenbos and Kassam (1979)* and others. Moreover, rainfall based agricultural drought assessment methods are in fact indirectly estimating actual evapotranspiration. But, since the satellite based approach to evapotranspiration is relatively unknown, we pay due attention in this report to the validation of these new data products.

4.1 Validation approach

Since the start of the EWBMS and ECGM system development, already in the early 1980's, EARS has carried out a range of validation activities in the framework of its projects. This culminated recently in a very detailed validation of the system in the Yellow River basin, where 4 dedicated flux-measuring systems were installed for this purpose. The system implemented at the Yellow River Conservancy Commission in Zhengzhou, now measures the water balance of the upper Yellow River basin (120.000 km^2) within 1%.

Validation is usually carried out at different levels or depth of the system products. Opportunities for validation of the EWBMS-ECGM system performance that all have been exploited are:

- Comparison and calibration of the received visual and thermal infrared channel, in particular vicarious calibration of the visual channel(s) using the known albedo of cumulonimbus cloud, sea, darkest and brightest land pixels.
- Validation of primary data products, such as temperature and albedo. The system generates air temperatures and these can be validated by comparison with measurements at meteorological stations.
- Validation of basic flux data products: (a) precipitation by comparison with rain gauge measurements, (b) radiation by comparison with radiometer measurements, (c) sensible heat flux by comparison with eddy correlation measurements or large aperture scintillometer measurements (LAS) (d) Actual evapotranspiration, being the difference of net radiation and sensible heat flux, through the previous two.
- Validation of the water balance: (a) in arid areas, without run-off, long term evapotranspiration should be more or less equal to precipitation, (b) at river catchment scale long term river discharge should be more or less equal to precipitation minus actual evapotranspiration.
- Validation of crop yields: by comparison of reported yields with yields simulated on the basis of the satellite data.
- Validation through human perception: a qualitative way of validation, where people with relevant field information conclude that the data provided comply with their knowledge and perception of the drought and food production situation.

- "Cross validation", i.e. comparison with other, independently derived satellite products. However this usually leads only to the conclusion that different products are alike or not. If they are not alike is does not tell which is closest to the truth. If they are alike, they will support each other.

4.2 Validation pitfall

When validating satellite data, we have to consider the following pitfall. In remote sensing one often speaks of "groundtruth" when ground data are considered that serve as a reference for the satellite derived data. However, "groundtruth" does not exist. All ground measurements or ground observations have smaller or larger errors.

For example, if we compare satellite derived air temperature with air temperatures measured at meteorological stations, then we compare an average of an area of 10-25 square kilometre with a point measurement made at a meteorological station in that area. These two do not necessarily have the same value. Therefore when we compare many such pairs of measurement and plot them in a XY-diagram, these points will never fit to a straight line. There will always be a lot of scatter. The quality of the relation between the satellite derived and ground measured data is expressed in terms of the correlation coefficient (R) and the standard deviation or root means square difference (RMSD). It should be noted that these are just measures of likeness between the two data sets and do not tell which data set is most accurate.

If we compare satellite and ground measured temperatures for stations in Africa and Europe, we usually find higher correlations and smaller RMSD's in Europe than in Africa, while the satellite measuring instrument remains the same. This outcome does not tell us that the satellite is performing worse over Africa than over Europe, but indicates that the quality of the ground measurements in Africa is less than in Europe. This all should be kept in mind when carrying out validation work. The example given was for the air temperature, but similar considerations apply to other ground data, such as rainfall and reported yields.

Rain gauge measurements are just very small samples from an extended and very variable rainfall field. Thus there are always sampling errors involved. The representativity of individual rain gauges for larger areas is very small and restricted to the spatial scale of a rainfall event. Particularly in relation to convective rainfall in Africa this may be only a few kilometres.

In relation to crop yields there are similar examples indicating that care should be taken when drawing conclusions from the comparison of satellite and ground data sets. When comparing satellite derived yields with ground assessments, we often have to rely on the FAOSTAT database of harvest and crop yield. The quality of the official yield assessments in Africa, however, is variable. Elaborate assessments are often hampered by lack of qualified people, road infrastructure and funding. A problem, often encountered in Africa, is that crop yield is derived by division of crop production and crop area. Usually, however, only harvested area is available and not planted area. In this way crop yields are overestimated, as failing crops may not be harvested. By consequence the area accounted for is to small. Therefore when comparing satellite derived yields with reported yields one always finds considerable scatter, and also here the fit between the data sets is usually better in Europe than in Africa.

4.3 Validation results

The actual validation of the EWBMS data products is presented in annex A to C of this report. Partly, the validation results come from earlier, though recently completed projects. New validation work has been done in the framework of the present FESA project, using ground data from Africa and Europe. To this end we have processed all Meteosat data from 1982 to 2009 to climatic data fields and crop yield estimates. These data were then compared with ground data sets collected from several sources.

In Annex A we compare EWBMS Meteosat derived data fields of temperature, radiation and sensible heat flux with similar point measurements made on the ground at various locations in Africa and Europe. Similar validation results from recent other projects in China, Mongolia and the Netherlands are presented in Annex C. Overall good correlations and small average differences are found. Random differences disappear when working with 10 daily moving averages.

In Annex B we have validated crop yield estimates obtained with the EWBMS-ECGM. Good results are demonstrated for maize yields at the national level in West Africa and Southern Africa and at the provincial level in Burkina Faso and Tanzania.

Given these validation results, it is concluded that the Meteosat derived climatic data are a valid data source for crop micro-insurance.

5 DATA BASE GENERATION AND DATA PROPERTIES

In the first part of this chapter the work done to generate the Meteosat based drought information database, for the period 1984 to date, will be reported. Thereafter the relative evapotranspiration data, being the prime candidate as satellite based drought index, will be studied and compared with rainfall data for 29 stations in Tanzania.

5.1 Extracting a long term data set from Meteosat

Meteosat is in orbit since 1978. There are two generations: Meteosat First Generation (MFG) from 1978 to 2006, and Meteosat Second Generation (MSG) from 2004 to date. EARS has been processing Meteosat data since the early 1980's and is operating a satellite receiving station since 1992. However, storage limitations in the early days and later technical modifications in the processing chain have caused an incomplete historical data set, which was not suitable to satisfy the present need for all Africa drought and crop performance statistics. With kind support of EUMETSAT in Darmstadt and the Royal Netherlands Meteorological Institute (KNMI), it has been possible to compose the following data base of hourly visual (VIS) and thermal infrared (TIR) data:

- MFG: May 1982 – April 2006	from EUMETSAT archive
- MSG: April 2004 – December 2005	from KNMI archive
- MSG: January 2006 – date	EARS reception and archive

In this way we have created an archive of satellite input data with almost 30 year of hourly visual and thermal infrared images, suitable for processing to relative evapotranspiration (RE) and relative yield (RY) data fields.

The visual (VIS) and thermal infrared (TIR) bands on the MFG and MSG satellites are somewhat different. For example, in the visual wavelength range, there are 2 bands on MSG and only 1 on MFG. In the MSG case we combine the 2 separate bands into one, in such a way that the result provides the same information as the single band on MFG. Both are then in the same way converted to the planetary albedo (reflectivity). For the period of overlap in MFG and MSG reception, i.e. between April 2004 and April 2006 we have done extensive inter-calibration between the two generations of satellites so as to generate the same results with both. Another difference between MSG and the preceding MFG is the difference in spatial resolution. MFG had 5 km, while MSG has 3 km spatial resolution.

The climatic data products of each satellite are generated with the EWBMS system for almost the whole hemisphere in the original Meteosat projection, i.e. as observed from space. The ECGM crop growth model, however, runs for separate data subsets, corresponding to the African regions: West, East and Southern Africa. To this end the EWBMS global radiation and relative evapotranspiration products are reprojected and resampled to an equal latitude and equal longitude (lat-long) grid, with a resolution of 0.04^{o}. Resampling is done on the basis of the "nearest neighbour" method. After resampling, the regional subsets are cut out and then processed to crop yields. The resulting relative yield (RY) and difference yield (DY) may finally be combined with land-use and other geographic information (usually also available in lat-long) so as to derive yield figures averaged by administrative regions and excluding non relevant land use classes. The complete Meteosat hourly data set, from 1982 to date, has been processed in this way. RE and RY indices have been generated for each grid cell in the three African regions. The next step is to derive the corresponding statistics that will enable to assess drought probability and yield loss risk.

5.2 Similarity and difference of evapotranspiration and precipitation data

There is fundamental similarity in the precipitation based and the evapotranspiration based approach to agricultural drought insurance. Both are based on direct or less direct estimates of actual and potential evapotranspiration. Though the fundamental background of these approaches is the same, there are considerable differences in the data used: ground measured rainfall versus satellite derived actual evapotranspiration. Rainfall is relatively irregular and only indirectly related to crop growth. There are several factors that disturb a direct relation with plant water uptake: (1) run-off/run-on, (2) deep percolation, (3) intermediate storage in the soil. On the other hand, evapotranspiration is almost identical to crop water use and is therefore a direct measure of crop growth.

In the next sections we study and compare the characteristics of the two types of data. The evapotranspiration data were extracted from the FESA database as 10-day (dekad) averages pertaining to the period 1984-2007. The rainfall data are WMO standard rain gauge data from 29 meteorological stations in Tanzania, made available through MicroEnsure. Figure 5.1 provides an overview of the locations of these rainfall stations, superimposed on a Meteosat derived actual evapotranspiration map. This map pertains to a single dekad and is derived from hourly Meteosat data. What strikes is the abundance of evapotranspiration data points compared to the limited number of rain gauge stations. When considering the spatial variation in these data, it seems questionable whether a single rain gauge can reliably represent an area with a radius of 25 km or 8*8 pixels.

5.3 Comparison of evapotranspiration and precipitation time series

We have extracted from the FESA database the time series of 10-daily evapotranspiration at the location of the rain gauge stations in Tanzania for the period 1994–2008. In figure 5.2 the average of all 29 time series of both: ground measured rainfall and satellite derived evapotranspiration are plotted. The data clearly show an overall division in a “wet” and a “dry” season, while sometimes also a split in the wet season may be observed. It strikes that evapotranspiration is phase-shifted relative to precipitation. High precipitation precedes high evapotranspiration. This is logical: when the rains start the soil is depleted and evapotranspiration is low. During the period of rainfall the soils are replenished but evapotranspiration first remains low because there are many clouds and radiation is not providing sufficient energy. Only after the rainfall is decreasing again, also cloudiness decreases and there is more and more solar radiation to evaporate the water. Thereafter, during the dry season, evaporation is gradually decreasing as a result of soil water depletion.

Crop growth depends on (i) radiation, which provides the energy for the photosynthesis reaction, and (ii) CO_2 uptake, which is only possible if the plant has open stomata and is evaporating fully. In fact the relative evapotranspiration is known to be proportional to crop production (*Doorenbos and Kassam 1979*). Therefore, considering figure 5.2, crop production is proportional and in phase with relative evapotranspiration (red graph) and not with rainfall (blue graph). Consequently precipitation is preceding crop growth. Rain water is stored in and buffered by the soil. In this respect it is not well understood why in current rainfall based insurance schemes only precipitation is considered that occurs during the crop growing period, while rain that falls before that period is also relevant.

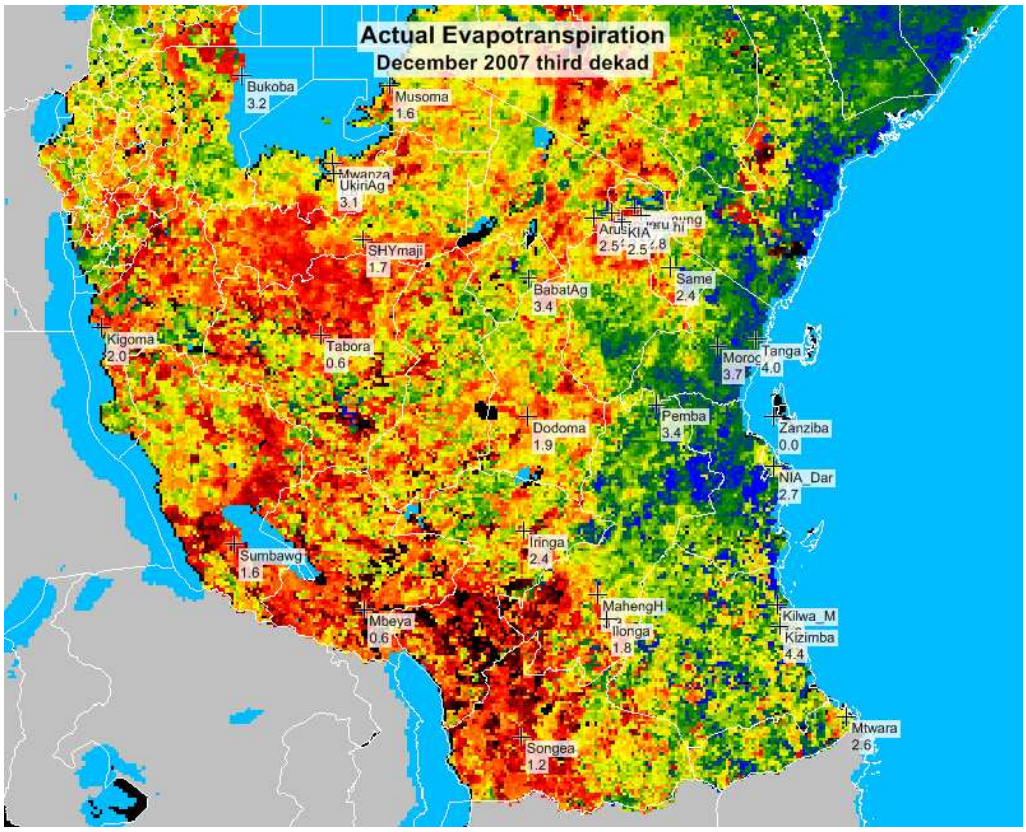

Figure 5.1: Dekadal evapotranspiration map indicating the locations of 29 meteorological stations in Tanzania. Values vary between 0 (black) and 5 mm/day (blue)

Besides lack of simultaneity, there are other interfering circumstances which disturb the relation between rainfall and crop growth. In hilly or mountainous areas rain may run down the slope. In the plains there may be considerable run-on from mountain slopes, both at the surface and sub-surface. Also shallow groundwater tables may disturb the relation between precipitation and crop production. Evapotranspiration, on the contrary, has a direct, simultaneous and proportional relation to crop growth. This means that considerable improvement in pay-out accuracy may be possible, when basing drought insurance on actual evapotranspiration data.

5.4 Mass balance of evapotranspiration and precipitation

In this section we want to verify the water mass balance, i.e. the balance of total rainfall and total evapotranspiration at the 29 rainfall stations. It is noted, however that rainfall and evapotranspiration do not necessarily have to be equal at each station. The reason is that water may be transported laterally, both at the surface and in deeper layers, and in some cases groundwater may be in reach of the plant roots. Nevertheless, taking the 29 stations together, we would expect an approximate mass balance. To evaluate this balance, the long term average of evapotranspiration and precipitation at the 29 stations has been plotted in figure 5.3. The regression line is almost 1:1, indicating that the overall water volumes correspond very well.

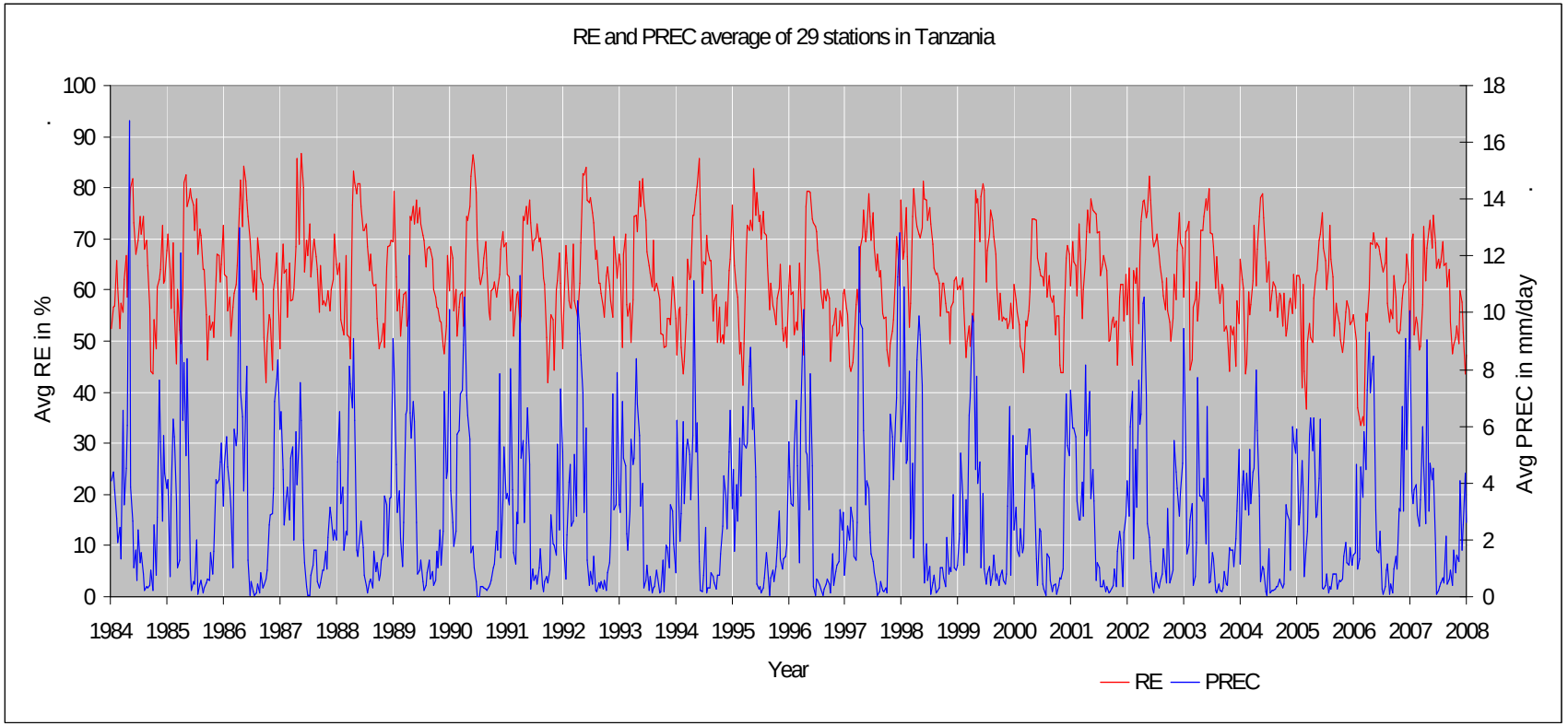

Figure 5.2: 10-Daily ground measured rainfall and Meteosat derived relative evapotranspiration for the period 1984-2000. The data are the averaged records of 29 meteorological station locations in Tanzania. The data show a phase shift of evapotranspiration relative to the rainfall.

5.5 Phase shift between evapotranspiration and precipitation

Earlier in this chapter, it was shown that rainfall is preceding evapotranspiration and crop growth. This is also observed in the time series presented in figure 5.2. So, between the two data sources a phase shift may be expected. We have invested this phase shift by cross correlating the evapotranspiration and the rainfall data, allowing a variable phase shift between the two. The result is shown in figure 5.4. The highest correlation between the evapotranspiration and rainfall data is found if we allow for a phase shift of 4-6 dekad, the rainfall being ahead of evapotranspiration. This suggests that in designing insurance contracts on the basis of evapotranspiration, the phasing may have to be somewhat different from a precipitation based contract.

5.6 Distribution of dekadal evapotranspiration and precipitation data

Figure 5.5 and 5.6 present the distributions of the dekad relative evapotranspiration and precipitation data, respectively, as derived from Meteosat and as measured at the meteorological stations. The difference between the two distributions is remarkable. While the rainfall distribution is very skew, the evapotranspiration distribution is almost normal. This illustrates that the erratic rainfall inputs are buffered by the soil and later used by the plants in a much more gradual way. The overall data set may be characterized by the distribution parameters that are presented in table 5.1.

5.7 Determination of percentile trigger values

In drought insurance the trigger serves to tune pay-out to a desired frequency. The trigger is usually set at a certain percentile of the data series pertaining to each area. The higher the percentile, the higher the number of pay-outs. The use of percentiles also guarantees a more or less equal number of pay-outs in different climatic zones, which prevents adverse selection. It is important that a trigger can be determined accurately from the available historic data, in particular from the climatic mean. This is a basic property of the available data set, which is highly relevant for drought micro-insurance. Therefore we will study this relation. If this relation appears not well defined and stable, then there is risk of inappropriate and unexpected pay-outs.

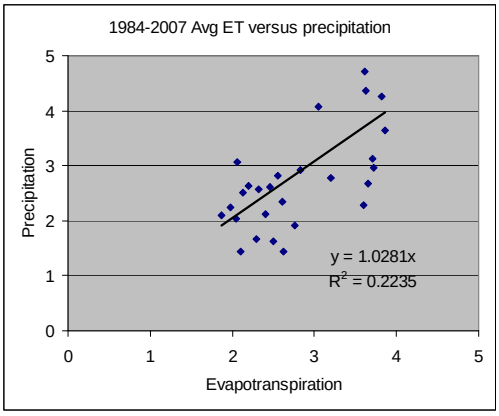

Figure 5.3: Scattergram of daily average rainfall against evapotranspiration, both in mm/day, at 29 stations in Tanzania.

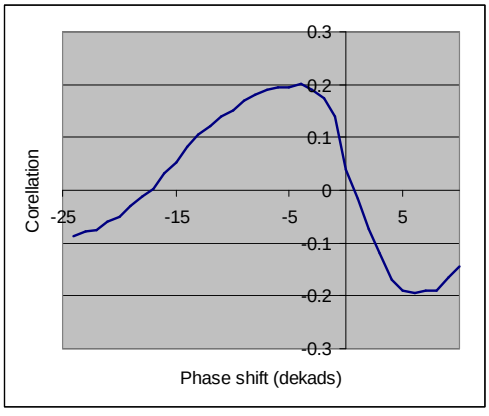

Figure 5.4: Correlation of dekad rainfall and evapotranspiration for variable phase shift. Average shift is 5 dekads

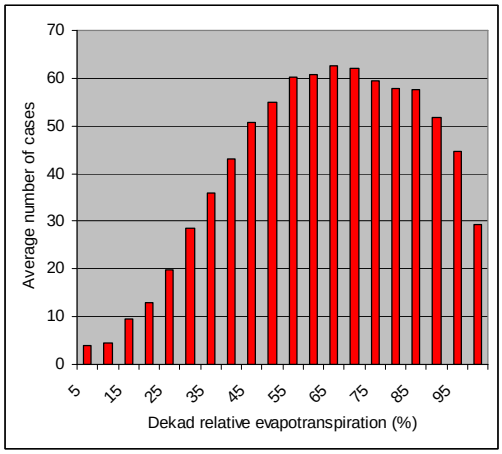

Figure 5.5: 1984-2007 distribution of all dekad relative evapotranspiration at 29 station locations in Tanzania.

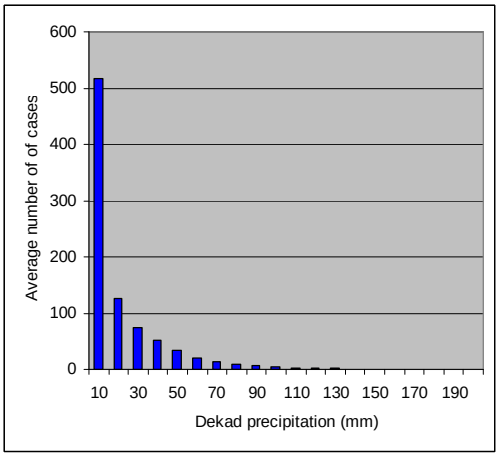

Figure 5.6: 1984-2007 distribution of dekad precipitation data for 29 stations in Tanzania.

Table 5.1: General distribution parameters of dekad rainfall and evapotranspiration at 29 meteorological stations in Tanzania.

	Station average		stand deviation		skewness		kurtuosis	
	Range	avg	range	avg	range	avg	range	avg
Precipitation	14 / 59	30	25 / 81	43	1.5 / 4.0	2.4	2 / 24	8.2
Evapotransp.	44 / 91	62	16 / 25	20	-1.6 / 0.2	-0.4	-0.6 / 4.6	0.4

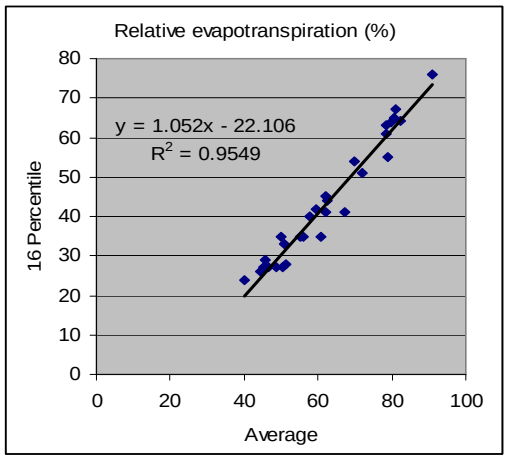

Figure 5.7: Relative evapotranspiration: 16-percentile as a function of 1984-2007 average for 29 locations in Tanzania.

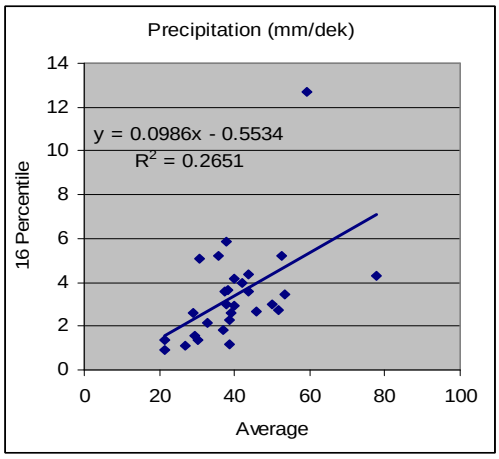

Figure 5.8: Precipitation: 16-percentile as a function of 1984-2007 average precipitation for 29 locations in Tanzania.

In figures 5.7 and 5.8 we have plotted the 16-percentiles of evapotranspiration and precipitation against the corresponding climatic mean values for the period 1984-2007. The coefficient of determination is 0.955 for the relative evapotranspiration and 0.265 for the precipitation data set. This result implies that there is considerably more intrinsic uncertainty in setting the precipitation trigger, than in setting the evapotranspiration trigger. This causes a risk of inappropriate pay-out and unforeseen high pay-out levels when using a rainfall based insurance. This problem is even magnified by the fact that there are usually no co-located data when ground measured precipitation is used to design the drought insurance. This subject is addressed in more detail in section 6.4.3.

6 ELEMENTS OF CONTRACT DESIGN

In this chapter we will discuss some elements of the design of a Meteosat evapotranspiration based drought insurance. Section 6.1 addresses the current state of the art in drought micro-insurance design, which is concluded to be sensitive to the exact start of the growing season. Therefore in section 6.2 and 6.3 the automatic timing of the growing season and sowing window is developed. Section 6.4 discusses the set-up of a multiphase burn analysis and discusses the evapotranspiration and precipitation based pay-outs in dependence of trigger settings and growing season structure. In section 6.5 steps are set to scaling up by means of introducing trigger modelling and a contract zoning approach. Section 6.6 finally addresses the subject of building trust among stakeholders. Section 6.7 summarizes this chapter's findings.

6.1 Current state of the art

We consider the current state of the art to be best represented by the multi-phase contract structure developed by *D. Osgood et al*. (2007) as described in the report: "*Designing Weather Insurance Contracts for Farmers in Malawi, Tanzania and Kenya*". This report was prepared for the Commodity Risk Management Group of the World Bank by the International Research Institute for Climate and Society (IRI) at Columbia University.

The design process followed by IRI is also guided by the Stewart, Doorenbos & Kassam or "SDK relation"

$$RY = 1 - k\,(1-RE) \qquad (31)$$

In the IRI approach, however, the relative evapotranspiration is called the Water Requirements Satisfaction Index (WRSI) and is estimated from precipitation data using a soil water budget model. The soil is viewed as a bucket that is filled by rainfall and depleted by evapotranspiration. The actual evapotranspiration is assumed to be proportional with the degree of filling of the bucket. For proper WRSI calculations it is necessary to have additional information on surface run-off and infiltration, soil type, soil depth, and deep percolation. The growing season of a crop is approximately 4 months. Crops have different growth phases with different sensitivity to drought.

In the earlier mentioned FAO document *Yield Response to Water* (*Doorenbos and Kassam 1979),* five growth phases are discerned: (1) Establishment, (2) Vegetative, (3) Flowering, (4) Yield formation and (5) Ripening. The FAO report documents the different drought response factors (k in equation 31) pertaining to each phase for a range of crops. Examples for groundnut, maize and sorghum are presented in table 6.1. It is noted from these figures, that the crop is most sensitive to drought (high k-value) in the flowering period, followed by the grain filling period. In the establishment, vegetative and ripening period the sensitivity is fairly low.

Given these growth phases and considering the fact that crops may fail because of drought during a relatively short period, IRI has developed a multi-phase contract structure. The development of these contracts is the result of a careful and complex process of studying weather and yield data, as well as by consultation of experts and farmers.

Table 6.1: Growth phases, their length and yield response factors to drought (k)

	Groundnut		*Maize*		*Sorghum*	
	days	k	days	k	days	k
Establishment	10-20	0.2	15-25	0.4	15-20	0.2
Vegetative	25-35	0.2	25-40	0.4	20-30	0.2
Flowering	30-40	0.8	15-20	1.5	15-20	0.55
Yield formation	30-35	0.6	35-45	0.5	35-40	0.45
Ripening	10-20	0.2	10-15	0.2	10-15	0.2
Total period	115-140	1.1	100-145	1.25	95-125	0.9

Table 6.2: Parameters of IRI drought insurance contracts. W=sowing window (dekad nr), R=sowing requirement (mm), L=length of phase (dekads), T = trigger (mm), E=exit (mm).

MAIZE	Sowing		Phase 1			Phase 2			Phase 3		
	W	R	L	T	E	L	T	E	L	T	E
Malawi											
Kasungu	11-17	25	5	50	30	3	80	30	4	30	20
Chitedze	11-17	25	5	40	30	3	125	30	4	25	20
Lilongwe	11-17	25	5	40	30	3	130	30	4	25	20
Nkhotakota	11-17	25	4	150	30	3	140	30	4	50	20
Mchinji	11-17	25	5	100	30	3	110	30	4	140	20
Tanzania											
Babati	16-20	25	4	80	0	5	120	10	-	-	-
Mbulu	15-19	30	5	30	0	7	170	10	-	-	-
Kenya											
Eldoret	10-12	80	4	300	0	6	500	0	6	900	0
Kitale	8-12	80	4	600	0	6	1200	0	6	1500	0
Nakuru	10-12	80	3	300	0	3	375	0	6	750	0
GROUNDNUT	Sowing		Phase 1			Phase 2			Phase 3		
	W	R	L	T	E	L	T	E	L	T	E
Malawi											
Kasungu	11-17	25	3	40	30	3	40	30	8	190	20
Chitedze	11-17	25	3	35	30	3	35	30	8	220	20
Lilongwe	11-17	25	3	40	30	3	40	30	8	230	20
Nkhotakota	11-17	25	3	120	30	3	120	30	8	240	20
Mchinji	11-17	25	3	100	30	3	70	30	8	170	20

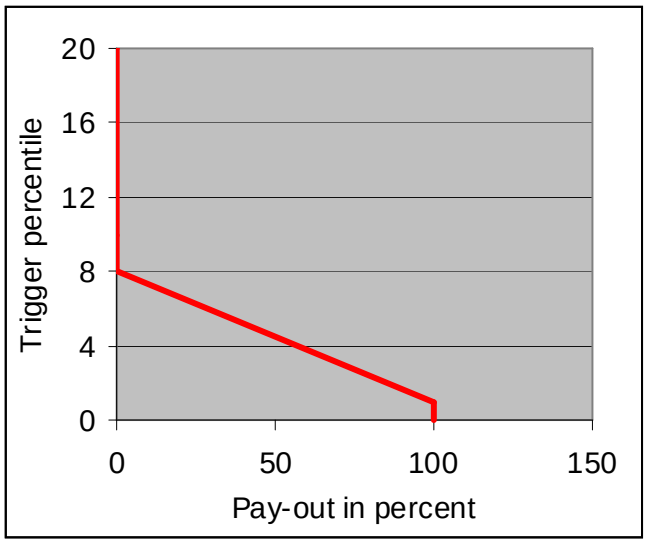

Figure 6.1: Insurance pay-out function for the case of an 8-percentile trigger and a 1-percentile exit.

The contracts developed by IRI for Malawi, Tanzania and Kenya, take a fairly straight forward approach based on measured rainfall. Only the most important three phases are discerned: (1) vegetative, (2) flowering and (3) yield formation. Each phase is assigned a length in dekads, as well as a trigger and an exit, expressed in mm precipitation. Below the trigger partial pay-out starts. When the exit is reached pay-out is full and the contract is terminated. The pay-outs of different phases are added up to a maximum of 100% of the insured sum.

The start of the growing season is determined by a sowing window. Within the sowing window a sowing requirement applies (in mm/dekad). If this requirement is met, the growing season is assumed to start and the crop is supposed to go through the 3 growth phases of predefined length. At the end of each phase a pay-out is possible, depending on the total rainfall measured. Figure 6.1 presents an example of the pay-out function, which is also used in the present study. Table 6.2 summarizes the parameters of the contracts developed by IRI for Malawi and Tanzania.

6.1.1 Starting the growing season

The current IRI contract structure and our ECGM crop growth model use a similar way of starting the growing season. For crop growth to start the ECGM requires the dekad relative evapotranspiration to be at least 40%. At a potential evapotranspiration of about 5 mm/day, this would correspond to 20 mm evapotranspiration per dekad. This is not very different 25 mm/dekad precipitation sowing requirement used by IRI, also considering that part of the rain may be lost by run-off.

6.1.2 Contract parameters vary considerably

When considering table 6.2 it strikes that, for the same crop, the contract parameters may differ considerably. Possibly the relation between measured precipitation and reported or recollected crop damage is variable and leads to different trigger settings. A more physical explanation would be that hydrological situation is different from place to place and leads to a different fractions of the precipitation being available to the crop and consequently to differences in how much rain is required for the crop to grow successfully. The variation in contract parameters, particularly phase length and trigger, suggest that these contracts need careful tuning for each location. This requirement may be a barrier to scaling up drought insurance, while keeping the contracts transparent and the costs low. When using evapotranspiration, this problem should not exist.

6.1.3 Critical dependence on growing season start

The IRI contract structure is an effort to more closely represent the phenology of crop development and to address the effects of drought in the different stages of crop development as experienced by the farmers. At the same time this contract structure exposes some new limitations, which are not so clear in single phase, i.e. total growing season contracts. In the case of maize, for example, a standard phasing of the growing season could be: vegetative: 5 dekads, flowering: 3 dekads, and yield formation: 5 dekads. Since during flowering the crop is most drought sensitive and since the flowering phase is relatively short, the outcome of the contract becomes critically dependent on the accurate timing of the growing season start.

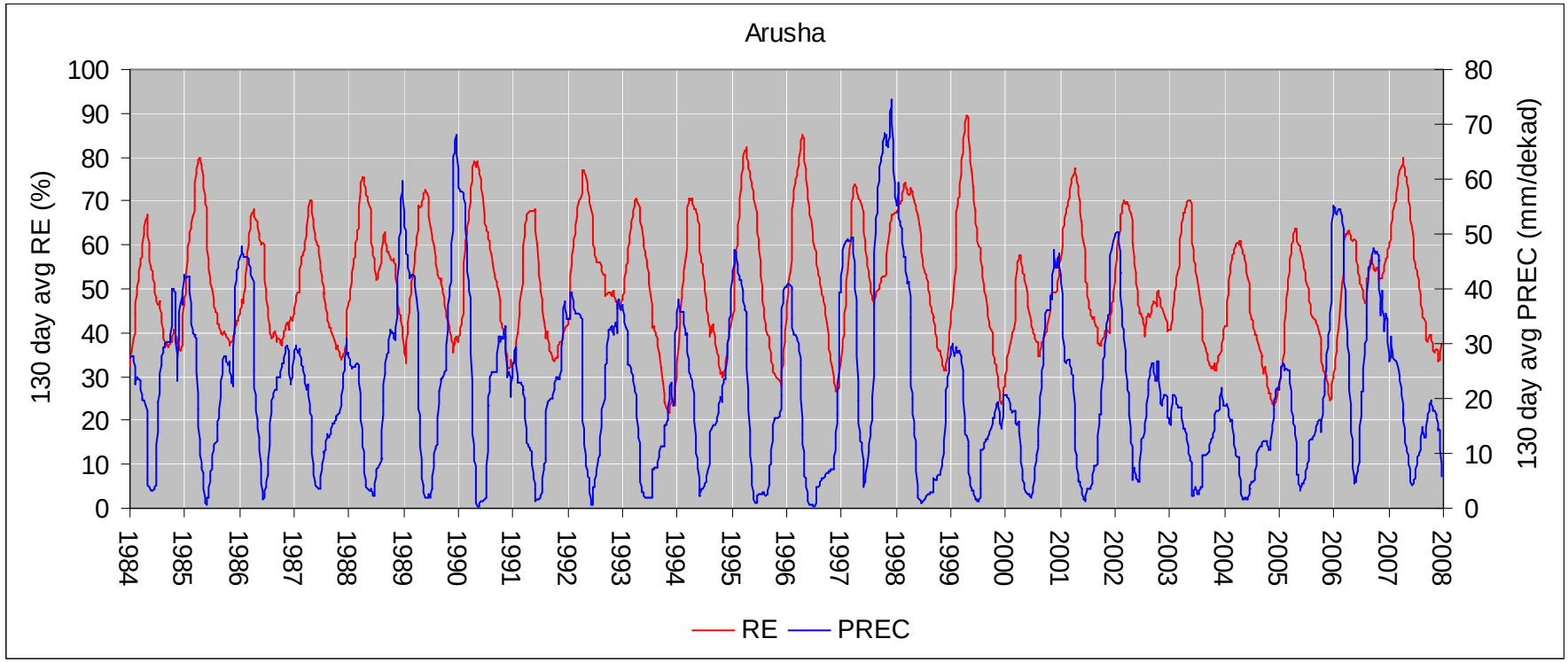

Figure 6.2: Evolution of the 130 day forward floating average of relative evapotranspiration (RE) and precipitation (PREC) in Arusha, NE Tanzania. The maxima in these curves mark the start of the growing season. Good growing seasons are characterised by high maxima. Note that 1998 had high rainfall. In 1999 precipitation falls dramatically but soil water stock is high and provides for another good growing season. In 2000 precipitation is low again, but this time soil water stock is depleted and evapotranspiration falls dramatically, leading to the worst growing season in the whole 1984-2007 period. 2001 and 2002 bring a short revival of precipitation, but in the 3 following years, precipitations falls again and soil water stocks are depleted leading to agricultural drought and bad production in the period 2004-2006.

Our analysis indicates that the standard crop calendars used by FAO and USDA are not accurate in this respect and that the actual start of the growing season may vary quite widely from year to year and from place to place. Since it is our objective to develop a drought insurance that can be scaled up easily, we will explore a more general approach. Therefore in the next section we will address the subject of location-specific growing season timing and triggering on the basis of the Meteosat derived climatic data set.

6.2 Using historic data series for timing the growing season

In the IRI multi-phase contract structure, a sowing window is defined during which the sowing conditions are monitored and a sowing trigger is applied to start the growing season. Accurate timing of the growing season becomes critically important in a multi-phase insurance contract structure. Standard growing seasons have been documented and published by FAO and USDA. These, however, do not provide sufficient detail to cover the large spatial and year to year variations, to allow for an adequate timing of the sowing window. This would imply that one always has to rely on local information, which restricts scaling up and cost-effectiveness of the insurance system. Therefore we will explore in this section the extraction of growing season and related sowing window from the historic data sets.

Farmers grow their crops during the period that, on the basis of experience and tradition, is known to provide the best conditions for crop growth. We will reproduce the development of this traditional knowledge by analysing the full historic data series and identifying the periods which provide the highest water availability during the growing season. We will particularly address the timing of maize growth, which has a growing season of about 130 days. The analysis is done in the following steps:

- Calculate the 130 day forward floating average
- Find the yearly maximum in the 130 day forward floating average and determine the corresponding dekad. This dekad represents the start of the growing season
- Given the start of the growing season in 28 years, determine the frequency distribution and mode of the growing season start. The latter represents the most likely start of the growing season.

An example of the result of the first step is shown in figure 6.2, which presents the 24 year time course of the 130 day forward floating average of the relative evapotranspiration and precipitation at Arusha, in north-east Tanzania. The maxima in these curves are well defined and can be easily extracted. Note that there is phase difference between the precipitation and actual evapotranspiration.

Using the approach described above, we have determined the maize growing season for each of the 29 locations in Tanzania. The result is shown in figure 6.3. This approach may be applied to any location in the region and thus regional maps of the start of the growing season may be developed. These may provide more accurate information on the start of the growing season and the sowing window than currently available. This approach will be useful when scaling up the insurance system.

6.3 Determination of the sowing window

The width of the sowing window may be studied by considering the frequency distribution of the growing season start. Two examples of this distribution are shown

in figure 6.4 and 6.5. The start of the growing season as shown in figure 6.3, is determined by the mode of the distribution, i.e. the most frequent starting dekad. For Mbeya this is dekad 7, and for Arusha dekad 11. For Arusha the sowing window should be ± 4 dekads, so as to include all starts during the period 1984-2007. In the case of Mbeya the sowing widow should be wider, preferably ± 6 dekads. The latter is a good general choice.

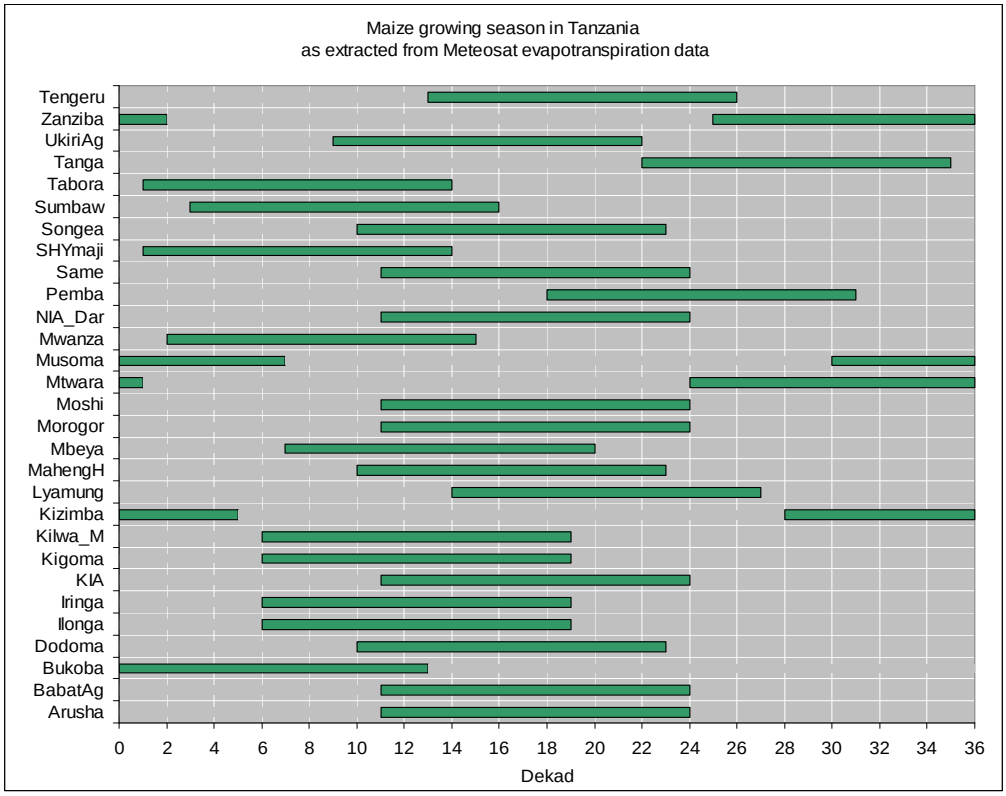

Figure 6.3: Maize growing season for different locations in Tanzania, as extracted from Meteosat relative evapotranspiration data during the period 1984-2007. The start of the growing season differs considerably between locations.

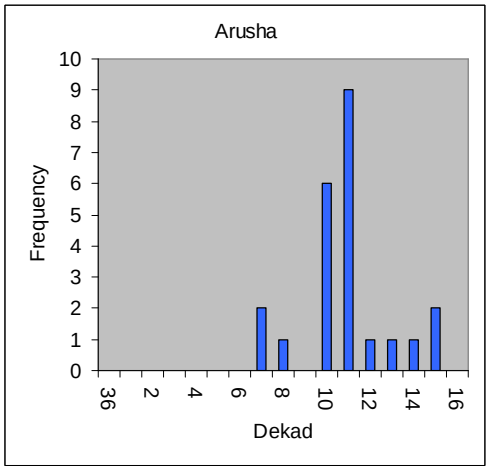

Figure 6.4: Frequency distribution of the start of the growing season at Arusha.

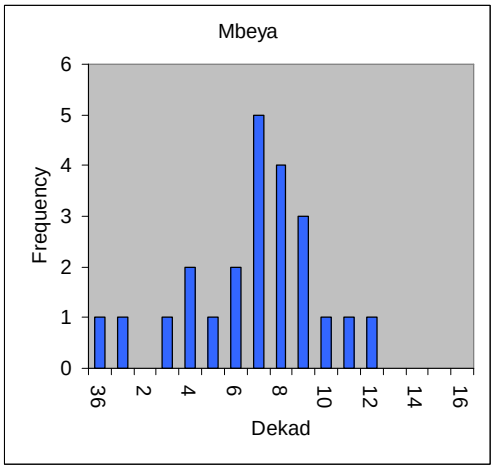

Figure 6.5: Frequency distribution of the start of the growing season at Mbeya.

6.4 Comparing evapotranspiration and precipitation based insurance performance

We have implemented the 3-phase insurance contract structure, as proposed by IRI in *Osgood et al. (2007),* in an Excel Workbook and have carried out a comparative burn analysis for the 29 station locations on the basis of both, the evapotranspiration and precipitation data. An important difference is that the start of the growing season and sowing window are determined location specific on the basis of the historic data records. An overview of the calculations is presented in table 6.3. The input for the calculations include: sowing requirement, length of the three growing phases, trigger percentile, exit percentile, and precipitation cap. The sowing requirements have been set equal to those already in use: RE=0.40, according to the ECGM crop growth model and PREC=25 mm/dekad, as used by IRI. We have taken the precipitation cap at 50 mm/dekad, i.e. roughly equal to the potential evapotranspiration. However the pay-out simulation shows little sensitivity to its precise choice, as long as the trigger percentile is at a low level. A cap of 100 mm/dekad gives almost the same result. In the following analysis, we will therefore study in particular the effect of the choice of the trigger percentile and the growing season structure.

Table 6.3: Spreadsheet inputs and calculations used to carry out a pay-out burn analysis for the period 1984-2007.

Spreadsheet	***Calculations***
Input	*Basic data set:* • Dekadely RE and PREC data by location in columns. *Parameters:* • Sowing trigger for RE (%) and PREC (mm/dekad). • Length of phase 1 (vegetative) in dekads. • Length of phase 2 (flowering) in dekads. • Length of phase 3 (yield formation) in dekads. • Trigger percentile. • Exit percentile. • Precipitation cap.
Sowing window	• Calculate growing season forward floating RE/PREC averages. • Determine maximum values of 130-day RE/PREC, and corresponding growing season yearly start. • Determine starting dekad frequency distribution and mode.
Season start	• Test within sowing window the RE/PREC sowing condition. • Find actual growing season start dekad.
Phase-1	• Calculate forward floating phase length average of RE/PREC. • Extract RE/PREC phase average for each year, given that years growing season start and phase length. • Calculate the RE/PREC trigger and exit from the corresponding percentiles, given the phase averaged values in each year. • Assess the trigger and calculate pay-outs as: (phase trigger – phase average value)/(phase trigger – phase exit).
Phase-2	Idem.
Phase-3	Idem.
Summary results	• Sum-up phase pay-outs and calculate total pay-out up to a maximum of 1.00, i.e. the insured sum. • Sum pay-outs by location and calculate location averages.

The basic approach that has been followed, with variable growth phases and percentile triggers, gives on average the same pay-out at every location. If the trigger is set at the 4-percentile and the exit at the 1-percentile, then over the years almost all stations get a mean pay-out of about 4 percent of the insured value in each phase, adding up to 12% for the whole growing season. This neat behaviour is reached by expressing both trigger and exit as percentiles of the phase averaged relative evapotranspiration and precipitation values. It indicates that the current drought insurance approach would not suffer from adverse selection. Although farmers in more favourable climates may not need drought insurance, this at least guarantees that they have the same probability of pay out. Also in terms of participation in the insurance, and thus economic feasibility, this may be considered an advantage.

6.4.1 Trigger percentiles

Figures 6.6a-c present the calculated pay-outs for both the evapotranspiration and rainfall based insurance with the trigger set at the 4, 6 and 8 percentile, respectively. The results for both data sources are not exactly the same. This, however, should not surprise when considering the differences between the two types of data. These differences are related to the irregular nature of the rainfall, the buffering function of the soil, and the gradual and delayed use of the soil water by crops.

Evapotranspiration is considered to be the better index as it is directly related to crop growth, while the faith of rainfall is unknown and thus precipitation is less directly related to crop growth. Over the years, however, the average pay-out of the evapotranspiration and precipitation based insurance is about the same. Using the 4-percentile trigger and 1-percentile exit, the total growing season pay-out value is 10.3% in the case of the evapotranspiration data and 11.4% for the rainfall data. The number of locations receiving pay-out is 69 for the evapotranspiration and 76 for the precipitation data set. Table 6.4 presents similar data for the 6-percentile and 8-percentile triggers.

The percentage of locations that would receive pay-out in both cases is 12.4% at the 4-percentile level and 22.7% at the 6 and 8 percentile trigger level. The same pay-out percentage does of course increase with the trigger percentile. For example at a 36% trigger the number of same pay-outs is 66.3%.

Table 6.4: Pay-out characteristics for several trigger percentiles and growing season phasing structures. Start of growing season is automatic. Exit at 1-percentile level.

Phasing structure	Trigger percentile	RE		PREC		Same PO
		PO nr.	PO value	PO nr	PO value	
5,3,5	8	137	14.6 %	145	16.6 %	22.7 %
5,3,5	6	137	13.2 %	145	15.2 %	22.7 %
5,3,5	4	69	10.3 %	76	11.4 %	12.4 %
5,7	4	53	7.9 %	56	8.4 %	12.8 %
12	4	28	4.2 %	28	4.2 %	10.7 %

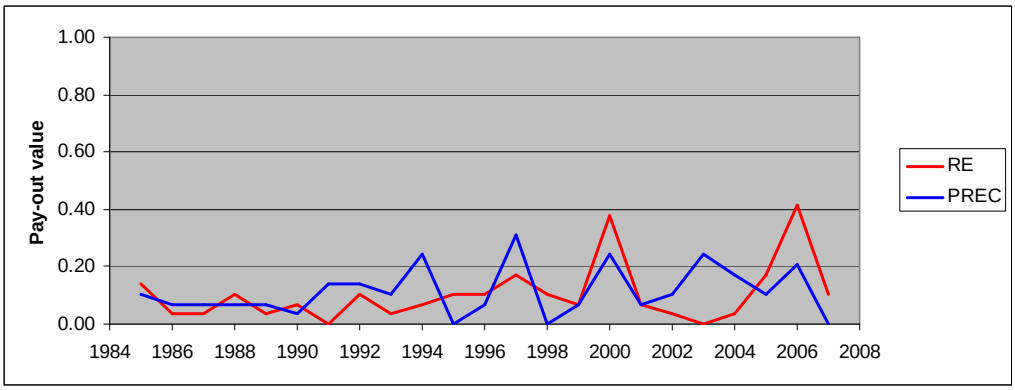

*Figure 6.6a: Average pay-out by year for the 29 locations in Tanzania at **4 percentile trigger** and 1 percentile exit level. Rainfall capped at 50 mm/dekad. Three phases of 5,3,5 dekads.*

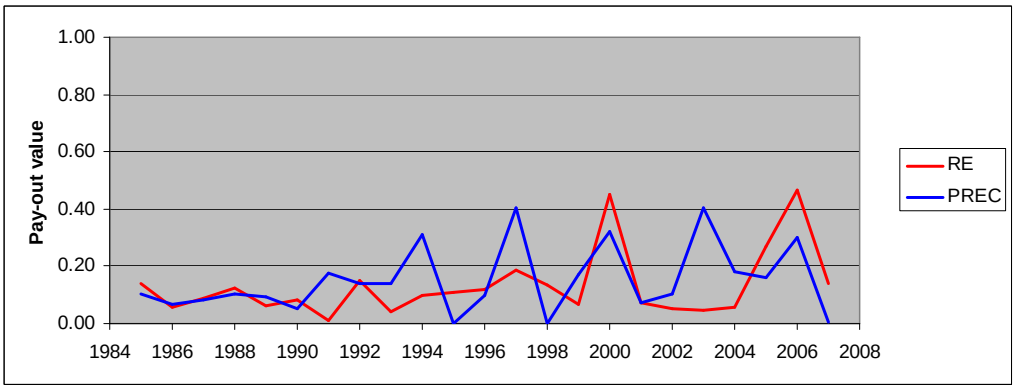

*Figure 6.6b: Idem for **6 percentile trigger.***

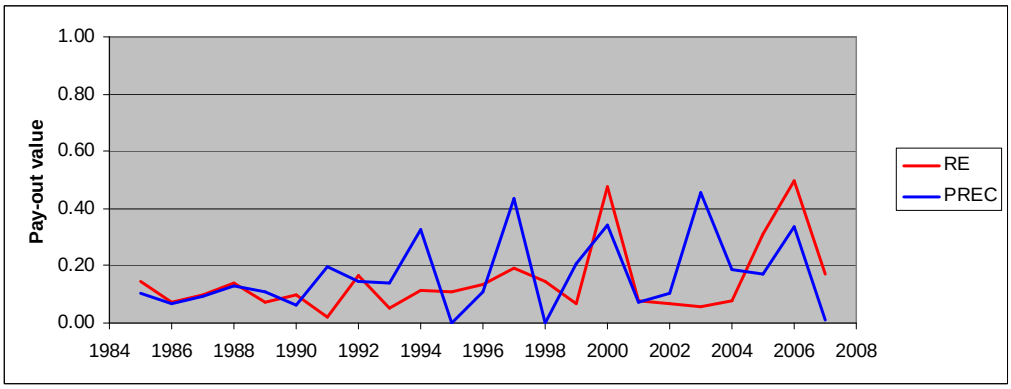

*Figure 6.6c: Idem for **8 percentile trigger**.*

6.4.2 Growing season structure

Figures 6.7a-c illustrate the effect of growing season structure. This does not concern its start, which is automatic and based on the variable and location specific sowing window extracted from the climatic data base. This was explained in sections 6.2 and 6.3. Here we consider the effect of how the growing season is built-up in terms of different growth phases. We have considered the following 3 alternatives, of which the first two are originating from the *Oswood et al. (2007)* paper.

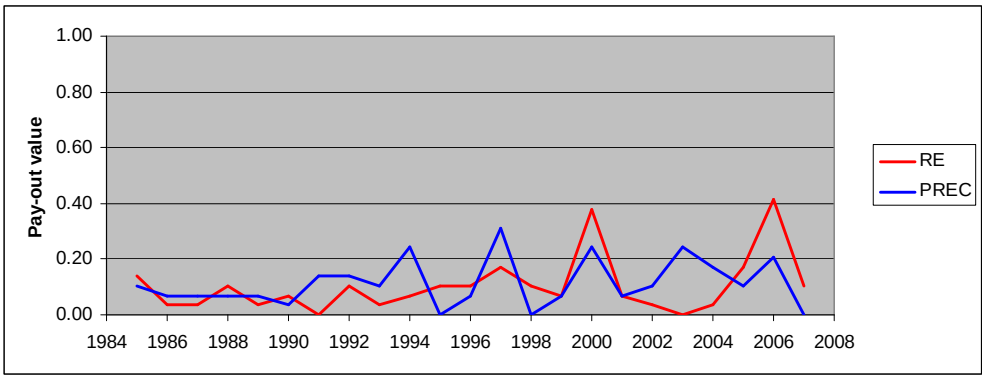

Figure 6.6a: Average pay-out by year for 29 locations in Tanzania at 4 percentile trigger and 1 percentile exit. Rainfall capped at 50 mm/dekad. ***3 phases of 5,3,5 dekads****. Average PO values: RE 12.4%, PREC 12.9%. Same PO: 5.9%*

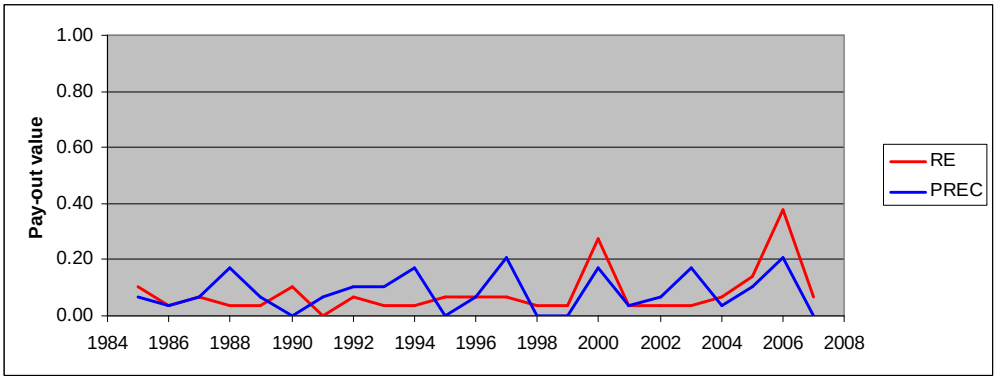

Figure 6.6b: Idem, but ***2 phases of 5,7 dekads****.*
Average PO values: RE 8.2 %, PREC 8.2 %. Same PO: 6.2 %

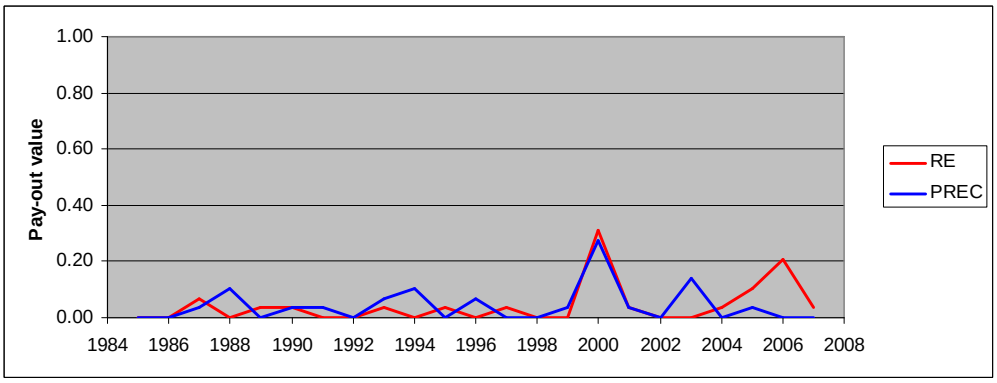

Figure 6.6c: Idem, ***1 phase of 12 dekads****.*
Average PO values: RE 4.2%, PREC 4.2%. Same PO: 12.6%

- A 3-phase structure of 5,3,5 dekads for the vegetative, flowering and yield formation periods.
- A 2-phase structure of 5,7 dekads. The second phase, in this case, combines the flowering and yield formation periods.
- One single phase of 12 dekads, representing the whole growing season in one time.

A burn analysis has been done for these three alternatives and the pay-out results, for both the RE and PREC data, are presented in figures 6.6a-c. The last three rows in table 6.4 summarize the results. As expected, the number of pay-outs and the total pay-out value increases with the number of growth phases discerned. Thus, at the same trigger level, a multiple-phase structure is considerably more expensive than a single phase, total growing season set-up. Also because of the high sensitivity of the multi-phase contract to inadequate triggering of the start of the growing season, it remains questionable whether a 3-phase structure pays off. A two or single phase approach may also be adequate to cover the most serious losses and will be much more affordable.

6.5 Towards scaling up and cost reduction

In this section some further steps are explored that may help to scale up the micro-insurance approach, while keeping data processing and administrative costs down. Modelling trigger and exit levels, as discussed in section 6.5.1, provides an easy way of setting the variables of a contract without need of extensive database calculations Thus it allows for scaling up while keeping overhead costs down. It could particularly be useful in combination with climatic zoning, as discussed in section 6.5.2.

6.5.1 Trigger modelling

It will not always be possible or practical to determine the trigger and exit for each possible location or pixel, particularly not when drought insurance is to be applied at larger scales. Therefore it is useful to investigate if it is possible to model the percentiles as a function of the climatic averages. This is done by means of regression. Examples are shown in figure 6.7 for phase 1 and phase 2 of the 5,3,5 dekad phasing structure. Table 6.5 presents an overview of the regression results. For the relative evapotranspiration (RE) the coefficient of determination (R^2) varies between 0.62 and 0.91. For the precipitation R^2 varies between 0.09 and 0.68. Clearly the modelled triggers based on evapotranspiration are considerably better defined than those based on precipitation. Lack of definition could lead to considerably higher pay-outs than anticipated on the basis of the trigger percentile, 4% in this case.

This expectation has been tested by carrying out a burn-analysis with the modelled 4-percentile triggers. The results are presented in table 6.6. The calculated pay-outs in this case are notably higher than in the case of triggers that are determined as percentiles directly from the data set. For the evapotranspiration data the increase in pay-out is 30-60%, for the precipitation data the increase in pay-out is considerably higher: 60-140%.

Table 6.5: Results of modelling the 4-percentile as a linear function of the climatic average of relative evapotranspiration and precipitation, respectively

Phasing structure	Phase nr	RE			PREC		
		slope	intercept	R^2	slope	intercept	R^2
5,3,5	1	0.845	-2.51	0.758	0.314	12.51	0.089
	2	0.892	-0.586	0.624	0.453	6.53	0.159
	3	0.940	1.506	0.810	0.651	1.13	0.335
5,7	1	0.930	-5.735	0.781	0.231	14.99	0.053
	2	0.897	5.301	0.819	0.662	3.45	0.481
12	1	0.947	1.724	0.911	0.720	5.02	0.682

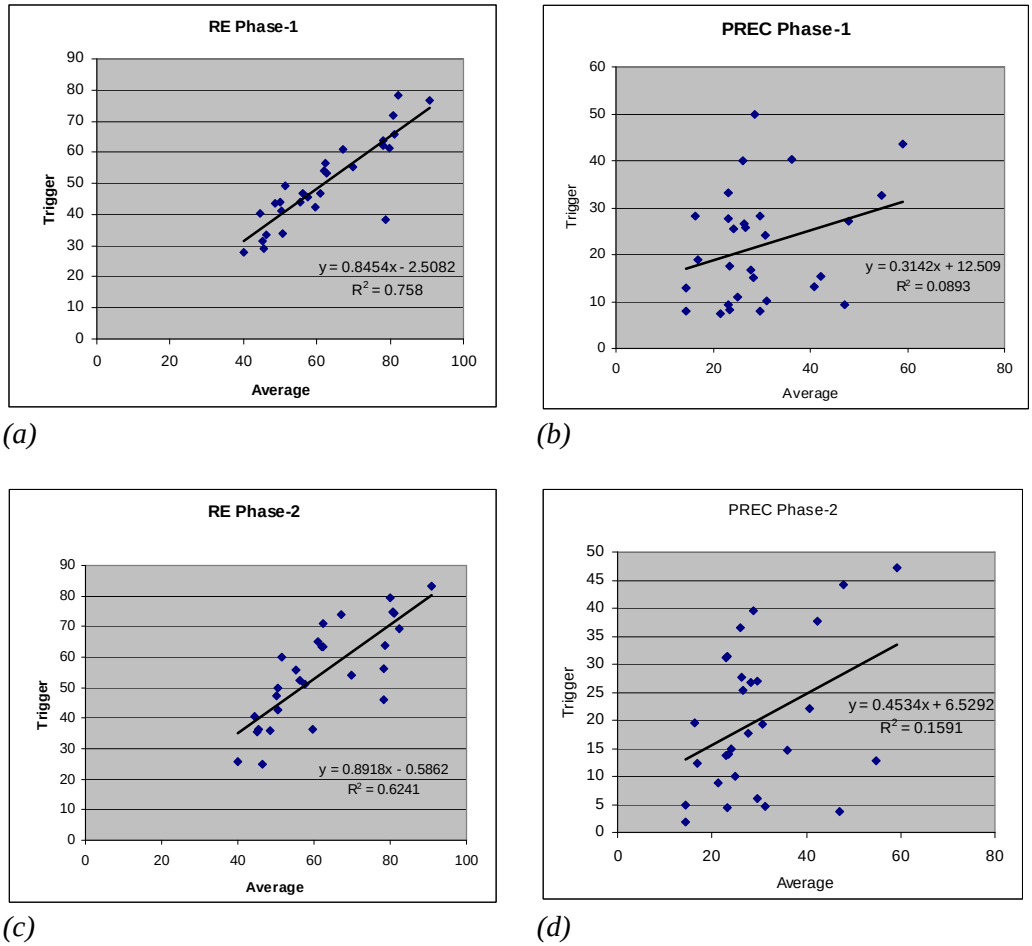

Figure 6.7: Regression of 4-percentile triggers against climatic average of relative evapotranspiration (left) and precipitation (right) for phase 1 (top) and phase 2 (below) of a 5,3,5 dekad multi-phase contract structure. Regression model providesbetter trigger definition in the case of evapotranspiration than in the case of precipitation.

Table 6.6: Pay-out characteristics for several trigger percentiles and growing season phasing structures. Start of growing season is automatic. Exit at 1-percentile level. ***Trigger and exit are modelled on the basis of regression against climatic mean of RE and PREC respectively****.*

Phasing structure	Trigger percentile	RE		PREC		Same PO
		PO nr.	PO value	PO nr	PO value	
5,3,5	8	190	19.3 %	248	30.7 %	34.7 %
5,3,5	6	152	17.0 %	226	29.1 %	29.6 %
5,3,5	4	128	15.2 %	209	27.1 %	27.3 %
5,7	4	101	12.7 %	145	19.4 %	25.2 %
12	4	60	6.6 %	54	6.4 %	19.3 %

6.5.2 Zoning approach

In the case of satellite evapotranspiration based insurance we have long evapotranspiration data series for every location, which would allow to define individual triggers and write individual contracts for almost every farmer. This however results in a high amount of administrative work. It would be necessary to know the precise location/coordinates of the individual farmer and to verify and calculate each individual pay-out. Although computers do allow for such an approach, it seems less appropriate.

In the previous section we have discussed the modelling of triggers as a tool to reduce the required data assessment when scaling-up the insurance and writing contracts suitable for a large number of clients, which are living in different climatic conditions all over the country or region. It the trigger can be modelled and be determined on the basis of the climatic average of water availability, i.e. relative evapotranspiration, then the next cost reducing step is to reduce the number of climatic conditions discerned. This approach is called climatic zoning.

We have seen in the previous section that RE based triggers are quite well related to the climatic averages of relative evapotranspiration. Thus zoning according to the RE climatic average (24 years) could be an approach to reduce the number of different contracts. An example of such a zoning map is shown in figure 6.8. It is noted that within each zone there may still be different growing seasons and corresponding sowing windows. The sowing window is usually defined in the contract as well. Thus it will also be necessary to create a start of the growing season map and to zone this map in a similar way. When this map is also available it is possible to write individual contracts for each combination zone, characterised by a certain level of evapotranspiration and a certain location of the sowing window. In fact, when the trigger modelling and zoning approach would be adapted, it may be possible to develop a single contract, in which the triggers and sowing windows are specified in more general terms and whereby the zoning maps and settings for each zone would be added in annex. In this way a national scale insurance with low administrative costs, could be realized.

6.6 Building trust

In the current rainfall based drought insurance pilots it is considered good practice to develop the insurance set-up in close cooperation with farmers, or rather their representatives, as well as other stakeholders. This participatory approach is democratic and recommendable, but at the same time becomes labour intensive and costly when scaling-up the insurance. Moreover the participatory approach may also have some unwanted side effects, particularly if both sides become partners, sharing responsibility and thus developing a joint interest. The participatory approach is costly and less sustainable when scaling up the insurance to the national and possibly regional level. It is believed, that when developing the insurance system to larger scales, emphasis should shift from end-user involvement to a sound scientific and multi-disciplinary approach, that could be refined in cooperation with and verified by the national and international scientific and professional community.

In addition it remains important to communicate the insurance system to the farmers, so as to explain it and to build trust among the farmers community. This is particularly important as farmers may have little notion of evapotranspiration and the measurement of this quantity by satellite.

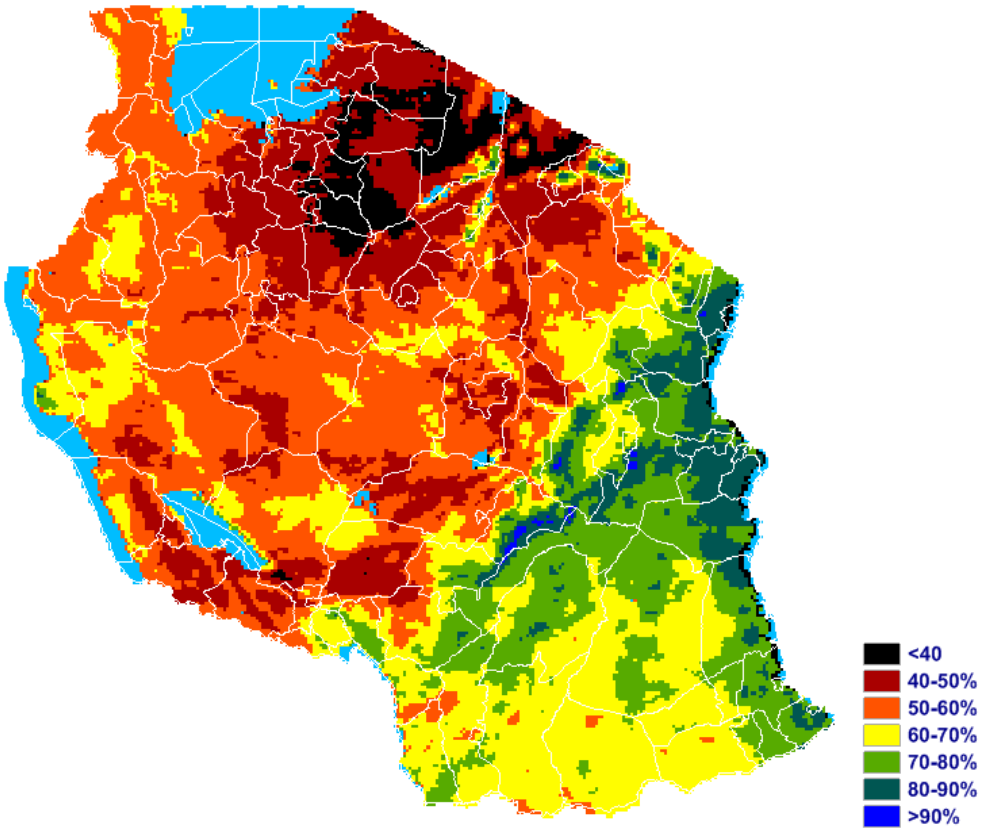

Figure 6.8: Example of a contract zoning map, defining a limited number of relative evapotranspiration levels within each GAUL-2 administrative region.

Building trust, in this case, starts with getting aware of and getting accustomed to the type of information. One can think of a range of actions to improve awareness and trust. A number of possible actions is listed below.

Involving national institutions

1) Involve the National Meteorological Service (NMS) in the validation of the data.
2) Possibly implement the EWBMS satellite data collection system at their premises so as to locally receive and process the data and generate the required products and data sets that are used for the drought insurance. In addition the NMS could use the EWBMS data products to communicate the drought situation through existing channels in near real time.
3) Involve the National Agricultural Extension Service to present the insurance product to farmers and farmer organisations and to act as an intermediary to promote and possibly sell the drought insurance.
4) Involve NGO's and farmer organisations in the same way.

Addressing the farmers

5) Develop an information booklet explaining the satellite based approach in simple pictures and notions related to real life situations.

6) Provide for a training session during meetings of farmer unions and similar organisations.
7) Broadcast crop water availability (= relative evapotranspiration) maps every 10 days through television and radio.
8) Create a national website for the drought micro-insurance and publish all relevant drought information on this site.
9) Publish crop water availability maps in national and local newspapers.
10) Create an SMS service for providing similar drought information to farmers.

Provide additional services

11) Provide micro-insurance in combination with micro-credit through trusted local insurance companies and banks.
12) Combine micro-insurance with contract farming, and sell through trusted institutions in this field.
13) Provide sowing information as an additional free service through, TV, radio, SMS or internet.
14) Provide crop yield forecasts as an additional free service through TV, radio, SMS or internet.

These are all actions which are within or next to the domain of the insurance data provider. There are other actions that could further complement the package, for example: dedicated advice in cooperation with the agricultural extension service.

6.7 Summarized findings in this chapter

In chapter 6 we have compared evapotranspiration and rainfall as alternative drought indices for designing crop drought insurance. We have also explored some simplifications that allow for scaling up the insurance while keeping costs low.

In general there are clear differences between the two types of data. Rainfall represents water supply and evapotranspiration reflects crop water use. In between is water loss by run-off and deep percolation and the accumulation and storage of water in the soil, from where it is gradually released for use and transpiration by the crop. As a result of this redistribution process the rainfall and evapotranspiration data show very different characteristics. Rainfall is distributed very skew (figure 5.6). Evapotranspiration has an almost normal distribution (figure 5.5). The satellite derived evapotranspiration shows a logical response to the seasonal precipitation events (figure 5.2), with a phase shift of typically 5 dekads (figure 5.4). The long term water volumes involved in rainfall and evapotranspiration are about the same, as they should be (figure 5.3).

Evapotranspiration is almost identical to crop water use. Relative evapotranspiration is known to be proportional to relative biomass production, i.e. crop growth. Therefore evapotranspiration is synchronous with and a direct measure of crop production, while rainfall precedes the main phase of crop growth. In between precipitation events and crop growth the faith of the water is not exactly know. Water may run off or run on (from mountain slopes) and water may percolate to deeper layers. Therefore precipitation is only indirectly related to crop growth. Thus the intrinsic basis risk is lower in the case of evapotranspiration. Consequently this data source has the potential of providing more accurate pay-outs. At the same time and

for the same reason, evapotranspiration based drought insurance should not be expected to provide the same pay-outs as rainfall based insurance.

In chapter 6 we have also introduced the multi-phase insurance contract structure. It was also indicated that the relatively short and sensitive flowering phase makes the contract critically dependent on the growing season start. Existing crop calendars are insufficient for this purpose. For this reason we have developed an automatic method to locate the sowing window on the basis of the climatic database, while the actual start is done on the basis of a sowing trigger.

In the present drought insurance approach, triggers and exits are set on the basis of percentiles. This has resulted in a very even distribution of pay-outs between the various locations and related climates. This approach eliminates the risk of adverse selection.

It has been shown that both data-sets show a similar pay-out response to drought. But the variations in rainfall based pay-outs are larger than those based on evapotranspiration. On average the pay-outs are 9-13% lower in the case of the evapotranspiration data than for the precipitation data. These differences are thought to be related to the more stable behaviour of the evapotranspiration data as a result of the water buffering effect of the soil.

In the present chapter we have introduced the multi-phase contract structure, as pioneered by *Oswood et al. (2007)* of IRI, Columbia University. A 3-phase, 2-phase and 1-phase set-up were compared. With the possibility of a partial pay-outs in each phase, the total pay-out value increases with the number of phases. This effect is 6-12% stronger in the case of the precipitation data than when using the evapotranspiration data. In view of this effect and the earlier mentioned sensitivity of a short flowering phase to growing season start, a 2-phase structure, consisting of (1) a vegetative and (2) a flowering & grain filling phase, seems to be a good option for evapotranspiration based insurance. At the 4 percentile trigger average pay-out would be 7.9% of the insured sum.

The financial feasibility of a drought insurance depends on the costs involved. Current approaches are often hampered by costs of data collection and administration. Although the evapotranspiration data have such a high density that it would be possible to write individual contracts for each farmer, such an approach could increase the administrative overhead and might reduce the positive effect of scaling up. Therefore we have looked at two possible measures to reduce overhead costs. The first one is to model the trigger on the basis of the climatic average of the data used. The relation is found by means of regression. It has been shown that such an approach tends to lead to higher pay-outs. The evapotranspiration data, however, show less dispersion and therefore lead to a better defined model than the precipitation data. RE pay-outs increase with 30-60% while precipitation pay-outs increase with 60-140%.

To keep administrative costs down when scaling up the insurance, also a climatic zoning approach is proposed on the basis of levels of average water availability, i.e. relative evapotranspiration. A sample climatic zoning map has been prepared (figure 6.14). Similar creation of a zoned sowing window map is proposed. The resulting two-dimensional zoning approach could be the key to a single and uniform contract with zoning map(s) and/or tables in annex. Such contract could be offered to any farmer in the country or region.

7 SUMMARY AND CONCLUSIONS

Need for drought micro-insurance

Drought micro-insurance is considered a key to poverty alleviation, economic development and climate adaptation. Traditional crop insurance is expensive and sensitive to adverse selection and fraud, and hence has not been very successful yet. Index insurance has been considered a good alternative, but has also introduced some new problems. These are known as intrinsic and spatial basis risk, meaning that the measured index is (a) intrinsically not identical to the risk to be covered and (b) that the place of measurement of the index is not the same as the dwelling place of the insured. Drought micro-insurance has also not been very successful yet because of the high costs involved. Usually this type of insurance had to be subsidized.

Potential of satellite data

Satellite derived data are recognized as a possibility to address these problems. Satellites provide a dense grid of measurements, from which the relevant data that correspond to the location of the insured can be selected. Moreover, long time series of relevant satellite data exist. The data can also be low cost as it would not be necessary to maintain extensive ground-based measuring networks.

The NDVI reflection index has already been measured from polar orbiting meteorological satellites for a long time. Its accuracy, however, suffers from a highly variable viewing and illumination geometry. Moreover it is more a measure of ground cover by vegetation, and much less an indicator of crop biomass. This index also gives no information on drought stress. The lack of relation to crop yield may introduce high intrinsic basis risk.

Another satellite-based approach is the estimation of rainfall fields. These methods are usually of a statistical nature and require intensive calibration with reliable rain gauge data, which in Africa are insufficiently available. The calibration is usually variable in space and time and has to be repeated frequently. Moreover rainfall data need additional models to estimate water availability to the crop. Other complications are (a) lateral flow of water(run-on/off) and (b) rainfall and crop growth are not synchronous. Therefore satellite-derived rainfall also suffers from considerable basis risk.

Evapotranspiration based approach

In this report we present a less known source of satellite climatic data that can be used for drought micro-insurance, which is based on the derivation of the actual evapotranspiration through measurement of the earth surface albedo and temperature and making use of the surface energy balance. A data set of 28 years of Meteosat data has been acquired and has been processed with the EWBMS system to temperature, radiation and actual evapotranspiration data covering all Africa. The latter two are used to run the ECGM crop growth model, which converts the radiation and actual evapotranspiration data in estimates of crop yield.

Methodology and validation

This report first focuses on the explanation of the scientific backgrounds and processing methodology. Chapter 2 discusses the EWBMS climatic data extraction and energy balance calculations. Chapter 3 explains the ECGM crop growth modelling approach. In chapter 4, the validation of the satellite derived data products is discussed. Detailed validation reports are presented in annex A to C at the end of this publication. In general the validation results show small average differences and high correlations between the satellite derived data and the independent ground data used for validation. Also the comparison of the satellite derived crop yields and the ground census data shows good results. It is therefore concluded that the Meteosat derived data are highly consistent with the available ground data and are a reliable basis for developing a drought micro-insurance product that can be used across Africa.

Proposed insurance indices

The Meteosat-derived indices proposed for drought micro insurance are:

- Relative evapotranspiration (RE) accumulated during the growing season
- Relative crop yield (RY), simulated throughout the growing season

RE is proportional to the level of CO_2 assimilation and crop dry matter production and is therefore a pre-eminent agricultural drought indicator. Therefore as an insurance index it has a low basis risk. Its derivation is based on physics and mathematics. Calibration is necessary only once and has already been done. Once calibrated, no external data are required, which implies that this approach can be applied very easily all over Africa, any time and anywhere. Since geostationary meteorological satellites span the earth, such drought insurance could even be introduced world wide.

RY provides a crop specific measure of yield deficit due to drought. From a theoretical point of view, it has the lowest intrinsic basis risk, certainly when compared to the satellite based indices explored so far: NDVI and precipitation. Deriving this index, however requires an additional crop yield processing step which is done on a regional basis: i.e. separately for the West, East and Southern Africa region. 28 years of EWBMS data products have been processed to maize yields for the East African region. Similar yield data sets can easily be extracted for other crops and other regions in Africa and Europe.

The Meteosat derived RE and RY indices provide not only a relatively low basis risk, but can also be produced very economically. There is no need for costly extensive measuring networks on the ground, which have to be managed and maintained. Moreover the approach can easily be scaled up. Larger scales, with a high number of insurance clients, will enable not only economies of scale, but also allow for better risk spreading and therefore lower re-insurance costs.

Database development and data properties

In chapter 5 the database development is discussed and the properties of the evapotranspiration data is studied by comparison with rainfall data for a number of locations in Tanzania. The evapotranspiration data are shown to be related, but

different. Precipitation and evapotranspiration represent different phases of the water cycle, with the soil as water buffer in between. While overall water volumes appear to be almost the same, there is a phase shift of about 5 dekads between precipitation and evapotranspiration. Evapotranspiration is known to be proportional to crop growth, whereas water and CO2 exchange with the atmosphere share the same diffusion path that is controlled by the plant stomata. Therefore evapotranspiration has a lower intrinsic basis risk than precipitation and offers the potential of improving the accuracy of pay-outs.

Elements of contract design

In chapter 6 we have studied some elements of contract design. Given the current state of the art, a multi-phase contract structure has been implemented. However such a multi-phase structure, with a relatively short flowering phase, becomes critically sensitive to an accurate start of the growing season. For this reason the multi-phase insurance approach is extended with a method of timing the start of the growing season and determining the corresponding sowing window automatically from 24 years of satellite data.

Pay-out performance

Finally from section 6.4 on we compare the performance of the evapotranspiration and precipitation based drought insurance in a burn analysis, pertaining to 29 locations (weather stations) in Tanzania. This is done in exactly the same way for both data sets, except that a cap is applied to the rainfall data set when calculating the pay-out.

Trigger and exit are defined in terms of data percentiles. This approach guarantees a predictable and even pay-out, independent of the location and local climate. This will prevent adverse selection. Calculated pay-out based on evapotranspiration and rainfall show similar year to year variations. Evapotranspiration based pay-out is less variable than precipitation based pay-out, which is attributed to the water buffering action of the soil. Evapotranspiration based pay-outs are also 9-13 % lower, than those based on precipitation. Introduction of a multi-phase structure, with possible pay-outs in each phase, also increases the overall pay-out. However the increase is 6-12 % more in the case of the precipitation than in the case of the evapotranspiration data.

Approach to insurance scaling up

We have explored ways to keep data processing and administrative costs down when scaling up the insurance. The first one is modelling of the trigger on the basis of climatic averages of evapotranspiration and precipitation, respectively. The linear regression models based on the evapotranspiration data are shown to be considerably better defined that those based on precipitation. Modelling the trigger leads to increased pay-out, but this was only 30-60% in the case of evapotranspiration, but 60-140% when using the precipitation data set.

Here we conclude that the precipitation based insurance provides notably higher risks to the (re-)insurer than the evapotranspiration based approach. This is based on arguments related to intrinsic basis risk and does not yet address uncertainties related to spatial basis risk, i.e. the dislocation between rain gauge stations and insured

farmers. The latter is expected to be high for precipitation in view of the limited number of rainfall stations and given the scale of convective precipitation.

A good relation between climatic average and trigger also offers the possibility of a climatic zoning approach, being another step to keep costs down. It is expected that a two dimensional zoning approach, for both: (1) evapotranspiration climatic mean and (2) growing season start, would enable a low cost, single drought insurance contract at national and possibly regional level.

Conclusions

Overall it is concluded that the Meteosat evapotranspiration data provide an excellent alternative for the precipitation based approach. The data are uniform, objective, validated and abundant. In terms of data properties, they are shown to perform better than precipitation. As an insurance index they are expected to give more accurate pay-outs. They also offer solutions for scaling up, while keeping costs down. Because of their high spatial resolution and wide extension they may indeed bring affordable and reliable drought micro-insurance to every farmer in Africa.

But evapotranspiration based drought insurance is new. It is necessary to build trust among farmers and other stakeholders. Collaboration at the national level with weather services and national extension services is recommended. Local implementation of the data collection system with the national weather service and publication of crop water availability maps through a variety of media may support habituation to the data. Strategic cooperation with local insurance companies, banks and agricultural input providers could help to package the insurance product in a logical and attractive way. In addition training material and courses could be developed in cooperation with NGO's and the national extension service.

-.-

ACKNOWLEDGEMENTS

We gratefully acknowledge:

Bert Koenders, former Netherlands Minister of Development Cooperation for his trust in the new technology and enabling this project.

Ronald Goldberg of the Netherlands Ministry of Development Cooperation for his supportive attendance and guidance of this project.

Kees Stigter, founding president of the International Society for Agricultural Meteorology, for writing his supportive introduction to this report.

Steve Coffey and James Sharpe of Micro-Ensure for their cooperation and experience contributed to this project, as well as for making available the precipitation data set.

David Gerbrands of RABO Development, Erik Klaassens and Jacqueline Barendse of ECORYS, for their constructive and enthusiastic cooperation and support.

Jamie Anderson and Francesco Rispoli of IFAD, Rome, for their interest and constructive discussions.

Bastiaan Mohrman of IFC, Washington as well as Rose Goslinga and Fritz Brugger of the Syngenta Foundation for their visit, interesting discussions and useful suggestions.

Jonas Ardö and Almut Arneth at the Department of Physical Geography and Ecosystems Analysis of Lund University in Sweden for making available the CARBOAFRICA flux tower data of Demokeya and Maun for the validation work.

REFERENCES

Alados I and Alados-Arboledas L (1999) "Validation of an empirical model for photosynthetically active radiation" Int. J. Climatol. 19: 1145–1152 (1999)

Arneth A, Veenendaal EM, Best C, Timmermans W, Kolle O, Montagnani L and Shibistova O (2006) "Water use strategies and ecosystem-atmosphere exchange of CO_2 in two highly seasonal environments", Biogeosciences, 3, 421–437.

Arnold M (2008) "The role of risk transfer and insurance in disaster risk reduction and climate change adaptation", Policy brief for the Commission on Climate Change and Development, Kräftriket 2B, SE 10691, Sweden.

Aubinet M, Grelle G, Ibrom A, Rannik U, Moncrieff J, Foken T, Kowalski AS, Martin PH, Berbigier P, Bernhofer C, Clement R, Elbers J, Granier A, Grunwald T, Morgenstern K, Pilegaard K, Rebmann C, Snijders W, Valentini TR, Vesala (2000) "Estimates of the annual net carbon and water exchange of European forests: the EUROFLUX methodology",Advances in Ecological Research 2000, 30:113-175.

Barrett EC and Martin DW (1981) "The Use of Satellite Data in Rainfall Monitoring", Academic Press, 340 pgs.

Brotzge JA and Crawford KC (2003) "Examination of the Surface Energy Budget: A Comparison of Eddy Correlation and Bowen Ratio Measurement Systems", Journal of Hydrometeorology, pp. 160–178, volume 4, issue 2, April 2003.

Businger, J.A. (1975) "Aerodynamics of vegetated surfaces", in: Heat and mass transfer in the biosphere, part 1, Transfer processes in the plant environment, DA de Vries and NH Afghan, eds., Scripta Book Company, pp 139-165.

Doorenbos J, Kassam AH (1979) Yield response to water. FAO Irrigation and Drainage Paper 33. FAO, Rome, 193 pp.

Frère M, Popov GF (1986) Early Agrometeorological Crop Yield Assessment. FAO Plant Production and Protection Paper 73. FAO, Rome, 124 pp.

Genovese G. (1998) The methodology and the results of the MARS bulletin: an integrated crop production assessment and forecast bulletin. Agrometeorological applications for regional crop monitoring and production assessment, Office for Publications of the EC. Luxembourg. volume 17735, 67-120.

Gommes R (1983) Pocket computers in agrometeorology. FAO Plant Production and Protection Paper 45. FAO, Rome, 140 pp.

Hazell P, Anderson J, Balzer N, Hastrup Clemmensen A., Hess U, Rispoli F (2010) Potential for scale and sustainability in weather index insurance for agriculture and rural livelihoods, International Fund for Agricultural Development and World Food Programme, March 2010, 152 pp.

Hellmuth ME, Osgood DE, Hess U, Moorhead A and Bhojwani H, eds.(2009) "Index insurance and climate risk: Prospects for development and disaster management", Climate and Society no 2. International Research Institute for Climate and Society (IRI), Columbia University, New York, USA.

Jonas Ardö, Meelis Mölder, Bashir Awad El-Tahir and Hatim Abdalla Mohammed Elkhidir (2008) “Seasonal variation of carbon fluxes in a sparse savannah in semi arid Sudan”, Carbon Balance and Management 2008, 3:7.
Kidder SQ and Vonder Haar TH (1995) “Satellite Meteorology”, Academic Press, San Diego California, 466 pgs.

Kondratyev, K.Y.(1969) ‘Radiation in the Atmosphere’, Academic Press, New York, London.

Monteith JL (1977) Climate and efficiency of crop production in Britain. Phil. Trans. R. Soc., London, Series B, 281: 277-294.

Morduch J (2004) “Micro-insurance: the next revolution?”, in: What have we learned about poverty, Banerjee a, Benabou R, Mookherjee D, eds. Oxford University Press
Papale D, Reichstein M, Aubinet M, Canfora E, Bernhofer C, Longdoz B, Kutsch W, Rambal S, Valentini R, Vesala T, Yakir D (2006) “Towards a standardized processing of Net Ecosystem Exchange measured with eddy covariance technique: algorithms and uncertainty estimation”, Biogeosciences, 3, 571-583.

Pierro R (2008?) “Micro-insurrance & disaster risk reduction: challenges and opportunities in the context of climate change”, Report Christian Aid, www.climategovernance.org.

Pierro R and Desai B (2008?) “The potential role of disaster insurance for disaster risk reduction and climate change adaptation”, Report Christian Aid.

Reichstein M, Falge E, Baldocchi D, Papale D, Aubinet M, Berbigier P, Bernhofer C, Buchmann N, Gilmanov T, Granier A and others (2005) “On the separation of net ecosystem exchange into assimilation and ecosystem respiration: review and improved algorithm”, Global Change Biology (11) 1424-1439.

Rosema A, Snel JFH, Zahn h, Buurmeijer WF, Van Hove LWA (1998b) The Relation between Laser-Induced Chlorophyll Fluorescence and Photosynthesis. Remote Sens. Environ. 65: 143-154.

Roth j, McCord MJ, Berold R (2008) “Agricultural microinsurance, global practices and prospects”, The MicroInsurance Centre, LLC, 1045 N. Lynndale Drive, Ste. 2A5; Appleton, WI 54914, USA.

Slabbers PJ, Sorbello Herrendorf V, Stapper M (1979) Evaluation of simplified water-crop yield models. Agric Water Managm 2:95-129.

Stewart JI, Hagan RM, Pruit RJ, Hanks RJ, Riley JP, Danielson WT, Franklin WT, Jackson EB (1977) Optimizing crop production through the control of water and salinity levels in the soil, Technical report, Utah Research Laboratory, Utah State University, Logan.

Stewart, J.I.and R.M. Hagan (1973) "Functions to predict effects of crop water deficits", ASCE J. Irrigation and Drainage Division 99, p. 421-439.

Supit I., A.A. Hooijer, C.A. van Diepen (1994)"System description of the WOFOST 6.0 crop simulation model implemented in CGMS. Volume 1: Theory and Algorithms", EUR 15956, Office for Official Publications of the European Communities, Luxembourg.1994-146 pp. cat.no: CL-NA-15956-EN-C.

Veenendaal EM, Kolle O and Lloyd J (2004) “Seasonal variation in energy fluxes and carbon dioxide exchange for a broad leaved semi-arid savannah (Mopane woodland) in southern Africa”, Global Change Biology, 10, 318–328, 2004.

Warner K, Ranger N, Surminski S, Arnold M, Linnerooth-Bayer J, Michel-Kerjan E, Kovacs P, Herweijer C (2009) “Adaptation to climate change: Linking disaster risk reduction and insurance”, United Nations International Strategy for Disaster Reduction Secretariat (UNISDR), Palais des Nations, CH-1211 Geneva 10, Switzerland.

ANNEX A: FESA VALIDATION OF EWBMS CLIMATIC DATA

The validity of the EWBMS climatic monitoring system and the products generated is assessed by comparison with independent ground measurements. It was however difficult to find good quality ground data for this purpose because of the low density of the network of climatic stations in Africa. Therefore, some data from locations in Europe were used as well.

Using data from a single site for satellite validation can pose serious problems because of measurement uncertainties in the ground data and the heterogeneity of the ground surface within one pixel. Field measurements are usually point data, while the satellite derived EWBMS products consist of much larger satellite pixels of 3x3 km for MSG and 5x5 in the case of MFG. Both, point measurements in the field and EWBMS satellite derived data have their own limitations. Therefore, perfect correspondence between field measurements and EWBMS pixel values cannot be expected. Results of the validation are presented, focussing on the ability of the EWBMS to reliably derive the variables and energy fluxes that determine the relative evapotranspiration as agricultural drought measure.

In section A.1 the EWBMS observation height air temperature data are compared with the readily available air temperature data from the Global Telecommunications System (GTS). These data were first extracted from our GTS database for several years in Tanzania, Burkina Faso and Ghana. However after a first data quality assessment it was decided not to use this dataset because of the limited geographical coverage, the many data gaps and evidently erroneous values. Instead an extensive and dense dataset of GTS observation height air temperatures, covering Spain, Portugal and a part of Morocco and Algeria were used for the evaluation.

Ground data on radiation were obtained from the World Radiation Data Centre in St. Petersburg, Russia and compared with EWBMS results for two sites in Africa, one in the Sahara in the South of Algeria during 1995 to 2007 and one at Mount Kenya for 2004 to 2007. The data owners of 2 CARBOAFRICA flux tower sites (Reichstein M. et al., 2005) provided sensible and latent heat fluxes data along with radiation data. One station is located in Botswana and has data for 1999, 2000 and 2001 (Veenendaal et al., 2004). and one station is located in Sudan with data for 2005, 2007 and 2008 (Ardo et al., 2008). In addition FLUXNET Marconi conference gap-filled flux and meteorology data from 12 European sites of the period 1996 to 1999 were used to evaluate the EWBMS sensible and latent heat fluxes in France, Netherlands, Italy, Sweden, UK, Denmark, Belgium and Germany. Results of the comparison of radiation are presented in section A.2 and the evaluation of sensible and latent heat is discussed in section A.3.

A.1 Validation of air temperature

Daily averaged observation height air (oha-) temperature data from the WMO-GTS are compared to corresponding EWBMS pixels with a grid size of 0.04^{o}. The oha-temperatures are measured with a sensor that is placed between 1,2 and 2 meter above the surface and is protected from precipitation and sunlight by a white painted louvered box. The EWBMS daily average oha-temperatures are derived from the

Figure A.1: Location of the 87 GTS oha-temperature stations used for comparison

EWBMS surface temperature and boundary layer air temperature outputs as discussed in section 3.2.4. In this section the oha-temperatures obtained from Meteosat are compared with those measured on the ground and reported through the WMO-GTS system. In a first attempt, GTS oha-temperatures in Tanzania, Burkina Faso and Ghana were selected for comparison with EWBMS results. After a data quality assessment it soon became clear that this dataset was not suitable because of the low geographical coverage, many data gaps and erroneous values. Therefore it was decided to do the comparisons with the data from stations in Spain, Portugal, Algeria and Morocco. Figure A.1 shows the geographic distribution of the 87 GTS stations that were finally selected for the analysis. Only data from stations that report at least every six hours on a daily regular basis were retained for the comparison. Incomplete data series, locations nearby the sea and mixed pixels were excluded from analysis. Standard statistical procedures were applied to check for normality and for removal of outliers. A scatter plot of all satellite derived and ground measured temperatures during 2008 is shown in figure A.2.

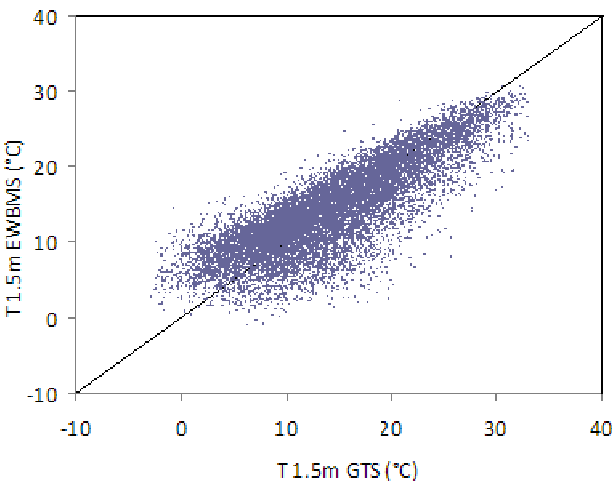

Figure A.2: GTS versus EWBMS observation height air temperatures

Table A.1: Average difference, RMSD and correlation of oha-temperature in 2008

	Δ ($T_{1.5m, EWMS}$-$T_{1.5m, ground}$)			RMSD	R
	avg	min	max		
Daily average temperature	+0.01	-2.07	4.14	3.64	0.83
10 Daily average temperature	-0.03	-2.16	4.14	2.31	0.94

Table A.2: Average difference, RMSD and correlation of oha-temperature by season

	Daily temperature			10 daily average temperature		
	Δ	RMSD	R	Δ	RMSD	R
spring	-1.03	3.82	0.70	-1.03	2.44	0.81
summer	-1.24	3.29	0.74	-1.24	2.06	0.90
autumn	0.93	3.77	0.74	0.93	2.33	0.92
winter	1.39	3.74	0.53	1.38	2.37	0.77

Δ = average difference T_{EWBMS}-T_{GTS}.

The summary statistics of the oha-temperature comparison are presented in table A.1 and A.2. In 2008 the average difference on a daily basis is 0.01 °C, the rms-difference is 3.64°C and the correlation coefficient is 0.83. For 10-daily averaged temperatures, the average difference changes to -0.03°C, the RMSD reduces to 2.31°C and the correlation coefficient increases to 0.94. For the daily temperatures the rms-error of the individual stations varies between 2.92°C and 5.18°C and correlation coefficient varies between 0.71 and 0.89. The differences are small and randomly distributed with 51% of the differences being positive and 49% of the differences being negative. Overall agreement between the ground data and EWBMS temperatures is good. In Appendix A the summary statistics are provided for each station.

The results indicate that the 10-daily GTS and EWBMS temperatures show less random difference than the daily data. For this reason we use the 10-daily moving averages of the EWBMS temperature as input for the crop growth model. In summer and autumn, the correspondence with ground temperatures is better than in spring and winter (table A.2). Examples of time series for 2 locations are presented in figures A.4 and A.5. The graphs show fairly good agreement between GTS and EWBMS measured oha- air temperature.

Finally it should be noted that this comparison mainly serves to show that the EWBMS system reproduces climatic changes fairly well. Sometimes there are notable differences. What matters for the calculation of the evapotranspiration, RE and the consequent effects on crop growth and RY, is not the absolute value of the -temperature at observation height, but the difference in temperature between the surface and the atmospheric boundary layer. This difference is derived from the satellite data in a consistent way. First noon and midnight surface temperature are mapped. Then the average surface temperature and the boundary layer air temperature are derived from the previous two (see sections 2.2.3-4). Finally the difference between the average surface temperature and the boundary layer temperature is obtained and used in the calculation of the actual evapotranspiration rate (sections 2.2.6-7, equations 13 and 14). This temperature difference is determined with a single instrument, in an internally consistent way and will therefore show relatively little error.

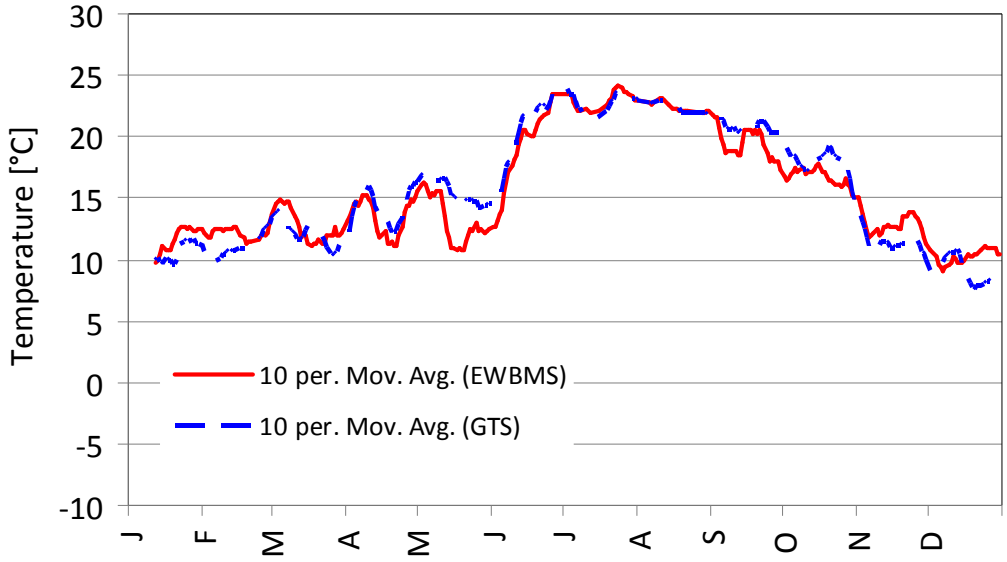

Figure A.3: Comparison between ten daily moving averages of EWBMS and GTS observation height air temperature in 2008 Evora, Portugal.

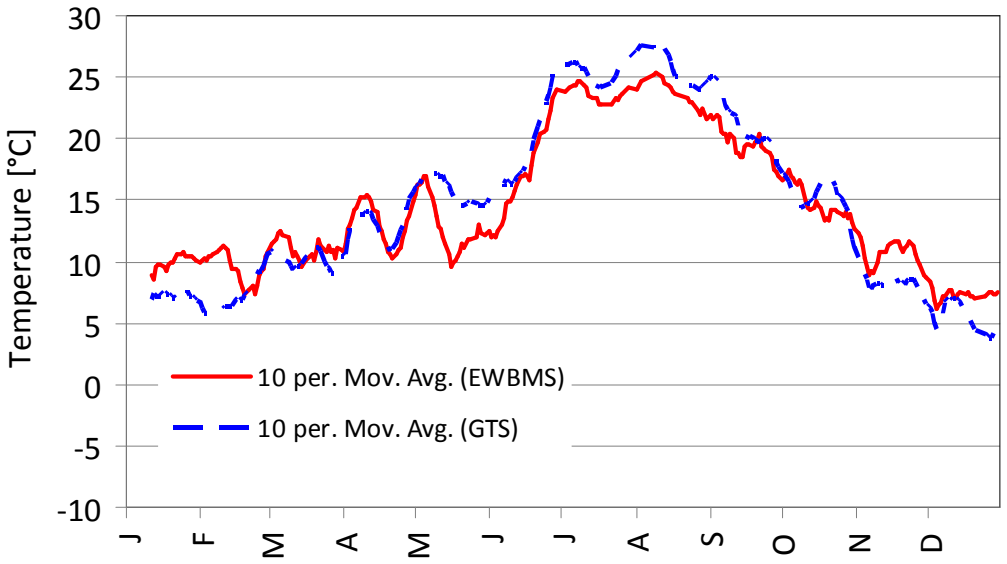

Figure A.4: Comparison between ten daily moving averages of EWBMS and GTS observation height air temperature at Madrid, Spain

Table A.3: Summary statistics for comparison of ground and satellite 1.5 m air temperature at 47 stations in Spain, Portugal and surroundings during 2008

GTS n°	country	station name	latitude	longitude	altitude	daily			10 daily average		
						Δ (°C)	RMSE (°C)	R	Δ (°C)	RMSE (°C)	R
7607	France	MONT DE M	43.92	-0.50	60	-0.29	3.79	0.76	-0.38	2.48	0.91
7621	France	TARBES OS	43.18	0.00	364	0.26	3.54	0.76	0.19	2.22	0.92
7627	France	ST GIRONS	43.00	1.10	412	0.48	4.05	0.71	0.39	2.75	0.88
7630	France	TOULOUSE	43.63	1.37	154	-0.31	3.88	0.77	-0.37	2.33	0.93
8055	Spain	LEON	42.58	-5.65	914	0.27	3.34	0.84	0.19	2.12	0.94
8075	Spain	BURGOS	42.37	-3.63	891	-0.03	3.27	0.85	-0.06	1.96	0.95
8080	Spain	VITORIA	42.88	-2.72	510	-0.25	3.48	0.79	-0.31	2.20	0.91
8084	Spain	LOGRONO	42.45	-2.33	363	-0.93	3.76	0.81	-1.00	2.40	0.92
8085	Spain	PAMPLONA/NOAIN	42.77	-1.63	453	-1.43	4.16	0.79	-1.49	2.94	0.91
8094	Spain	HUESCA/MO	42.08	-0.33	554	-0.59	3.99	0.85	-0.65	2.60	0.96
8130	Spain	ZAMORA	41.50	-5.75	660	0.80	3.96	0.75	0.77	2.44	0.89
8140	Spain	VALLADOLID/VILLANUBLA	41.72	-4.85	846	0.15	3.52	0.85	0.11	2.29	0.94
8141	Spain	VALLADOLID	41.65	-4.77	739	0.69	3.74	0.83	0.66	2.41	0.93
8160	Spain	SARAGOSSA	41.67	-1.02	258	-1.07	4.28	0.80	-1.17	2.65	0.93
8171	Spain	LLEIDA	41.62	0.63	199	-0.98	4.41	0.82	-1.08	2.95	0.96
8202	Spain	SALAMANCA	40.95	-5.50	795	0.84	3.48	0.86	0.81	2.24	0.95
8210	Spain	AVILA	40.65	-4.70	1131	1.28	3.66	0.85	1.26	2.33	0.94
8213	Spain	SEGOVIA	40.95	-4.12	1006	0.16	3.48	0.86	0.16	1.96	0.96
8215	Spain	NAVACERRADA	40.78	-4.02	1888	4.14	5.18	0.89	4.14	4.55	0.96
8221	Spain	MADRID	40.45	-3.55	582	0.12	3.75	0.84	0.05	2.24	0.96
8223	Spain	MADRID/CUATRO VIENTOS	40.38	-3.78	687	-0.55	3.33	0.88	-0.59	2.08	0.97
8224	Spain	MADRID/GETAFE	40.30	-3.72	617	-0.80	3.69	0.85	-0.88	2.47	0.95
8261	Spain	CACERES	39.47	-6.33	405	-0.56	3.65	0.83	-0.58	2.17	0.95
8272	Spain	TOLEDO	39.88	-4.05	516	-1.22	3.88	0.84	-1.29	2.70	0.94
8280	Spain	ALBACETE	38.95	-1.85	704	0.11	3.76	0.84	0.04	2.32	0.95
8330	Spain	BADAJOZ/T	38.88	-6.82	192	-0.88	3.55	0.85	-0.91	2.26	0.96
8391	Spain	SEVILLA	37.42	-5.90	31	-2.07	4.12	0.79	-2.16	3.03	0.93
8397	Spain	MORON DE LA FRONTERA	37.15	-5.62	88	-1.55	3.65	0.83	-1.60	2.48	0.95
8410	Spain	CORDOBA	37.85	-4.85	92	-1.07	3.91	0.83	-1.10	2.62	0.95
8419	Spain	GRANADA	37.18	-3.78	570	1.21	3.77	0.84	1.19	2.55	0.95
8451	Spain	JEREZ	36.75	-6.07	28	-0.46	3.42	0.82	-0.45	1.98	0.94
8548	Portugal	COIMBRA/C	40.15	-8.47	179	-0.25	3.07	0.76	-0.21	1.46	0.92
8558	Portugal	EVORA/C.	38.53	-7.90	246	-0.16	3.05	0.82	-0.15	1.49	0.95
8560	Portugal	VISEU	40.72	-7.88	644	0.82	2.92	0.85	0.82	1.46	0.97
8561	Portugal	BEJA/B. A	38.07	-7.92	203	0.25	3.07	0.81	0.23	1.72	0.94
8562	Portugal	BEJA	38.02	-7.87	247	0.23	3.08	0.80	0.23	1.65	0.93
8567	Portugal	VILA REAL	41.27	-7.72	562	0.66	2.96	0.85	0.64	1.62	0.95
8568	Portugal	PENHAS DO	40.42	-7.55	1388	3.20	4.23	0.88	3.19	3.46	0.97
8570	Portugal	CASTELLO	39.83	-7.48	384	0.10	2.95	0.85	0.10	1.41	0.96
8571	Portugal	PORTALEGR	39.28	-7.42	590	0.43	3.41	0.81	0.41	1.55	0.95
8575	Portugal	BRAGANCA	41.80	-6.73	692	0.50	2.96	0.86	0.46	1.60	0.96
60430	Algeria	MILIANA	36.30	2.23	721	-0.44	3.56	0.88	-0.46	2.11	0.96
60437	Algeria	MEDEA	36.28	2.73	1036	1.04	3.93	0.89	0.98	2.51	0.97
60511	Algeria	TIARET	35.35	1.47	978	0.11	3.84	0.89	0.06	2.50	0.97
60514	Algeria	KSAR CHELLALA	35.17	2.32	801	-1.19	4.22	0.89	-1.24	3.16	0.97
60520	Algeria	SIDI-BEL-ABBES	35.20	-0.62	476	-0.40	3.23	0.89	-0.41	2.09	0.96
60531	Algeria	TLEMCEN	35.02	-1.47	247	0.02	3.31	0.85	0.01	1.84	0.95

A.2 Validation of radiation

The World Radiation Data Centre (WRDC) in St Petersburg, Russia, recognized by the World Meteorological Organisation (WMO), publishes solar radiation data collected from the world radiometric network on its website. Two sites in Africa, one in Algeria and one in Kenya were selected for comparison with EWBMS radiation data. Solar radiation data for one site in Algeria and one site in Kenya were used for the validation of the EWBMS radiation data.

The first site is Tamanrasset (22.78°N, 5.52°E), located in the Ahaggar Mountains highland region in central Sahara, southern Algeria. A complete dataset of global radiation measurements is available for the period 1995 until 2007. The second location is near the top of Mount Kenya (0.062°S, 37.30°E), in central Kenya at an elevation of 3678 m. The vegetation on the site is dominated by mosaic forest, shrub land and chaparral plant communities. Here global radiation data are available for the period 2004 until 2007 but many gaps in the dataset are present. Also from the CARBOAFRICA data set, discussed in more detail in section A.3.1, global radiation measurements were available at Demokeya, Central Sudan, and Mayn, Botswana,

Exclusion of erroneous measurements is an important part of the data quality control process. It ensures that the data comparison does not suffer from a bias or errors due to obvious or common reasons. In a first step, erroneous data were removed for one of following reasons: energy imbalance, data outside tolerance range, instrument malfunction, heavy precipitation, etc. Daily averages of global solar radiation data, as measured on the ground, were then compared to the corresponding EWBMS global radiation data, extracted from the data fields for single pixels corresponding to the locations of the 4 stations.

Table A.3 shows the yearly average difference, the correlation coefficient and the rms-error for the daily average global radiation data at the 4 sites. The results are good. A very good correspondence between ground and EWBMS global radiation is observed at Mount Kenya, the station that is nearest to the FESA pilot areas.

Figure A.5 shows a scatter plot of the data measured at the Mount Kenya station for the period January 2005 until December 2007. The dataset in the plot consists of 364 data points. The comparison between EWBMS and CM11 global radiation at Mount Kenya shows that the satellite derived values and the values measured in the field are consistent. The relationship for the entire dataset investigated exhibits a Pearson's correlation coefficient of 0.91, an average difference of 9 W.m-2 and a RMSD of 32 $W.m^{-2}$ (16%) for the daily data. The discrepancies between the observed and modelled values are minor with absolute differences in magnitude larger than 70 $W.m^{-2}$ in only 3% of the cases.

Table A.3:Average difference, RMSD and correlation of global radiation by station

	Δ $W.m^{-2}$	RMSD $W.m^{-2}$	RMSD %	R	period
Tamanrasset	8	36	13	0.88	1995, 2004-2007
Mount Kenya	9	32	16	0.91	2005-2007
Demokeya	26	48	18	0.71	2005, 2007-2008
Maun	20	45	18	0.84	1999-2000

Δ = average difference Rg_{EWBMS}-Rg_{WRDC}.

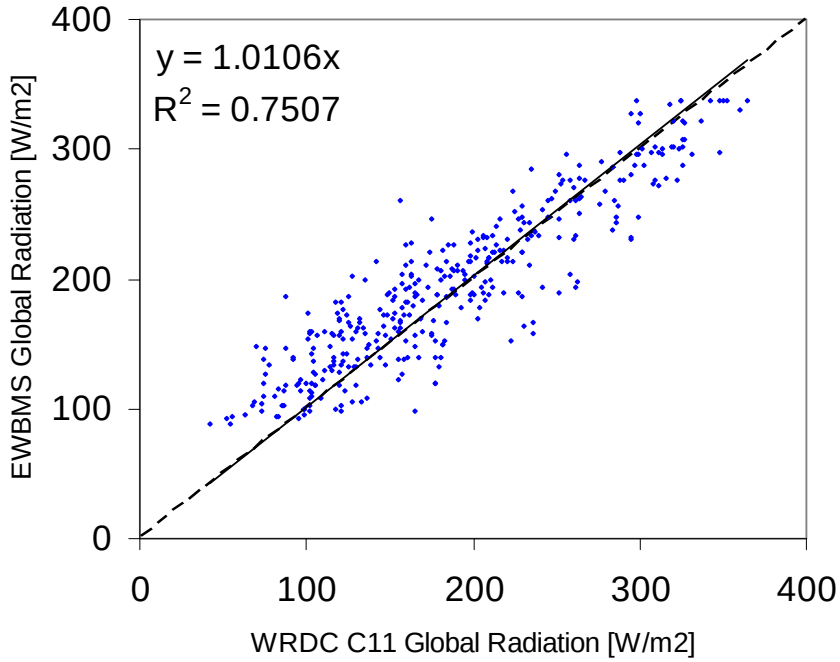

Figure A.5: Daily averaged global radiation measured by C11 (WRDC) versus EWMBS global radiation (2005-2007) at Mount Kenya

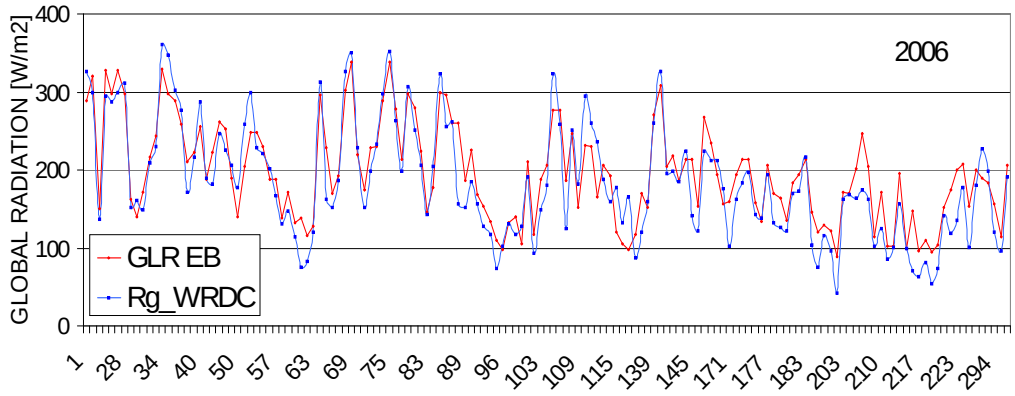

Figure A.6: EWBMS (red) and WRDC (blue) global radiation time series at Mount Kenya in 2006

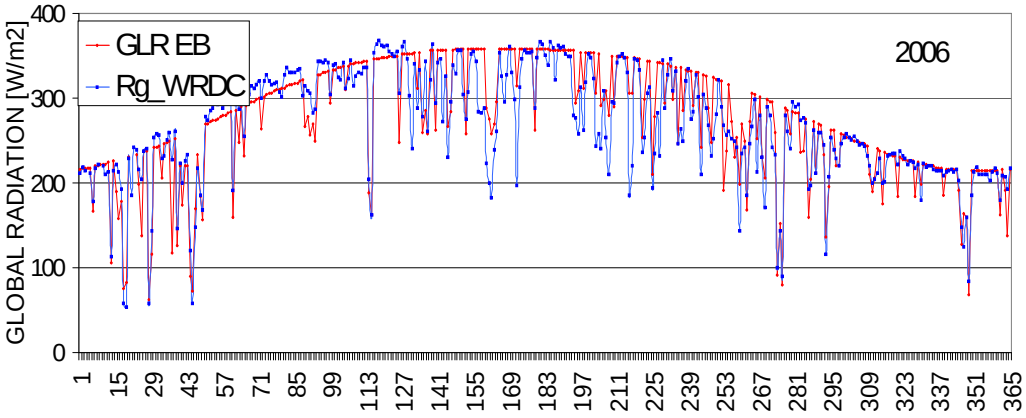

Figure A.7: EWBMS (red) and WRDC (blue) global radiation time series at Tamanrasset in 2006

Figures A.6 and A.7 show two examples of time series of daily average global radiation as measured at the WRDC ground stations Mount Kenya and Tamanrasset (in blue) and as derived from Meteosat with the EWBMS system (in red) during 2006. Differences in global radiation do not necessarily have their origin in the EWBMS, but could as well be caused by slight errors or drift in the calibration of the radiometer. They could also be caused by slight tilt of a sensor, or by pyranometer heating due to radiation. Degradation by a few tenths of a percent per year was observed by Alados et al. (1999) in the CM11 pyranometers.

A.3 Validation of sensible heat flux

In this section the daily averaged eddy correlation data from the CARBOAFRICA flux towers and from the 11 FLUXNET towers in Europe are compared to the corresponding daily EWBMS sensible heat fluxes, with a block size of 3*3 pixels.

A.3.1 Validation with CARBOAFRICA data

Sensible and latent heat flux data, based on eddy covariance measurements at two CARBOAFRICA flux tower sites (Reichstein M. et al., 2005) were obtained One CARBOFLUX station is located in Sudan and can provide data for 2005, 2007 and 2008. The other one is located in Botswana and has data for 1999, 2000 and 2001 (see Ardo et al., 2008).

The first site Demokeya (13°16’ N, 30°28’ E), is located in Kordofan, central Sudan, approximately 35 km north east of the town El Obeid. The savannah ecosystem is characterized by a sparse Acacia plantation with a canopy cover of 5–10% and a ground cover composed mainly of perennial grasses and some herbs. Average annual temperature is 26°C and average annual rainfall is 320 mm. Measurements are available for the years 2005, 2007 and 2008.

The second flux tower is located 20 km north east of Maun (19°55’ S, 23°34’ E) at the southern edge of the Okavango Delta in northern Botswana. The ecosystem is characterized by broadleaf, raingreen savannah woodlands dominated by Colophospermum mopane, the typical woodland species of Southern Africa with a canopy of approximately 8m tall and a sparse under story of grasses and herbs during the rainy season (Arneth et al., 2006, Veenendaal et al., 2004). Average annual temperature is 22°C and average annual rainfall is 464 mm. Measurements are available for the years 1999 to 2001.

The data were first quality controlled. Data with energy imbalances larger than 20% were removed. Only data on days where more than 66% of the half hourly eddy flux reports were available have been evaluated. The final dataset at Maun then consists of 674 data points and at Demokeya of 538 data points.

Figure A.8 shows the EWBMS daily sensible heat flux plotted against the eddy correlation results. The comparison shows that EWBMS and eddy correlation derived sensible heat fluxes are consistent. For the 1999-2000 Maun dataset, the relationship exhibits a Pearson correlation coefficient of 0.55, an average difference of -1 $W.m^{-2}$ and a RMSD of 21 $W.m^{-2}$. The errors are random and observed differences on a daily basis are balanced well with 52% of the differences being positive and 47% of the differences being negative. The relationship with the Demokeya dataset exhibits a

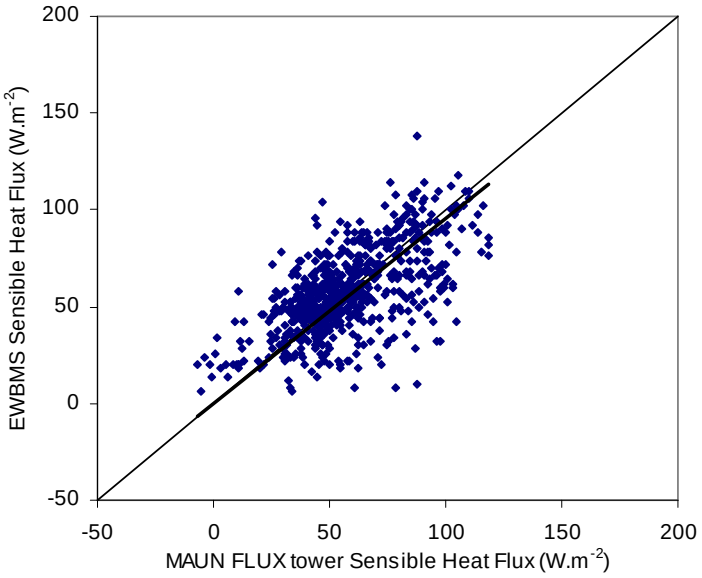

Figure A.8: Daily averaged sensible heat flux measured at Maun, Botswana in 1999 and 2000 versus EWMBS sensible heat flux

Pearson correlation coefficient of 0.41, an average difference of 1 $W.m^{-2}$ and a RMSD of 20 $W.m^{-2}$. The errors are random and observed differences on a daily basis are balanced well with 55% of the differences being positive and 45% of the differences being negative.

Figures A.9 and A.10 show the time series of the daily EWBMS sensible heat flux (in red) along with the sensible heat flux derived through eddy correlation from measurements on the CARBOAFRICA tower at Maun, Botswana (in blue) in 1999 and 2000, respectively. Accurate representation of the sensible heat flux across a landscape from measurements at a single tower remains difficult to achieve. The footprint of the eddy correlation measurement is much smaller than an EWBMS grid cell. Furthermore, distortions of the measured fluxes by the anemometer itself can also partially explain why considerable differences may occur between both measurements. Keeping this in mind, the EWBMS sensible heat flux data correspond quite well with the ground measured data. The averages are the same over larger time periods and no bias between the EWBMS and ground data is observed.

A.3.2 Validation with Marconi FLUXNET data

FLUXNET data were obtained, processed and gap-filled according to the recommendations of the Marconi conference (Falge et al. 2005). They are used to evaluate the EWBMS sensible and latent heat flux data in France, Spain, Belgium and Germany. These data come from 12 European sites in the period 1996 to 1999. Some site information is presented in table A.4.

The average temporal data coverage for these sites during one year is 65%. The data have standardized procedures for gap filling and data aggregation to day and night, weekly, monthly, and annual periods. Some meteorology data were also gap filled to support flux estimating methods and are reported along with non-filled meteorological data. The dataset is available free of charge on the Fluxnet website (http://daac.ornl.gov/FLUXNET/). Sensible and latent heat flux data from 12

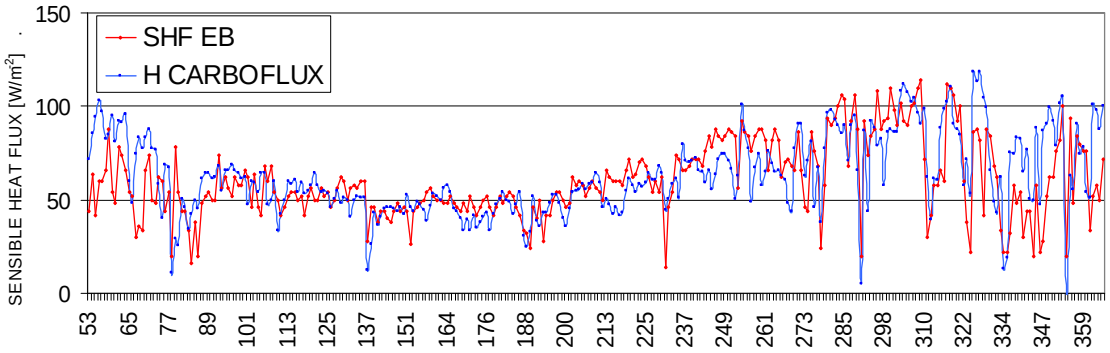

Figure A.9: Daily EWBMS (red) and CARBOFLUX sensible heat flux (blue) at Maun, Botswana in 1999

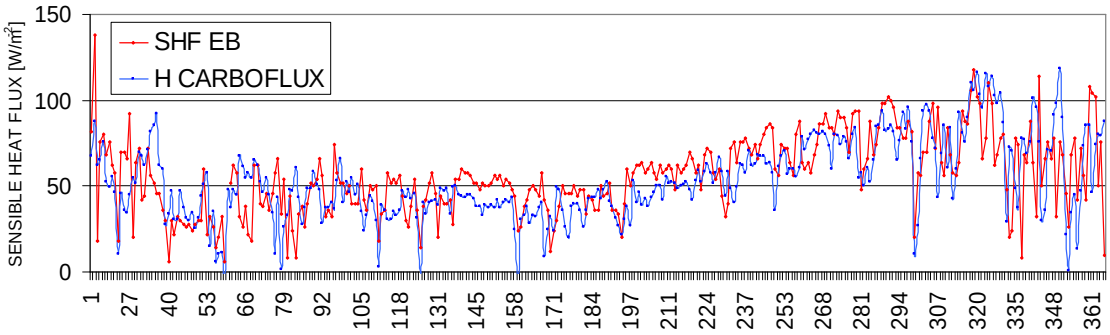

Figure A.10: Daily EWBMS (red) and CARBOFLUX sensible heat flux (blue) at Maun, Botswana in 2000

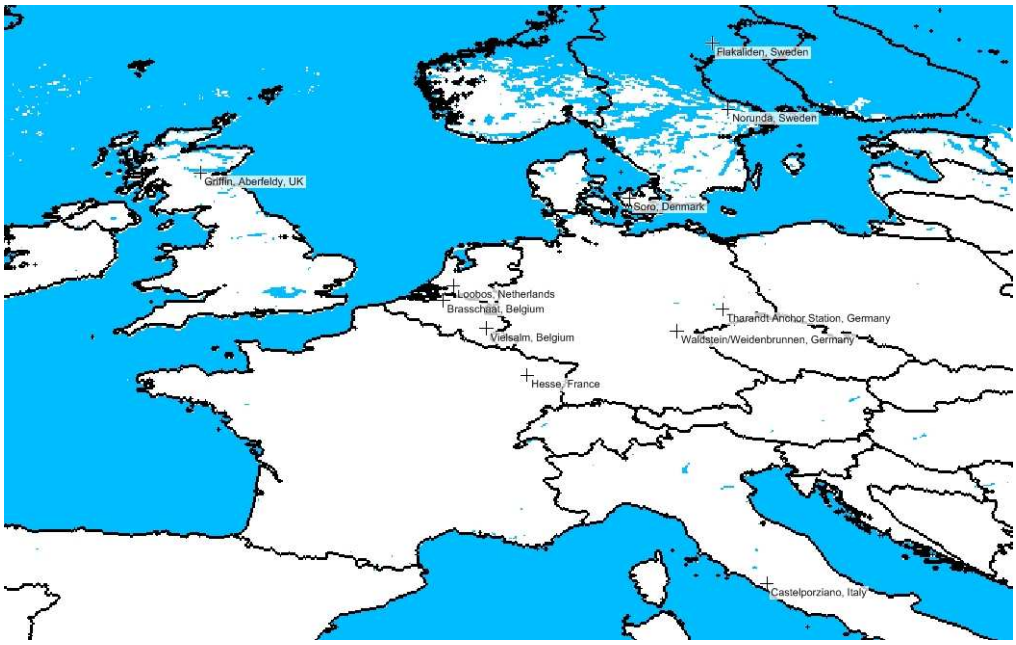

Figure A.11: Location of the Marconi conference flux towers (Falge et al. 2005) of the data are used for validation of EWBMS fluxes

Table A.4: Site information 11 European FLUXNET towers involved in the validation

Site name	Country	Lat	Long	Climate	Forest type
Brasschaat (De Inslag forest)	BE	51.31	4.52	Mediterranean	Mixed
Vielsalm	BE	50.31	6.00	Temperate	Mixed
Tharandt Anchor Station	GE	50.96	13.57	Mediterranean	Evergreen needleleaf
Waldstein/WeidenBrunnen	GE	50.14	11.87	Mediterranean	Evergreen coniferous, spruce
Soro (LilleBogeskov)	DK	55.49	11.65	Mediterranean	Mixed
Hesse	FR	48.67	7.06	Mediterranean	Deciduous broadleaf
Castelporziano	IT	41.71	12.38	Mediterranean	Evergreen broadleaf
Loobos	NL	52.17	5.74	Temperate	Evergreen needleleaf
Flakaliden	SW	64.11	19.46	Boreal	Evergreen coniferous
Norunda	SW	60.09	17.50	Boreal	Evergreen coniferous
Griffin, Aberfeldy	UK	56.61	-3.80	Mediterranean	Evergreen coniferous

Table A.5: Yearly average differences, RMSD and correlations of 10 daily average sensible heat flux during the months June, July and August for the European flux stations

Station name	Country	Year	10 Daily average		
			Δ	RMSD	R
			W.m-2	W.m-2	
Brasschaat (De Inslag Forest)	Belgium	1996	-15.72	18.05	0.97
		1997	5.12	16.67	0.70
		1998	17.83	24.95	0.70
Flakaliden	Sweden	1996	1.46	11.81	0.37
		1997	3.43	10.25	0.49
		1998	-0.20	9.60	0.77
Hesse	France	1996	16.39	20.78	0.52
		1998	20.25	29.80	0.34
		1999	31.59	33.40	0.35
Loobos	Netherlands	1996	1.74	15.67	0.03
		1997	-3.30	16.45	0.61
		1998	14.21	20.09	0.57
Norunda	Sweden	1996	-4.55	15.85	0.40
		1997	-13.04	19.46	0.85
		1998	11.22	15.09	0.44
Soro (LilleBogeskov)	Denmark	1996	2.38	20.55	0.43
		1997	-5.25	13.54	0.58
		1998	14.28	21.29	0.44
		1999	13.86	19.84	0.61
Tharandt Anchor Station	Germany	1996	11.81	18.99	0.03
		1997	1.61	12.32	0.31
		1998	0.64	14.76	0.34
		1999	2.24	11.93	0.58
Vielsalm	Belgium	1996	8.64	9.59	0.87
		1998	11.77	14.89	0.56
Waldstein/ WeidenBrunnen	Germany	1996	-21.43	26.84	0.18
		1997	6.41	14.97	0.72
		1998	19.62	25.30	0.79
Griffin, Aberfeldy	UK	1998	-13.26	18.22	0.81
Castelporziano	Italy	1997	-30.11	32.66	0.91

Δ = average difference in sensbible heat flux derived from satellite with the EWBMS system and measured at the FLUXNET towers.

European sites for the period 1996 to 1999 were selected for evaluation of EWBMS data in France, Netherlands, Italy, Sweden, UK, Denmark, Belgium and Germany. The location of these sites is shown in figure A.11.

Table A.5 presents an overview of the results of comparing the EWBMS sensible heat fluxes with those measured at the European FLUXNET sites during the months June, July and August. Reasonable good correspondences are seen between the European flux tower data and the EWBMS sensible heat fluxes for various stations. In some cases the differences were larger, which can partially be explained by sensor errors and the effects of surface heterogeneity.

Figure A.12 and A.13 provide two examples of time graphs of both data sets, one at the Tharandt anchor station in Germany and the other one from the Norunda station in Sweden. The average difference for all locations and years involved is 3 W.m-2, relatively small compared to the daily average sensible heat flux (37 W.m-2) of all stations involved. The errors are random and observed differences on a daily basis are balanced equally with EWBMS observations in 44% of the cases lower and in 56% of the cases larger than the eddy correlation measurements. Even when correlation on a daily basis is quite low at some locations, the sensible heat flux results are still good for unbiased estimations of evapotranspiration on a 10-daily basis, as used for crop yield simulation and monitoring.

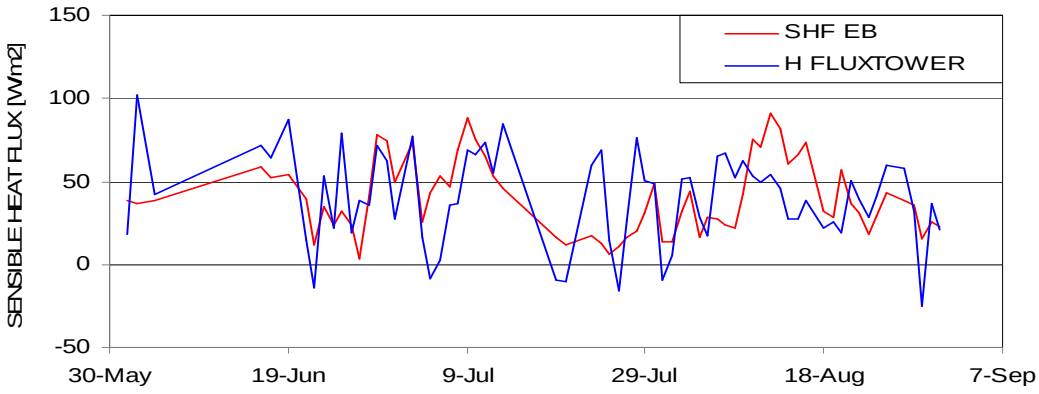

Figure A.12: Daily EWBMS (red) sensible heat flux and flux tower sensible heat flux (blue) at Tharandt Anchor Station, Germany in 1997

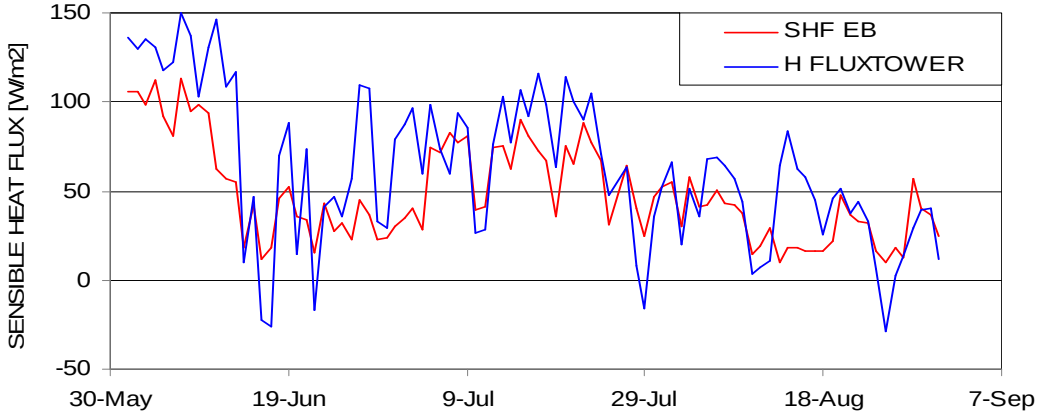

Figure A.13: Daily EWBMS (red) sensible heat flux and flux tower sensible heat flux (blue) at Norunda, Sweden (bottom) in 1997

An accurate representation of the sensible heat flux across a landscape from the measurements at a single tower is not possible. The footprint of the eddy correlation measurement is still much smaller than the EWBMS pixel, and varies with the wind direction. Furthermore, distortions of the measured fluxes by the anemometer itself may also occur. Given the complexity and limitations of the measurements the EWBMS satellite derived sensible heat flux compares quite well with the fluxes measured on the ground by eddy correlation.

A.4 Conclusion

In section A.1-3 we have compared EWBMS Meteosat derived data fields of temperature, radiation and sensible heat flux with similar point measurements made on the ground at various locations in Africa and Europe. Overall good correlations and small average differences were found. On a daily basis random differences can be quite large, which is to be attributed to the considerable differences in the footprint and method of both measurements. Such differences largely disappear when working with 10 daily moving averages. Given the fact that the satellite derived temperature, radiation and sensible heat flux data correspond well with ground observations and can be considered valid, we may also conclude that the actual evapotranspiration will be valid, as this flux follows by subtraction of the sensible heat flux from the net radiation. Thus the results of this validation work show that the basic EWBMS climatic data, on which the agricultural drought monitoring, crop yield estimation and insurance is based, are reliable, consistent and unbiased.

In the next chapter the validation of crop yield assessments with the EARS Crop Growth Model on the basis of the EWBMS radiation and evapotranspiration data is carried out.

ANNEX B: FESA VALIDATION OF ECGM CROP YIELD ESTIMATES

Crop yields have been simulated with the ECGM according to the methodology discussed in chapter 3. The ECGM is capable of giving a value of the relative yield (RY) and difference yield (DY) at every moment of the growing season. Earlier research (*Rosema et al., 2001; Roebeling et al., 2004*) has shown that after 60-80 days of the growing season these values are highly correlated to end of season reported yields and can be used to make a crop yield forecast. Although at that time the most critical stages of crop development have passed, the final outcome may still be subject to some change depending on how the second half of the season proceeds. Therefore our current crop yield forecasting practice consists of making a first forecast after 80 days and then updating this forecast every 10 days. In this evaluation, EWBMS based agricultural drought indicators are presented and the ECGM yield estimates are evaluated by comparing the end of season EWBMS crop yields against reported statistical yields.

B.1 Validation data sources

Validation of the ECGM yield estimates is done by comparison with census yields collected through the FAOSTAT and COUNTRYSTAT web sites. FAOSTAT data (http://faostat.fao.org) cover area harvested, yield per hectare and quantity produced at national level for major crops in all African countries. At the sub-national level, COUNTRYSTAT data are available for a number of African countries and crops (http://www.fao.org/economic/ess/countrystat/en/). Data on harvested area are given in hectares, yields in hectogram/hectare and production data in tonnes. In addition a maize yield dataset for several locations in Tanzania covering the period 1991-2007 was available from Tanzania through MicroEnsure.

The comparison between the satellite derived and ground data is done by regression analysis. The scatter between the two data sets is usually considerable and due to inaccuracies in both data sources. Particularly in Africa the uncertainties in reported yield data can be considerable. For example, it has been observed that, for some countries, the same crop yield has been reported for a series of years in a row, which is unlikely. Lack of adequate funding, insufficient training, political unrest and natural hazards may give rise to incompleteness and insufficient quality of crop yield data, or may even cause relevant statistics to be missing for several years.

B.2 Validation of satellite derived crop yield

To arrive at satellite based crop yield estimates, the end-of-growing-season difference yields are first derived with the ECGM on a pixel-by-pixel basis for the whole region. Thereafter the data are combined with existing geographic information, in particular land use maps (figure B.1) and FAO crop growing areas (figure B.2), and are then selectively integrated to the district, province and country level, using the FAO Global Administrative Unit Layers division (GAUL 0,1,2). Thereafter the difference yields are converted to absolute yields according to equation (30) in section 3.9. The resulting absolute satellite derived yields are then plotted against national or provincial level reported yields. The root mean square difference (RMSD) and the correlation coefficient (r) are used as measure to evaluate the relationship between predicted and reported yields (Genovese, 1998). The satellite based yields were compared to the ground reported yields at the end of the growing season.

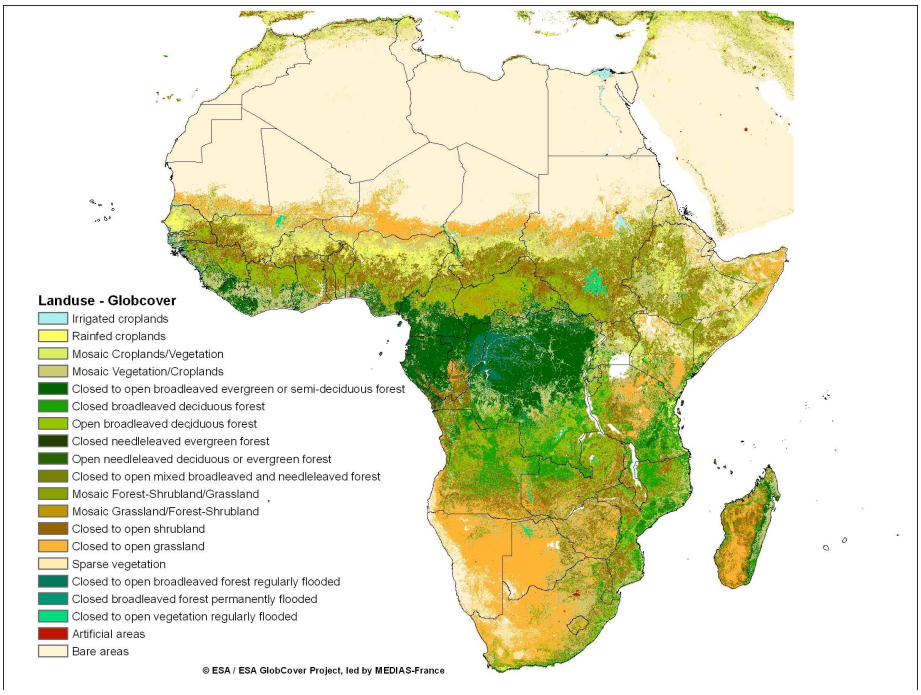

Figure B.1: Land use map (USGS-GLCC)

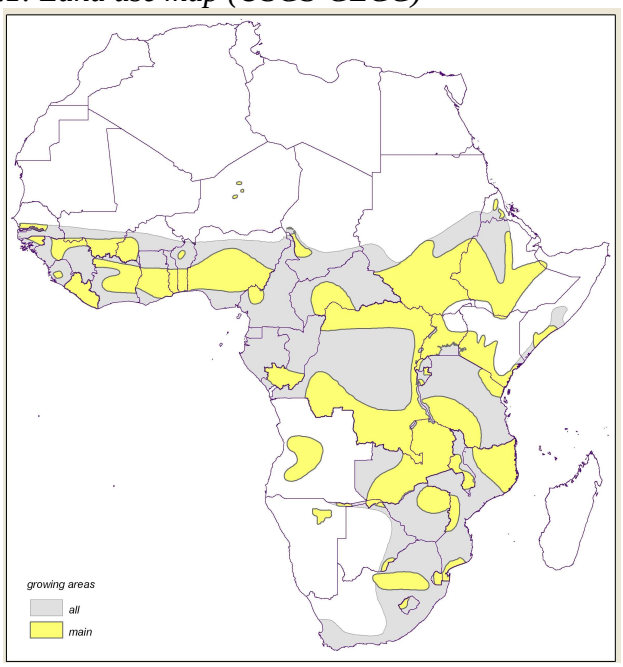

Figure B.2: Maize growing areas (FAO-GIEWS)

As land use information source, use has been made of the United States Geological Survey's Global Land Cover Characteristics database (http://edc2.usgs.gov/glcc). An overview of these data is shown in figure B.1. In addition use is made of the crop growing area maps, as available from FAO-GIEWS. The map for the crop growing areas of maize, as downloaded from the GIEWS website (http://www.fao.org/giews) is shown in figure B.2.

B.3 Crop yield validation results

B.3.1 West Africa

FAOSTAT reported national maize yields of 11 West African countries from 2002 to 2007 were compared to the ECGM estimates derived from Meteosat. Only national yield data were available and the satellite yield estimates hence were calculated with country average difference yields and historical reported yields from previous 5 years as described in the previous section. Maize data from following countries have been obtained: Benin, Burkina Faso, Cameroon, Cote d'Ivoire, Ghana, Guinea, Liberia, Nigeria, Senegal, Sierra Leone and Togo. The ground maize yield reports range from 743 kg/ha in Sierra Leone to 3000 kg/ha in Liberia with an average of 1700 kg/ha.

In figure B.3 the EWBMS maize yields are plotted against the FAOSTAT yields; the 1:1 line is added. In the plot three outliers are circled, which were all reports from Senegal (2002, 2004 and 2005). They were omitted from further analysis. The comparison results in an average difference of -4 kg/ha, an RMSD of 221 kg/ha and a Pearson correlation coefficient of 0.92. The differences are small and randomly distributed with 54% of the differences being positive and 46% of the differences being negative. Overall agreement between the national statistical ground yield reports and the ECGM satellite derived maize yield estimates in West African countries is good.

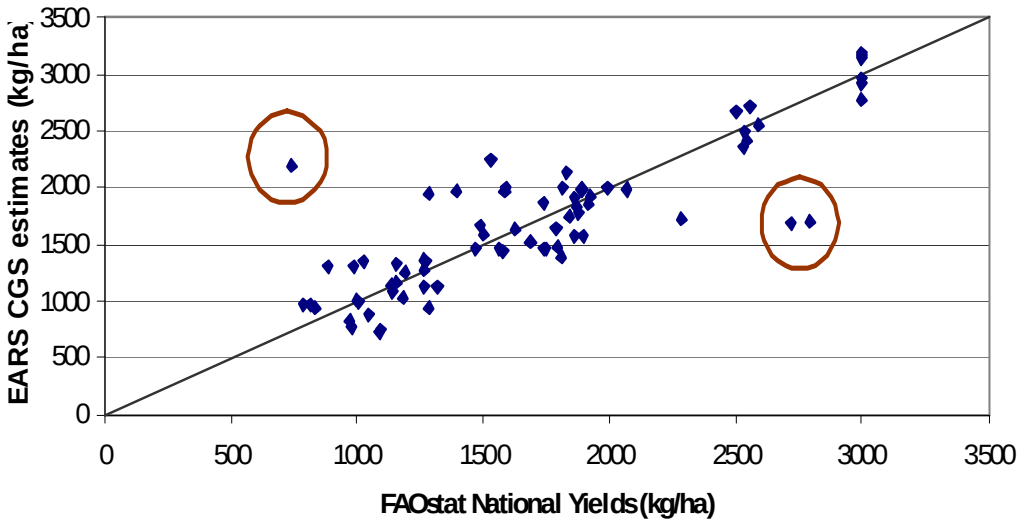

Figure B.3: ECGM maize yield forecast versus FAOSTAT reported maize yields for 11 West African countries from 2002 to 2007. Encircled data are outliers, reported from Senegal in 2002, 2004 and 2005. These were omitted in the further analysis.

B.3.2 Southern Africa

A similar comparison has been done with the FAOSTAT reported national maize yields of 10 countries in the Southern Africa region for the years 2003 to 2007. The reported maize yields in this dataset range from 182 kg/ha in Botswana to 3635 kg/ha in South Africa with an average of 1244 kg/ha. Maize yield data from following countries were used: Angola, Botswana, Lesotho, Malawi, Mozambique, Namibia, South Africa, Swaziland, Zambia and Zimbabwe.

In figure B.4 the ECGM satellite derived maize yields are plotted against the FAOSTAT ground reported yields. The 1:1 line is added. The comparison results in an average difference of 13 kg/ha, a RMSD of 265 kg/ha and a Pearson correlation coefficient of 0.95. The differences are small and randomly distributed with 56% of the differences being positive and 44% of the differences being negative. Overall agreement between the national statistical ground yield reports and the ECGM yield estimates in Southern African countries is good.

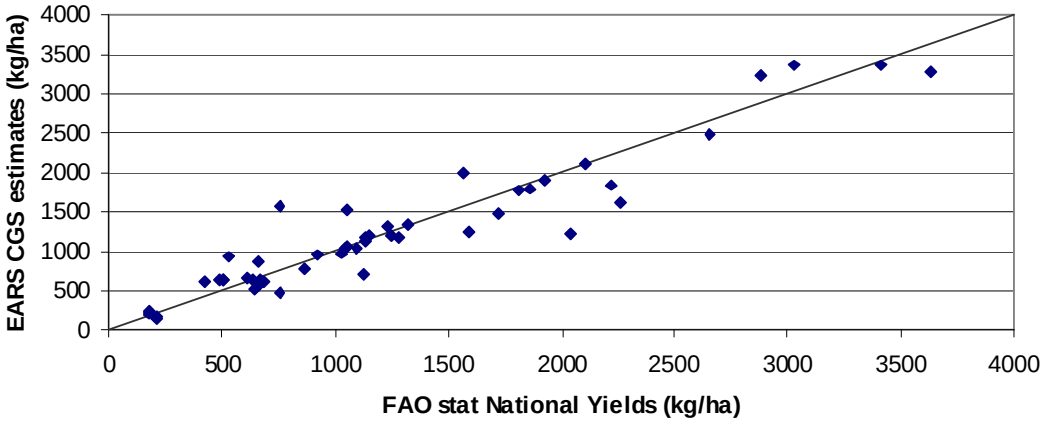

Figure B.4: ECGM satellite derived maize yield forecast versus FAOSTAT national reported maize yields for 10 Southern African countries from 2003 to 2007.

B.3.3 Burkina Faso

The ECGM maize yield results were compared against provincial census yields from Burkina Faso for the period 1996-2007. They are published on the COUNTRYSTAT website of FAO. The yield, production and growing area data concern 29 provinces during 12 years. The total number of data points used in the comparison is 348. The provincial maize yields in this dataset range from 125 kg/ha in Gnagna to 2795 kg/ha in Kenedougou with an average of 1051 kg/ha. No trend was observed in the data.

According to the FAO calendars, the maize-growing season in Burkina Faso lasts from 1 April until 11 August. These dates were used for the start and the end of the ECGM maize growing simulation. Figure B.5 shows the country's main maize growing areas. The most important maize growing provinces are Houet, Comoe and Kenedougou in the southwestern part of the country where 47% of the national maize staple of Burkina Faso is produced.

Since provincial data on maize yield and area were available, not only provincial satellite yield estimates could be calculated but also more accurate national maize yield estimates could be made by using the crop growing area of each sub-national administrative unit as weighing factor. Whereas the provincial data series on yield and growing area are continuous, the satellite yield estimates could be based on the satellite derived difference yields and the preceding 5 yr average census yields, as described in section 3.9, equation (30). Examples of the correlation between Meteosat derived provincial maize yield estimates and census yields are presented in figure B.6. The correlation is fairly good with coefficients of determination (R^2) between 0.62 and 0.8.

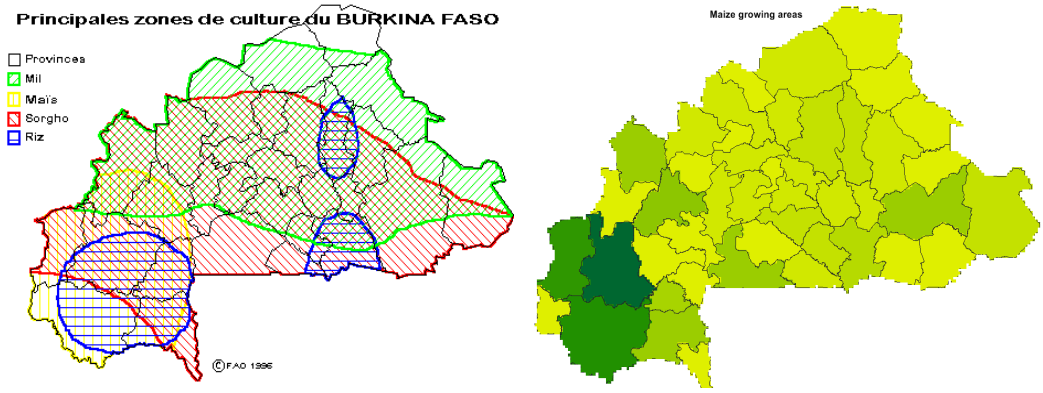

Figure B.5: Main cultivation areas of maize, sorghum, millet and rice in Burkina Faso(left). According to COUNTRYSTAT, the three most important maize growing provinces are Houet, Comoe and Kenedougou, shown in dark green on the right

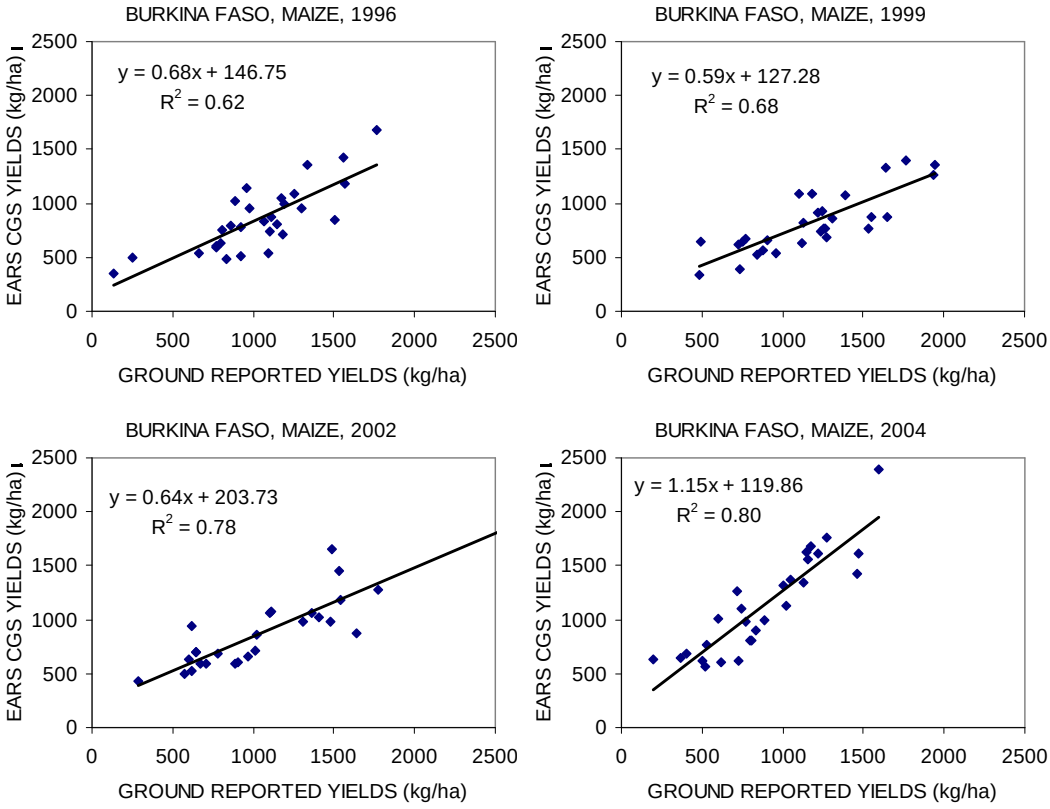

Figure B.6: End of season provincial reported maize yields plotted against EARS CGS (1st dekade August MDY) results at Burkina Faso in 1996, 1999, 2002 and 2004

Table B.1: Average yield, difference and RMSD of EWBMS and reported crop yields for all provinces and for the 3 most important maize growing provinces separately.

	Average Yield* (kg/ha)	Average Difference (kg/ha)	RMSD (kg/ha)	RMSD %
BURKINA FASO ALL PROVINCES	1051	-23	123	12
HOUET	1734	-35	127	7
COMOE	1626	-16	103	6
KENEDOUGOU	2017	-25	142	7

**(1996-2007 provincial averages)*

Table B.1 presents the average yield and RMSD for all provinces and the 3 most important maize growing areas in Burkina Faso. Reasonable good correspondences are seen between the ground reported and EARS-CGS provincial yields with small average differences and root mean square differences (RMSD) below 15%. Here it is noted again that differences between ground and satellite estimates are due to both data sources. In fact the RMSD presented in table B.1 represents the vector sum of the standard errors in the satellite derived yields and the ground reported yields.

B.3.4 Tanzania

The EARS-CGS model results were compared against provincial yield statistics from Tanzania for the period 1996- 2007. In principle the statistics on maize yields, productions and areas for 117 provinces during 12 years are available, but in practice many statistics are missing and the total amount of data points used reduces to 132. The maize yield reports in this dataset range from 200 kg/ha in Morogoro rural to 3000 kg/ha in Arumeru with an average of 1507 kg/ha. No trend was observed in the ground yield data.

According to the FAO calendars, the maize growing season in Tanzania lasts from 1 December until 1 June. These dates were used for the start and the end of the ECGM maize growing simulation. Figure B.5 shows the country's main crop zones and maize growing areas. Maize is grown widespread. The more important maize growing provinces are Kongwa, Kiteto and Simanjiro where 11% of the national maize staple of Tanzania is produced.

Since the data on yield and growing areas was interrupted and 5 consecutive years of data were only occasionally available, satellite yield estimates were not based on difference yields but on relative yields and historical reported maximum yield as described in section 4.1.

Examples of the accuracy of the provincial maize yield predictions are presented in Figure B.6, where the reported provincial maize yields are plotted against the

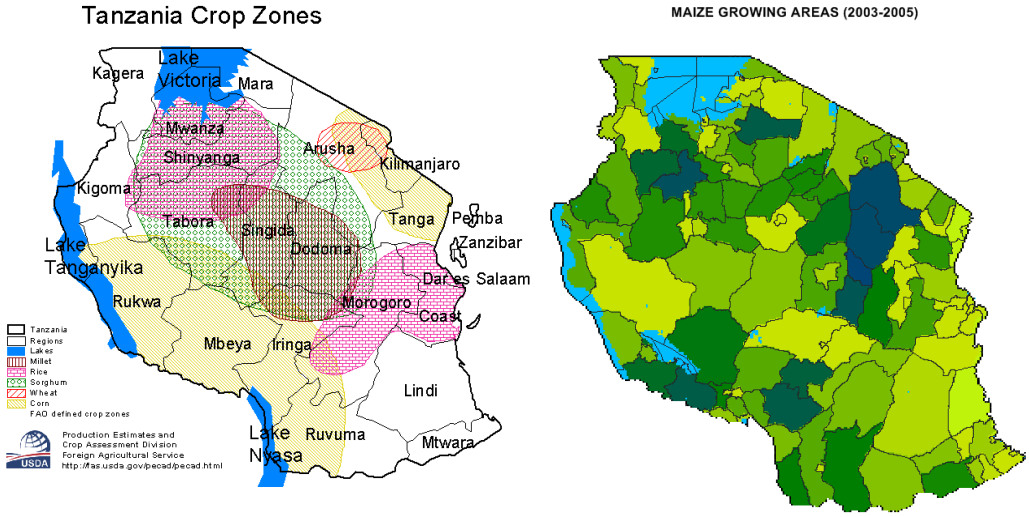

Figure B.5: Main cultivation areas of maize, sorghum, millet, wheat and rice in Tanzania (left). According to the statistical data, some important maize growing provinces are Kongwa, Kiteto, Simanjiro and Kahama shown in blue (right).

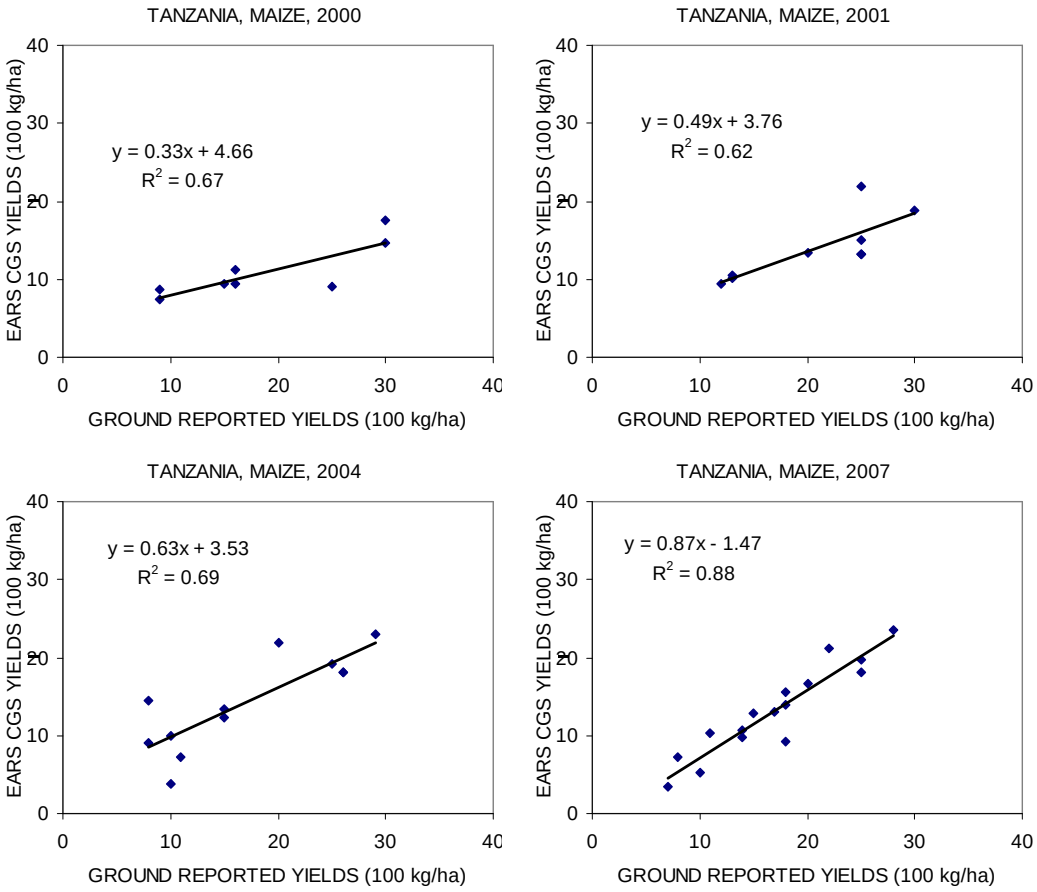

Figure B.6: End of season reported provincial maize yields plotted against ECGM results (1st dekad of June) in Tanzania in 2000, 2001, 2004 and 2007

EWBMS Meteosat based maize yield results. Spatial correlation is reasonably high with the coefficient of determination reaching values a high as 88%. Table B.2 shows the average yield and RMSD for all provinces and four important maize growing areas in Tanzania. There is fairly good correspondence between census and ECGM provincial yields with small average differences and RMSD<15%. Here it is noted again that differences between ground and satellite estimates are due to both data sources. In fact the RMSD presented in table B.2 represents the vector sum of the standard errors in the satellite derived yields and the ground reported yields. Differences between yield estimates could be attributed to varying harvest ratio and difference in measurement scale or both.

Table B.2: Average difference and RMSD between EWBMS and reported crop yields for some important maize growing provinces

	Average Yield* (kg/ha)	Average Difference (kg/ha)	RMSD (kg/ha)	RMSD %
MBINGA	2360	-540	577	24
NAMTUMBO	1029	-33	293	28
KITETO	2360	-540	577	24
SIMANJARO	2360	-629	670	28

**(1996-2007 averages)*

ANNEX C: VALIDATION RESULTS FROM RECENT PROJECTS

C.1 China: Yellow River Basin

The project "*Satellite Water Monitoring and Flow Forecasting System in the Yellow River Basin*" (*Rosema et al. 2008*) was carried out in the period 2004-2008 in cooperation with the Bureau of Hydrology of the Yellow River Conservancy Commission in Zhengzhou China with the objective to develop a drought monitoring and river flow forecasting system in the Yellow River. The project has been completed successfully and the flow forecasting system is fully operational in the Weihe and Upper Yellow river catchments, each some 100-120 thousand sqkm. The system is unique in the sense that it is the first operational flow forecasting system in the world that is almost entirely driven by satellite data. A large validation effort has been carried out during the project, which included 4 dedicated flux measuring sites.

Temperature

Daily averaged observation height air temperature ($T_{1.5m}$), as measured at the WMO-GTS meteorological stations in the basin were compared with the corresponding EWBMS air temperatures, derived from FY2c satellite data. The correlation between the two data sets during the year 2006 was 0.89 for the daily data and 0.96 for 10 daily averaged data. The average difference was 0.03 ^{o}C, the root means square difference (RMSD) 3.2 ^{o}C. Figure C.1 shows a plot of the data at two different stations. Random differences are particularly due to the large difference in measuring footprint.

Net radiation

Net radiation was measured through NR-Lite net radiometers (Kipp en Zonen) at 4 dedicated measuring sites belonging to the project. Three sites were on the Tibettan plateau, over 3000 m altitude, one in the Loess plateau area. Daily averaged net radiation data measured at the 4 sites with NR-Lite net radiometers (Kipp en Zonen)

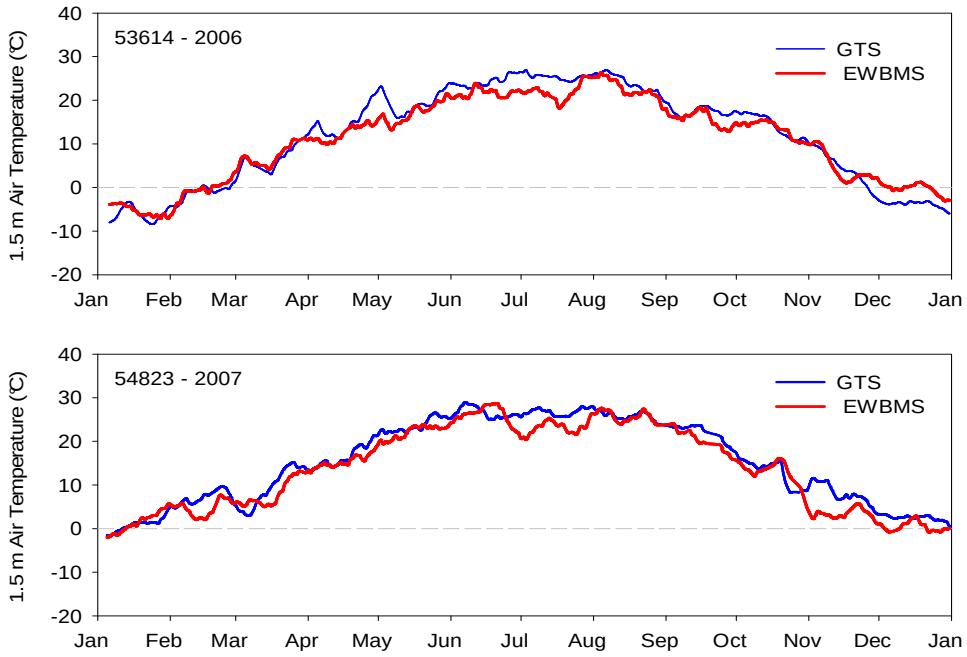

Figure C.1: Yearly course of ten daily average 1.5 m air temperatures in 2006 and 2007 for two stations in the Yellow River basin

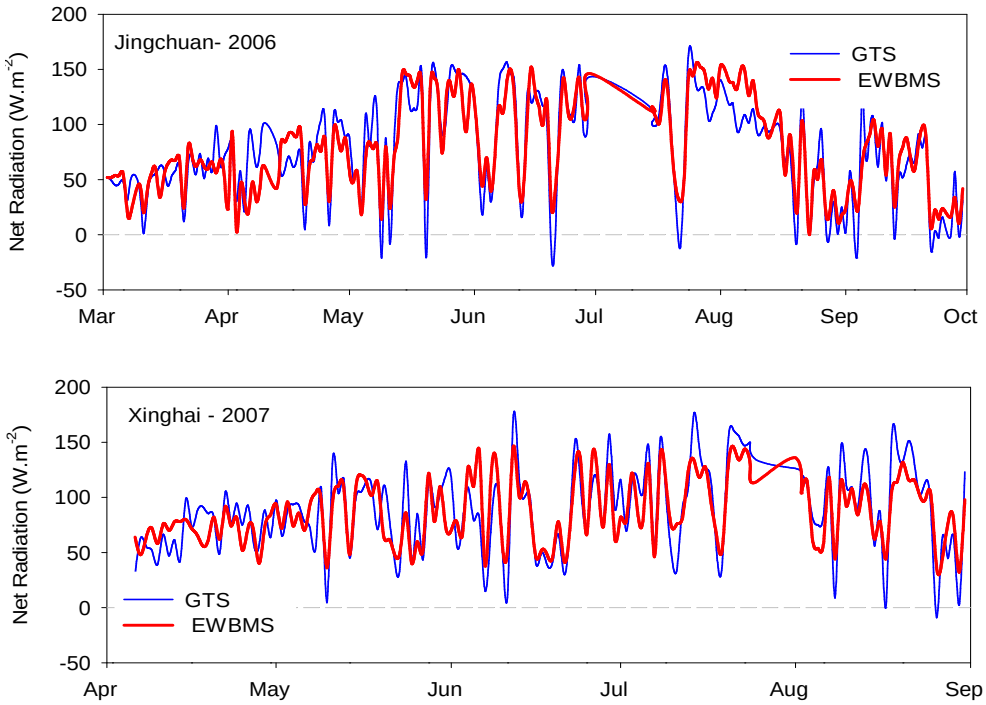

Figure C.2: EWBMS (red) and ground measured (blue) net radiation time series at Jingchuan and Xinghai

were compared with the corresponding EWBMS net radiation values. The correlation coefficients at these sites during 2005-2007 were 0.83 for the daily and 0.89 for the 10 daily average values. RMSE was respectively 25 and 13 W/m^2. The average absolute difference was between 0 and 13 W/m^2. Figure C.2 shows the course of the net radiation at Jingchuan and Xinghai as determined from satellite and measured on the ground.

Sensible heat flux

At the same 4 sites the sensible heat flux (H) has been measured with Large Aperture Scintillometers. The LAS sends a beams of light along a horizontal path of several km's through the atmosphere. The intensity fluctuations, caused by turbulent eddies of different temperature, are measured. From these the sensible heat flux is calculated. The grid size of the EWBMS data was 0.1°, or about 100 km^2. Figure C.3 shows two examples of time series sensible heat flux derived from the EWBMS and measured by LAS. The whole time series runs from 8/2005 to 8/2008. The correlation coefficients were 0.83 for the daily and 0.89 for the 10 daily average values. RMSE was respectively 25 and 13 W/m^2. Average differences are very small.

Catchment water balance

Rainfall and evapotranspiration were derived from the FY2 data through the EWBMS. Net precipitation of the upper river catchment (120,000 sqkm) was compared with river runoff. Figure C.4 presents the EWBMS net precipitation and the river discharge as measured on the ground. Figure C.5 shows the cumulative values of precipitation (blue), actual evapotranspiration (red), net precipitation (light blue), and river discharge (black line). The net precipitation and the river discharge should match and do so very well.

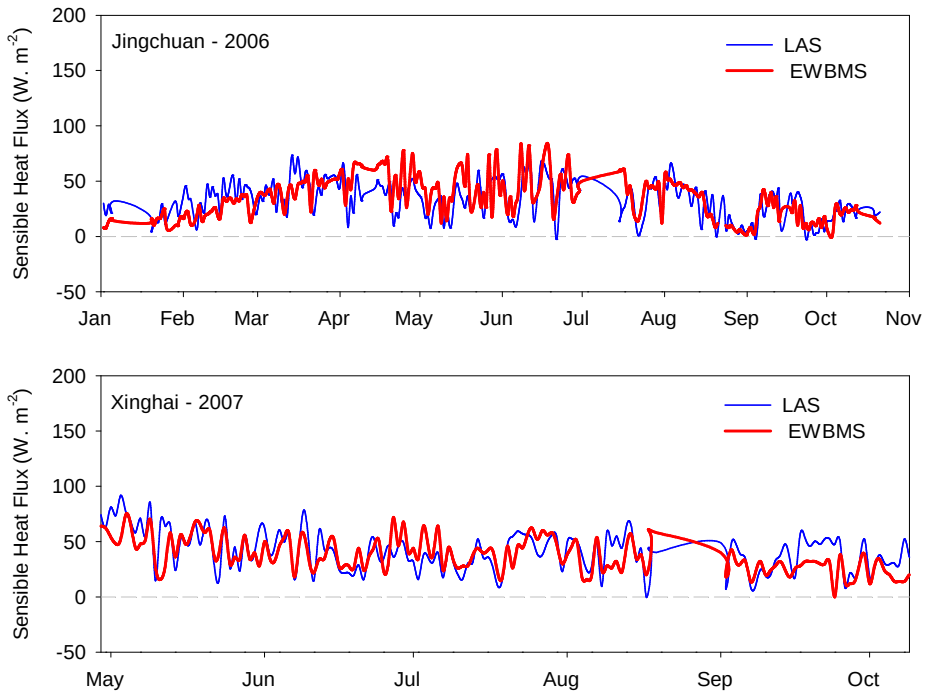

Figure C.3: Daily EWBMS (red) sensible heat flux and LAS sensible heat flux (blue) at Jingchuan in 2006 and Xinghai in 2007.

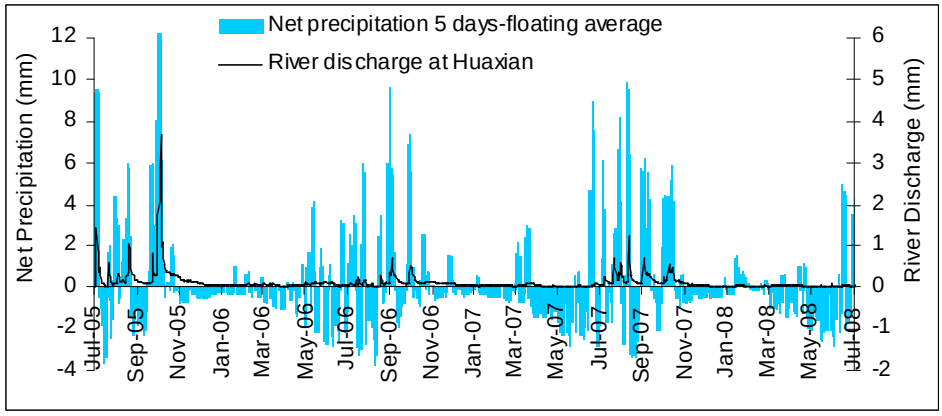

Figure C.4: Net precipitation (precipitation-actual evapotranspiration) on, and discharge from the upper Yellow River basin

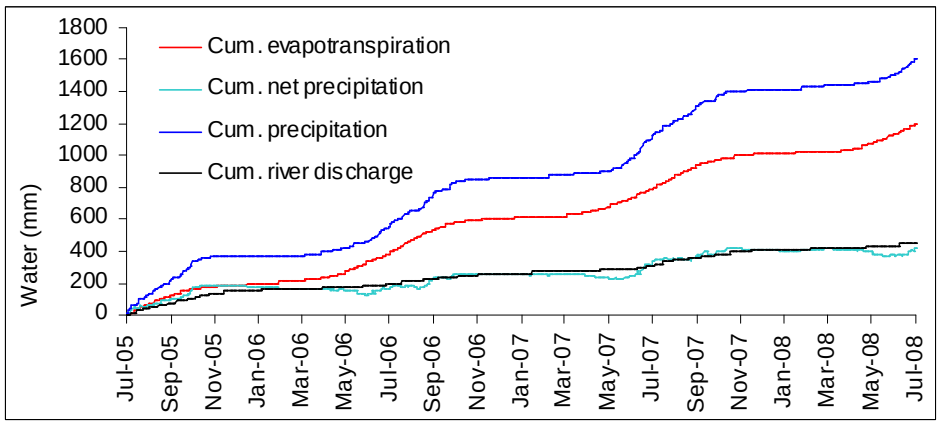

Figure C.5: Cumulative precipitation, actual evapotranspiration, net precipitation and river discharge from the upper Yellow River basin.

C.2 Mongolia

The EWBMS has successfully been implemented at the Ministry of Nature and Environment in Mongolia for pasture monitoring and management. Also here a considerable validation effort was made.

Observation height air temperature

Daily averaged observation height air temperature from regularly reporting WMO-GTS stations have been compared to corresponding EWBMS values with a grid size of 0.05° (about 25 km^2). The correlation coefficients for the years 2006-2008 are high: 0.89-0.90 for the daily and 0.93-0.97 for the 10 daily average values. The RMS differences are several degrees but this should amaze, given the large difference in footprint. The yearly average difference is less than 0.2 ^oC. Figure C.6 presents the yearly observation height air temperature course at two locations in Mongolia, as estimated from the satellite, and measured on the ground.

FigureC.6: Yearly course of ten daily average observation height air temperature during 2006 at two locations in Mongolia, as measured on the ground (blue) and as determined with FY2c satellite with the EWBMS system.

Net radiation

Daily averaged net radiation data measured with a Q7 net radiometer (Radiation Energy Balance Syst., Seattle) at the Arvaikheer PAM flux site, were compared with the corresponding EWBMS outputs from a single pixel (25 km^2). Figure C.7 shows the course of the measurements during 1999 and 2001, figure C.8 presents the corresponding scattergram. The satellite and ground data agree quite well. The entire data set shows a correlation coefficient of 0.84, an average difference of 1.35 $W.m^{-2}$ and a RMS difference of 20 $W.m^{-2}$. On a ten daily average basis the correlation improves to 0.89 and the RSM difference becomes 9 $W.m^{-2}$.

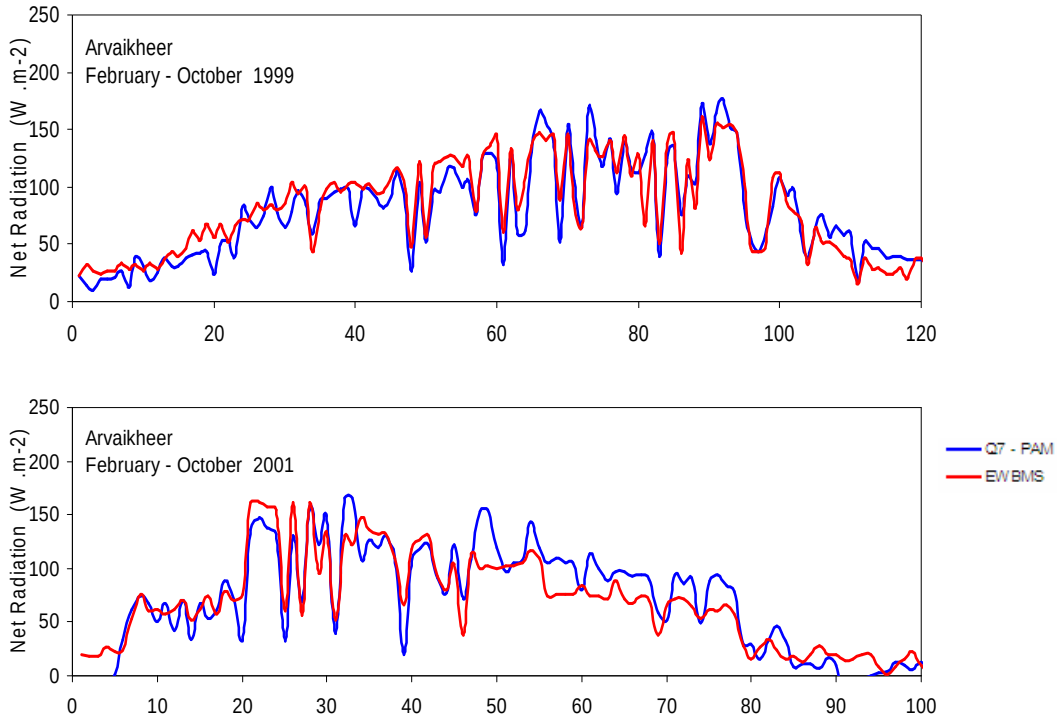

Figure C.7: EWBMS (red) and Q7 (blue) net radiation time series in 1999 and 2001, at the Arvaikheer PAM III flux site in Mongolia

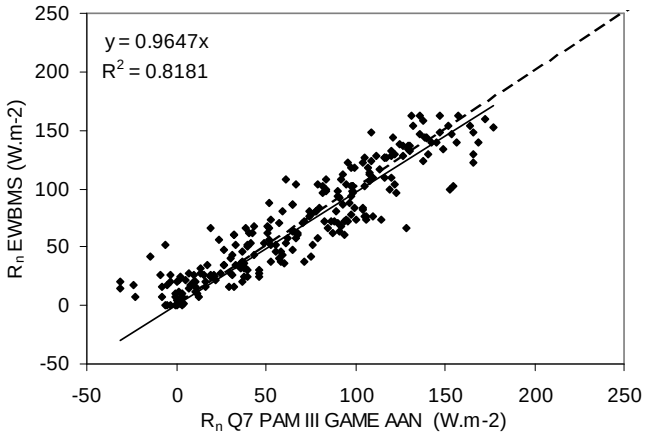

Figure C,8: Scattergram of daily averaged net radiation measured by Q7 versus EWMBS net radiation at the Arvaikheer PAM III flux site in 1999 and 2001.

Sensible heat flux

The PAM III station in Arvaikheer employs a 3-D sonic anemometer (Gill Inc., R3A) and a hygrothermometer (Vaisala, 50Y) to determine turbulent fluxes of sensible heat by eddy correlation. The instruments are mounted on the flux tower at 7.8m above the surface. Fore the entire dataset the correlation with the EBWMS values is 0.43, the average difference -1 W.m^{-2} and the RMSD 27 W.m^{-2}. Figure C.10 presents the time courses and figure C.11 shows the scattergram of both data sets. Given the differences in foot print the agreement is fairly good.

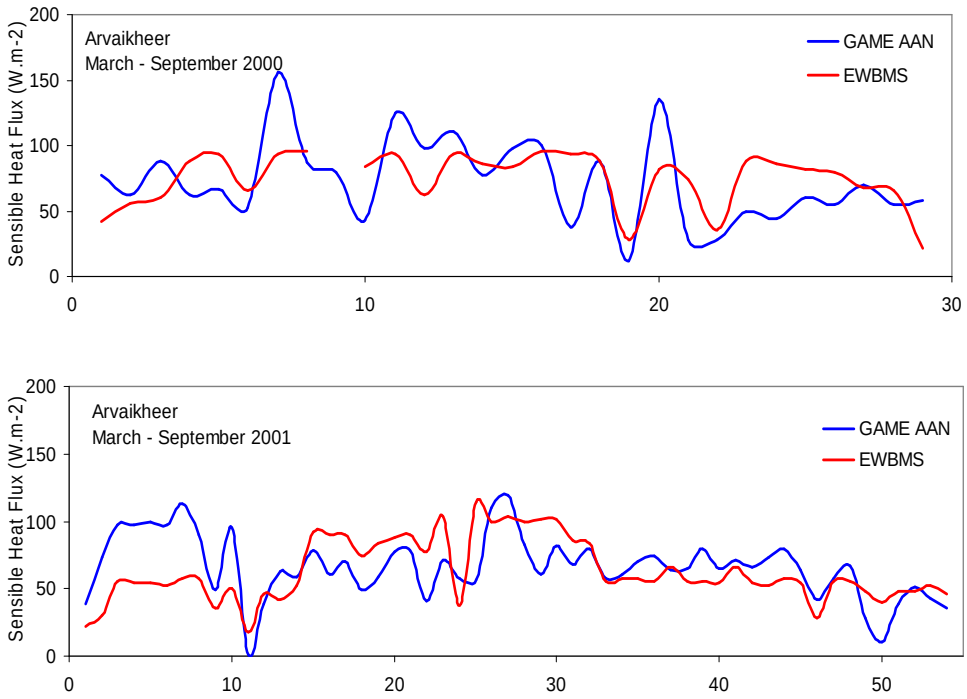

Figure C.10: Daily EWBMS (red) and ground measurements of sensible heat flux at Arvaikheer (blue)

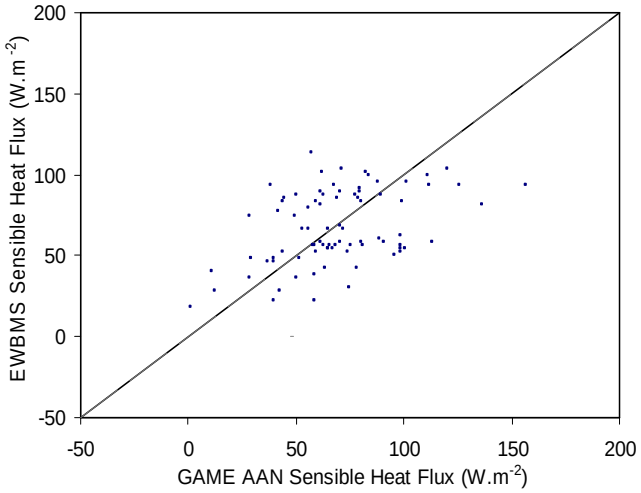

Figure C.11: Daily averaged sensible heat flux measured at PAM III in Arvaikheer versus EWMBS result

C.3 Netherlands

The project "High Water Forecasting by Satellite and Radar" (*Foppes et al. 2007*) was carried out during 2006 and 2007 in the Netherlands. Validation work was done on precipitation, radiation, sensible heat flux and latent heat flux (actual evapotranspiration) data. EWBMS radiation, sensible heat flux and latent heat flux data were compared with data from the meteorological mast at Cabouw, kindly provided by the Netherlands Meteorological Institute (KNMI).

Energy balance components

The comparison of KNMI measurements at Cabauw and the EWBMS results is presented in figure C.13. It shows global radiation, net radiation, sensible heat flux and actual evapotranspiration, respectively. The daily global radiation values correspond well, with an average difference of 12 W/m2 or 7% and a mean coefficient of determination of r^2=0.70. Daily net radiation differences are 12 W/m2 or 12% on average, with a mean coefficient of determination r^2=0.65. The sensible heat flux values are on average quite similar, except for the period of 25 June to 9 July, where the EWBMS output is too low for yet unknown reasons. Nevertheless the actual evapotranspiration during the whole period is quite similar, as shown in the lowest graph. The EWBMS actual evapotranspiration is on average some 25 W/m2 lower on a daily basis. Since the EWBMS radiation estimates are about correct, it is believed that the lower evapotranspiration values are the consequence of accounting for the photosynthetic electron flow, which amounts to 8% of the absorbed global radiation. It is also noted that the KNMI data were of recent date and not yet quality controlled. The overall validation result is considered satisfactory.

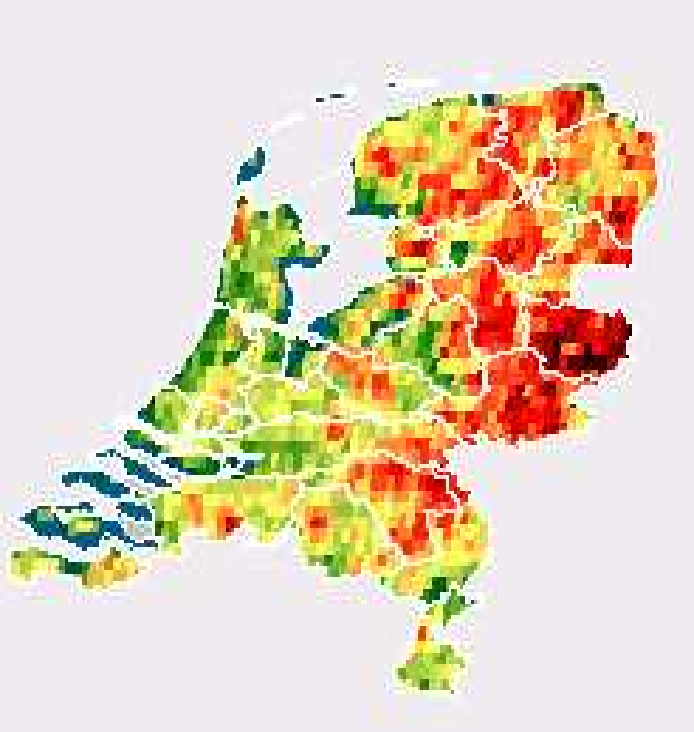

Figure C.12: EWBMS actual evapotranspiration in the Netherlands during 2006

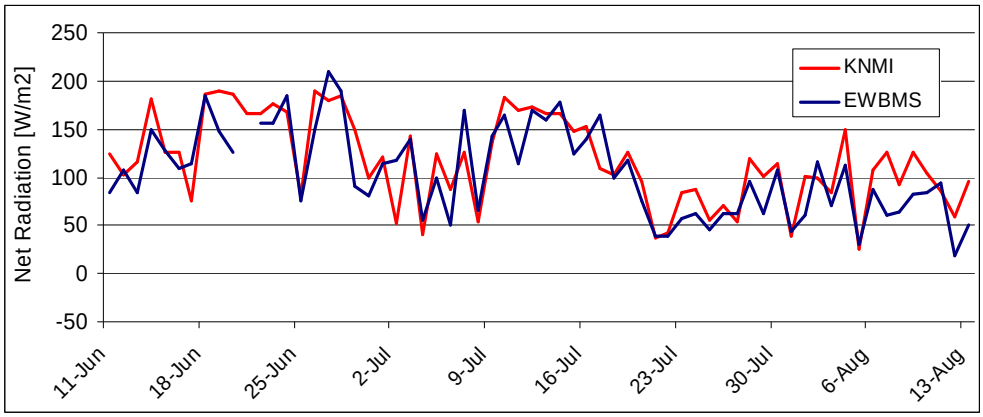

(a)

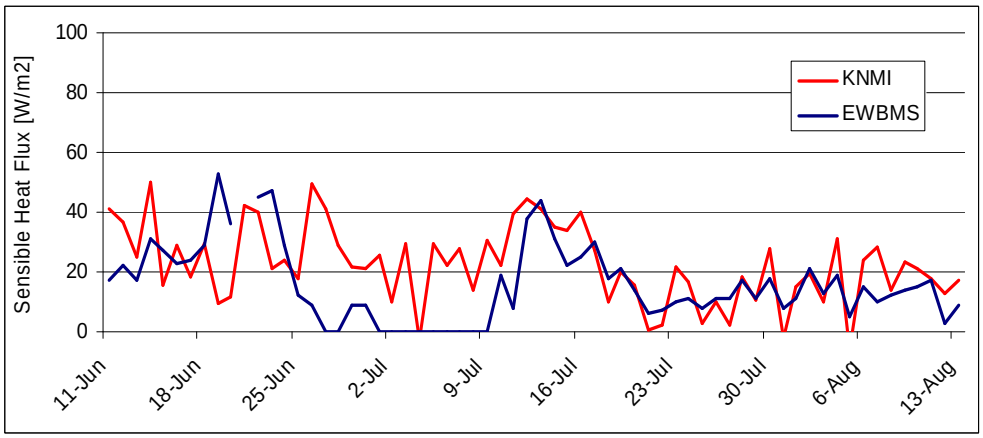

(b)

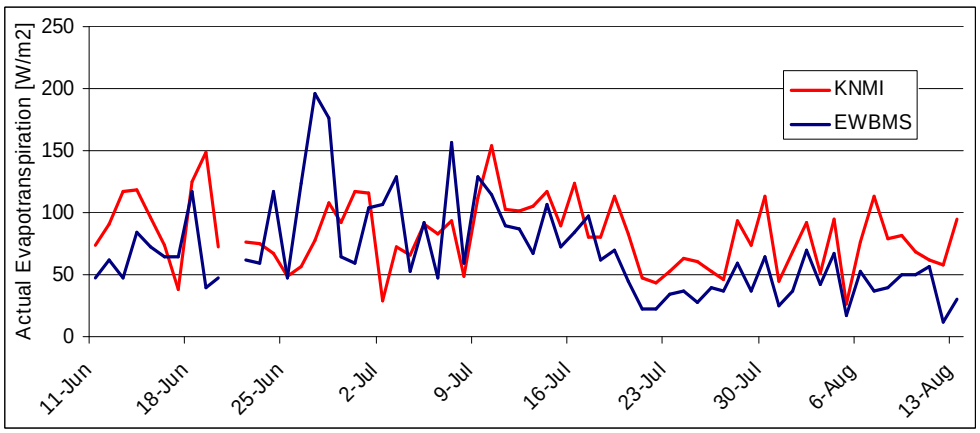

(c)

Figure C.13: Validation of EWBMS Meteosat derived fluxes with data measured at the Cabauw meteorological mast. (a) net radiation,(b), sensible heat flux and (c) actual evapotranspiratio. Period:, 11/6 –14/8, 2005